ABSTRACT

NIROUMAND, RAMIN. Joint Traffic Signal and CAV Trajectory Optimization for Mixed-autonomy Traffic Streams. (Under the direction of Dr. Leila Hajibabai and Dr. Ali Hajbabaie).

The Federal Highway Administration estimates that roughly 60% of the traffic delay happens in urban road networks, where bottlenecking caused by intersections plays a significant role. The literature has shown the effectiveness of incorporating new technologies in traffic signal optimization. For instance, using online data obtained from connected vehicles (CVs) helps to find proper signal timing plans to minimize vehicular delay at intersections. In addition, jointly optimizing connected automated vehicles' (CAVs) trajectory and signal timing plans in a fully connected and automated environment has shown to further decrease the delay. However, a fully CAV environment provides the possibility of removing signal heads and operating the intersection under the signal free intersection control logic. Although a fully CAV environment promises significant improvements, it is not attainable in the near future. The main objective of this study is to propose innovative intersection control logics and develop efficient and effective algorithms to solve them considering mixed-autonomy traffic streams.

As the first step, this study developed a mixed-integer non-linear program to control the trajectory of mixed fleets of connected-automated vehicles and connected human-driven vehicles (CHVs) through signalized intersections. CAVs are used as mobile traffic controllers and their trajectory is continuously optimized via a central methodology, while a new "white" phase is introduced to enforce CHVs to follow their immediate front vehicles. The movement of CHVs is incorporated in the optimization framework utilizing a customized linear car-following model. During the white phase, CAVs lead groups of CHVs through an intersection. The proposed formulation determines the optimal signal indication for each lane-group in each time step. A receding horizon control framework is developed to solve the problem. The case study results

indicate that the proposed methodology successfully controls the mixed CAV - CHV traffic under various CAV market penetration rates and different demand levels. The results reveal that higher CAV market penetration rate induces more frequent white phase indication compared to green-red signals. The proposed program reduces the total delay by 19.6% - 96.2% compared to a fully-actuated signal control optimized by a state-of-practice traffic signal timing optimization software.

Since the proposed white phase optimization model is not solvable in real-time, a vehicle-level distributed coordination strategy is developed to provide real-time solutions using the available computation power of vehicles. During the white phases, CAVs negotiate the right-of-way to lead a group of CHVs while CHVs must follow their immediate front vehicle. This problem is formulated as a distributed mixed-integer non-linear program and is solved using a methodology to form an agreement among all vehicles on their trajectories and signal timing parameters. The agreement on trajectories is reached through an iterative process, where CAVs update their trajectory based on shared trajectory of other vehicles to avoid collisions and share their trajectory with other vehicles. Additionally, the agreement on signal timing parameters is formed through a voting process where the most voted feasible signal timing parameters are selected. The numerical experiments indicate that the proposed methodology can efficiently control vehicle movements at signalized intersections under various CAV market shares. The introduced white phase reduces the total delay by 3.2% to 94.06% compared to cooperative trajectory and signal optimization under different CAV market shares in our tests. In addition, our numerical results show that the proposed technique yields reductions in total delay, ranging from 40.2% - 98.9%, compared to those of a fully-actuated signal control obtained from a state-of-practice traffic signal optimization software.

The proposed distributed framework could successfully provide near-optimal solutions in real-time. However, it could take up to 80% of the time step length to solve the problem leaving little or no time for communication delays. In addition, joint signal and trajectory optimization for isolated intersections can be used as a subroutine for corridor- and network-level signal and trajectory optimization problems. Therefore, a new methodology is developed to provide near optimal signal timing plans and CAV trajectories much faster than the distributed framework. A bi-level architecture is used to solve the joint signal and trajectory optimization problem. An efficient shooting heuristic is developed to optimize the trajectories of connected-automated vehicles (CAVs) while the trajectories of connected human-driven vehicles (CHVs) are estimated using a customized car-following model with a given set of signal timing plans in the lower level. The upper level enumerates all the feasible signal timing plans and selects the one with the best value to be implemented. The results indicate that the proposed methodology can successfully provide signal timing plans and CAV trajectories in a much shorter time than the updating time step length. The case study results show the capability of the proposed methodology in finding proper signal timing parameters and vehicle trajectories in at most 40 milliseconds, which is much shorter than the 500 milliseconds-long updating time step length. Moreover, efficient control of CAVs can decrease the average intersection delay by up to 50.1%, compared to a fleet of CHVs.

Our research shows the effectiveness of using CAVs as mobile controllers during white phases. Using white phases can drastically decrease the intersection delay by mimicking the signal free intersection logic within mixed-autonomy environments. Therefore, as the final step of this research, we introduce a shooting heuristic-based methodology that constructs vehicle trajectories while considering vehicle group safety constraints during white phases. A bi-level architecture consisting of a shooting heuristic for trajectory construction at the lower level and an enumeration

technique for intersection signal timing optimization at the upper level is developed to find proper signal timing parameters and CAV trajectories in real-time. In addition, a platooning logic is presented to operate platoons of vehicles containing one or more vehicle groups at a time during white phases to improve the quality of the solutions. Case study results indicate that the proposed framework can successfully operate demands as high as 1200 $veh/h/lane$ through an isolated intersection with computation times of at most 37 milliseconds. This affirms the capability of this framework to be used as a subroutine in network-level signal and trajectory optimization algorithms. Moreover, the proposed framework can reduce average delay by up to 65%, compared to a joint signal and trajectory optimization with different CAV market shares.

Joint Traffic Signal and CAV Trajectory Optimization for Mixed-autonomy Traffic Streams

by
Ramin Niroumand

A dissertation submitted to the Graduate Faculty of
North Carolina State University
in partial fulfillment of the
requirements for the degree of
Doctor of Philosophy

Civil Engineering

Raleigh, North Carolina
2023

APPROVED BY:

Dr. Ali Hajbabaie Committee Chair	Dr. Leila Hajibabai Committee Chair
Dr. Billy Williams	Dr. Sanmugavadivel Ranjithan
Dr. Munindar Singh	Dr. George F. List

BIOGRAPHY

Ramin Niroumand received his B.Sc. degree in civil engineering from the University of Tabriz, Tabriz, Iran, in 2014, and the M.Sc. degree in civil engineering from the Sharif University of Technology, Tehran, Iran, in 2017. He pursued his Ph.D. studies in the Department of Civil, Construction, and Environmental Engineering, North Carolina State University. Ramin's research interests include Operations Research analysis and their applications on improving the mobility of transportation systems.

TABLE OF CONTENTS

LIST OF TABLES

LIST OF FIGURES

CHAPTER 1: INTRODUCTION

1.1. Significance of the research

Traffic signals are traditionally used to preserve safety between conflicting lane-groups of intersections. To do so, the signal controller stops all the lane-groups using a red light and operates a group of non-conflicting lanes. However, safety comes at a price of bottlenecking that is one of the significant contributors of the traffic delay. Therefore, efficient ways of operating intersections can significantly improve the overall performance of the traffic. Recent technologies, especially connectivity and automation can help improving the efficiency of intersection control strategies. For instance, incorporating online vehicle information obtained from connected human driven vehicles (CHVs) into signal optimization methods can reduce vehicles' waiting time behind a red light (Goodall et al., 2013; He et al., 2012; Lee et al., 2013; Li and Ban, 2018). In addition, optimally operating connected automated vehicles (CAVs) through signalized intersections with a fixed signal timing can reduce the average delay (Asadi and Vahidi, 2010; Tajalli and Hajbabaie, 2018). Moreover, jointly optimizing CAV trajectories and intersection signal timing plans within a fully CAV environment can further decrease the intersection delay (Jung et al., 2016; Li et al., 2014; Yu et al., 2018). However, a fully CAV environment provides the possibility of using a signal-head-free intersection control logic that leads to the maximum capacity of the intersection (Dai et al., 2016; Dresner and Stone, 2008, 2004; Mirheli et al., 2019, 2018; Wu et al., 2012). Nevertheless, a fully CAV environment is not attainable in the near future. Therefore, preparing the infrastructure and traffic control methods for the transition period from human-driven vehicles to CAVs is crucial.

Some studies have jointly optimized CAV trajectories and signal timing parameters considering mixed-autonomy traffic streams (Guo et al., 2019; Li and Zhou, 2017; Moradi et al., 2021; Tajalli et al., 2020). However, these studies mostly considered simple intersection layouts or failed to provide real-time solutions. In addition, they use the traditional green and red signals to control the traffic stream that leads to creating bottlenecks. Rey and Levin (2019) have introduced a “blue” phase to utilize the presence of CAVs in a more efficient way. During the blue phases, only CAVs from CAV-dedicated lanes can access the intersection from conflicting movements. Note that traditional green and red signal indications are also used to control the movements of human driven vehicles. However, their numerical experiments on a network of 25 intersections revealed that their proposed methodology outperforms existing optimized signalized intersections when CAV market share exceeds 60%. Research shows that sufficiently penetrated traffic streams can be controlled by controlling the movements of CAVs (Qian et al., 2014).

In this dissertation, we aim to use CAVs as mobile controllers to gain indirect control over CHVs. Trajectories of CAVs are optimized along with intersection signal timing plans to provide overall intersection-level optimal solutions. A new “white” phase is introduced that can be assigned to conflicting movements simultaneously. During this phase, CAVs form groups of CHVs and navigate them through the conflicting area of the intersection while CHVs must follow their immediate front vehicles. Note that green and red signal indications are used when there are not enough CAVs in the vicinity of the intersection to control the movements of the entire fleet. The proposed white phase concept is formulated as a mixed-integer non-linear program. However, this formulation is too complex to be solved in real-time. Therefore, a vehicle-level distributed coordination scheme is developed to solve the mathematical program in real-time. The proposed framework takes up to 80% of the updating time step length to solve the problem. Hence, a shooting heuristic is proposed to solve the joint signal and trajectory optimization problem more efficiently. This methodology can solve the problem in less than 40 milliseconds that makes it suitable to be used as a subroutine for network-level signal and trajectory optimization frameworks.

1.2. Problem statement

The effectiveness of joint CAV trajectory and intersection signal timing optimization has been shown in several studies. However, these studies mostly considered a fully CAV environment, used simple intersections layouts, or failed to provide real-time solutions. Moreover, they stop vehicles behind a red light to preserve safety even with a fully CAV fleet. Hence, it is essential to propose new concepts to deploy the full potential of CAVs in improving the overall performance of intersections. Using CAVs as mobile controllers can provide indirect control over human driven vehicles. Therefore, the safety of sufficiently penetrated fleets can be preserved by mobile controllers (CAVs) instead of stationary controllers (traffic lights). This provides the possibility of operating vehicles from conflicting movements simultaneously.

In addition, controlling CAV trajectories and intersection signal timing plans require computationally efficient solution techniques to provide real-time solutions. However, there is a trade-off between the run time and the quality of the solutions. Real-time intersection-level solutions can be acquired using distributed techniques. However, a faster solution technique is also needed to be used as a sub-routine in network- and arterial-level signal and trajectory optimization problems. In this dissertation, a vehicle-level distributed optimization framework is proposed that provides near-optimal intersection signal timing parameters and CAV trajectories in real-time. To further reduce the run time and make it suitable as a subroutine for network-level signal and trajectory optimization algorithms, a shooting heuristic-based solution technique is developed that solves the problem in less than 40 milliseconds using some simplifying assumptions.

1.3. Research objectives and scope

The main objective of this dissertation is to study the effects of optimally controlling CAV trajectories and intersection signal timing plans on the performance measures of isolated intersections. In particular, this dissertation introduces a new “white” phase, during which CAVs act as mobile controllers and navigates groups of human driven vehicles through the intersection from conflicting movements simultaneously. A distributed optimization and coordination algorithm and a shooting heuristic-based algorithm are also introduced to solve the joint signal and trajectory optimization program in real-time. This dissertation focuses on answering the following fundamental research questions:

1. Can the control of CAVs lead to a better result by using them as mobile controllers?
2. How to solve the joint control of mobile (CAVs) and stationary controllers (intersection signals) in real-time?
3. How to solve the joint CAV trajectory and intersection signal timing optimization problem in a more efficient way to be useful as a subroutine in network-level signal and trajectory optimization algorithms?
4. How to solve the joint control of mobile (CAVs) and stationary controllers (intersection signals) in a more efficient way to be useful as a subroutine in network-level signal and trajectory optimization algorithms?

1.4. Contributions of research

Traditional signal control strategies can operate vehicles only from non-conflicting lane-groups even with high CAV market shares. However, it is possible to include CAVs in intersection control by using them as mobile controllers. This dissertation introduces a new "white" phase, during which CAVs act as mobile controllers by forming groups of human driven vehicles and navigating them through the intersection from conflicting movements simultaneously. The safety of the shared fleet is guaranteed by optimally controlling the trajectory of CAVs. A mathematical programming is developed to provide optimal control parameters for the moving and stationary controllers.

In addition, the existing intersection signal and CAV trajectory control methods are not scalable and do not use the available computational power of vehicles. Therefore, a distributed optimization is developed to decompose the signal and trajectory optimization program into vehicle-level programs. Moreover, a coordination algorithm is designed to push the vehicle-level optimal findings toward intersection-level optimality. This framework is scalable with the size of the problem and uses the available computational power of vehicles that eliminates the need for a central computation unit. In addition, near-optimal solutions are calculated to be implemented in real-time.

Furthermore, network-level signal and trajectory optimization algorithms need to solve the intersection-level signal and trajectory optimization problem multiple times as their subroutines. Hence, an efficient shooting heuristic-based algorithm is developed to construct CAV trajectories and provide near-optimal signal timing plans for an isolated intersection in the order of milliseconds that makes it suitable to be used in network-level intersection control algorithms.

Finally, the proposed shooting heuristic algorithm is extended to consider CAVs as moving controllers during the white phases. To so so, the vehicle-group formation and their safety are included in the CAV trajectory construction. In addition, operating single CAVs is not optimal in high CAV market shares. Therefore, a platooning algorithm is designed to form platoons of CAVs and operate them instead of operating individual CAVs.

1.5. Dissertation organization

The exposition of this doctoral dissertation is as follows.

Chapter 3 provides a novel problem formulation for joint signal and trajectory optimization in mixed-autonomy environments. A new white phase is suggested during which CAVs form groups of CHVs and navigate them through the intersection from conflicting movements simultaneously. A hybrid solution technique consisting of linearization and receding horizon framework is also proposed to solve the optimization model in a central way.

The proposed signal and trajectory optimization model is too complex to solve in real-time. Therefore, Chapter 4 provides a vehicle-level distributed coordination strategy that uses the available computational power of vehicles to find near-optimal intersection signal timings and vehicle trajectories in real-time.

The solution technique proposed in Chapter 4 uses up to 80% of the updating time step length, which makes it real-time for an isolated intersection. However, network-level signal optimization algorithms may need to optimize intersection-level signal and trajectories multiple times. Hence, Chapter 5 introduces a shooting heuristic-based methodology that can solve the joint signal and trajectory optimization problem in the order of milliseconds that makes it suitable as a subroutine for network-level signal and trajectory optimization algorithms.

Chapter 6 extends the shooting heuristic-based methodology to accommodate white phases and consider vehicle-group safety constraints in CAV trajectory construction process.

Chapter 7 summarizes the contributions of this research and highlights the findings.

CHAPTER 2: LITERATURE REVIEW

The Federal Highway Administration predicts that roughly 60% of the total travel delay occurs on urban street networks, where intersections play a prominent role as the bottlenecks of the system (Mirheli et al., 2019). A reach body of the literature has dealt with optimally controlling the signalized intersections to improve the overall efficiency of the system. However, due to low visibility of the traffic condition to the traffic control unit, it is very challenging to provide a suitable set of signal timing parameters. Connected vehicle (CV) technology has provided the possibility of incorporating the upcoming vehicles' information into the intersection signal timing optimization methods (Goodall et al., 2013; He et al., 2012; Lee et al., 2013; Li and Ban, 2018). Such an informed decision can significantly improve the efficiency of the intersection control methodologies. In addition, this information can help the intersection controller to be reactive to the dynamic traffic demand that happens throughout the day.

The emergence of connected automated vehicles provides additional benefits on top of improving the visibility of the traffic systems promised by CV technology. Optimally controlling the movements of CAVs approaching a signalized intersection with a fixed signal timing plan can lead to the maximum use of the available green signal times (Asadi and Vahidi, 2010; Tajalli and Hajbabaie, 2018). In addition, jointly optimizing the signal timing plans and CAV trajectories can further enhance the intersection control frameworks (Jung et al., 2016; Li et al., 2014; Yu et al., 2018). Furthermore, a considerable reduction in delay is reported when the signalized intersections are converted to signal-head-free intersections in a fully-automated vehicle environment (Dai et al., 2016; Dresner and Stone, 2008, 2004; Mirheli et al., 2019, 2018; Wu et al., 2012). Optimizing the trajectory of CAVs at signal-head-free intersections helps utilize the maximum capacity of intersections. While technology, regulation, and safety limitations influence the expansion of CAV market penetration rate for many years to come, there is a need to prepare for the transition from human-driven to self-driving cars with various CAV market penetration rates.

The following provides a thorough review of the existing studies on optimizing CAV trajectories through signal-free and signalized intersections.

2.1. Trajectory optimization of CAVs at signalized intersections

Optimizing CAV trajectories helps control the movement of vehicles approaching the signalized intersection and prevent an excessive number of stops. Tajalli and Hajbabaie (2018a) have developed a distributed optimization and coordination algorithm to dynamically optimize the speed of CAVs over a network of signalized intersections. Their algorithm first decomposes the network into intersection-level sub-networks to reduce the complexity of the problem. Then, it creates effective coordination among each pair of the sub-networks to push the intersection-level solutions toward network-level optimality. They incorporated their methodology into a model predictive control to further decrease the complexity and allow for additional consensus among the sub-networks. They have tested their methodology in networks with eight, twenty, and forty intersections under four various demand levels. Their numerical experiments show up to 14.8% and 9.7% - 13.4% reductions in travel time and speed variation, respectively. Moreover, they reported respectively up to 28% and 9.5% increase in the average speed and the total number of completed trips. Furthermore, their methodology successfully solves the CAV speed optimization problem in real time with an optimality gap of at most 2.7%. Furthermore, controlling the trajectory of CAVs reduces energy and fuel consumption significantly. As shown by Asadi and Vahidi (2010), an optimal eco-driving strategy with advance knowledge of signal timing plans can decrease fuel consumption by 47% at an arterial street with nine intersections. Moreover, controlling the trajectory of CAVs along with optimizing the signal timing plans can improve the operational performance of intersections.

Li et al. (2014) have jointly optimized signal timing and CAVs' trajectories through an enumerative technique in a fully-automated environment for a simplified intersection. They have shown that a cooperative signal timing and trajectory optimization reduces the average travel delay by 16.2%-36.9% and increases the intersection throughput by 2.7%-20.2% compared to a fully-actuated signal control. Jung et al. (2016) have developed a bi-level optimization model to minimize fuel consumption and delay at an isolated signalized intersection with 100% CAV penetration rate. Their experiments have resulted in a reduction of travel time and fuel consumption by 12% and 10%, respectively compared to fully-actuated and pre-timed signal control methods. Li and Zhou (2017) have jointly optimized signal timing plans and CAV trajectories in a mixed-autonomy environment. They represented the traffic dynamics and signal timing constraints with a phase-time traffic hypernetwork model to reduce the complexity of the problem. They developed a sequential branch and bound search algorithm to solve the problem more efficiently. Their case study results indicate their proposed framework can reduce the intersection total delay by 4.2% in comparison with fixed-time signal control with a 5% CAV market share. Yu et al. (2018) have proposed a mixed-integer linear programming model to optimize signal timing and trajectories of vehicles at an isolated intersection in a 100% CAV environment. They split vehicles into platoons and use an optimal control strategy to minimize fuel consumption of the platoon leaders. The numerical results reveal that their proposed models increase the intersection throughput by 0.55%-19.8% and decrease the average delay and average CO_2 emission by 41.16%-83.37% and 7.45%-49.31%, respectively compared to a fully-actuated signal control.

Feng et al. (2018) have also optimized the signal timing and trajectory of CAVs by splitting vehicles into platoons and controlling the trajectory of the platoon leaders. Their study shows reductions in vehicle delay and CO_2 emission up to 24.0% and 13.8% for a two-phase intersection, respectively. Li et al. (2018) have optimized the trajectory of CAVs and signal timing plans with the presence of conventional vehicles. They used a bi-objective and multi-stage model to minimize the traffic delay by optimizing signal timing plans and provide optimal trajectories for that signal timing plan. They utilized a hybrid heuristic method that combines genetic algorithm and particle swarm optimization. Their methodology provides optimal trajectories from each vehicle's perspective without coordination among vehicles, therefore, the solution may not improve system-level performance. Their numerical experiments on an arterial street with four intersections show 9.7%-12.2% and 0.6%-7.9% reduction in travel delay and energy consumption, respectively compared to fixed-time signal control with 10% electric vehicles. Liang et al. (2019) have developed a bi-level rolling-horizon methodology to jointly optimize signal phase and timing plan and CAV trajectories while considering traditional human-driven vehicles, connected human-driven vehicles, connected human-driven vehicles which receive speed guidance (human-cooperative vehicles), and autonomously-driven connected vehicles. The proposed methodology enumerates all possible departure sequences of naturally happening platoons to find the departure sequence with the least delay at the upper level. At the lower level, they first convert each departure sequence to a signal phase and timing and find the appropriate speed guidance for autonomous and cooperative human-driven vehicles to minimize the total number of stops. Then, the signal timings are adjusted based on the calculated speed guidance and the delay associated with the signal phase, and timing is calculated and sent back to the upper level. They tested the proposed methodology on an isolated intersection with exclusive left-turning lanes and showed that the intersection total delay and number of stops decreases as CV penetration rate increases and autonomous and cooperative human-driven vehicle penetration rate increases, respectively.

Pourmehrab et al. (2019) have proposed a framework to adjust an adaptive intersection control considering vehicles' arriving time to maximize the utilization of green phases. Their methodology provides a feasible signal phase and timing plan by using a set of rules to process all incoming vehicles. In addition, they split the fleet into platoons and only optimize the trajectories of automated leaders to minimize their travel delay. Their numerical experiments on a four-leg isolated intersection show a 38%-52% reduction in average travel time in comparison with a fully actuated signal control. Guo et al. (2019) have proposed a two-step approach to find near-optimal signal timing plans and CAV trajectories with different CAV market penetration rates. The proposed approach finds near-optimal signal timing plans to minimize intersection delay in the first step using dynamic programming. In the second step, they generate CAV trajectories and estimate movements of CHVs based on the determined signal plans using shooting heuristic. Their case study results indicate that the proposed approach reduces average travel time and fuel consumption by up to 35.7% and 31.5%, respectively compared to adaptive signal control. A sensitivity analysis also shows that increasing the CAV penetration rate significantly contributes to improvements in intersection performance. This study can handle a mixed-autonomy traffic stream with different CAV penetration rates, however, it stops vehicles behind the red light even in a fully automated environment which leads to higher delay compared to signal-free intersection control methods.

Moradi et al. (2021) have developed an integrated platoon-based round-robin algorithm for intersections within a mixed-autonomy environment while prioritizing special vehicles. They further improved their methodology by incorporating a speed advisory mechanism for CAVs.

Their methodology outperforms fixed-time and actuated intersection control methods with 5% and 35% CAV penetration rate, respectively. Du et al. (2021) have proposed a joint signal and trajectory optimization framework that improves the traffic efficiency and energy saving. Their methodology optimizes the signal timing plans to minimize vehicle delay at the macro level and optimizes the CAV trajectories to minimize fuel consumption at the micro level. A comparison with the Cooperative Adaptive Cruise Control (CACC) with a fixed time signal control shows 6%-14.5% fuel consumption reduction with 20% CAV penetration rate. Tajalli and Hajbabaie (2021) Have developed a methodology to jointly optimize the signal timing plans and CAV trajectories in mixed autonomy environments. Their methodology decomposes the joint signal and trajectory optimization program into smaller lane-level optimization problems using a Lagrangian relaxation technique. They reported a 5%-51% reduction in average travel time while having duality gaps of at most 0.1%.

Ghosh and Parisini (2022) have proposed a priority-based methodology to operate a mixed fleet of AVs and HVs through a signalized intersection. As a new vehicle arrives at the intersection cooperative area, the intersection controller re-evaluates the optimal departure sequence of vehicles. The controller then informs the AVs of their allocated time slot to cross the intersection while communicating with HVs using signal indications. Their numerical experiments on an isolated intersection indicate that their methodology outperforms the First-In-First-Out control logic. Jiang and Shang (2022) have developed a framework to dynamically allocate CAV-dedicated lanes while jointly optimizing CAV trajectory and intersection signal timing parameters. They weighted the delay and the number of stops to form an integrated performance index (PI) to evaluate the performance of their proposed framework. Their case study results show up to 15.7% reduction in the PI per vehicle, compared to a fully actuated intersection control. Ma et al. (2022)

have proposed a shared-phase-dedicated-lane (SPDL)-based traffic control model to operate a mixed fleet of CAVs and HVs through an isolated signalized intersection. They assumed CAV-dedicated lanes that are shared among left-turn and through CAVs. A three-level optimization model is designed to solve the proposed model. The upper level uses a NEMA ring barrier structure to optimize the barrier durations using dynamic programming to minimize the total vehicle delay. The middle level enumerates all phase sequences and durations for the given barrier from the upper level to find the combination with the minimum vehicle delay. Finally, the lower level conducts the CAV platooning and trajectory planning tasks based on the given signal timing and ring barrier information. They used a rolling-horizon scheme to implement their framework dynamically with a time varying demand. Their case study results reveal delay reductions by up to 51%, compared to the blue phase framework proposed by Rey and Levin (2019) with 50% CAV market share.

Nguyen et al. (2023) have proposed a bi-level control framework to design traffic signal timing parameters at a network-level while providing a detailed trajectory control policy for CAVs at a link-level. The lower level of their framework uses a group-based longitudinal trajectory planning scheme to coordinate vehicular trajectories. The upper level decides on signal timings and end-to-end vehicle routings. Their proposed framework could successfully provide near-optimal solutions while increasing the average intersection throughout by up to 17%. Zhang and Du (2023) have developed a system optimal platoon-centered control for eco-driving. Their developed methodology guides platoons of mixed CAVs and HVs to smoothly pass signalized intersections while reducing sharp deceleration and red idling. They used a solution technique consisting of three model predictive controllers for platoon trajectory control and an MINLP for optimally splitting the platoons as needed. Their case study results with platoons of 10 and 16 vehicles show respectively 50% and 7% reduction in fuel consumption and emission, compared to an existing cooperative adaptive cruise control and eco-driving strategy.

2.2. Trajectory optimization at signal-head-free intersections in a fully-automated environment

Traffic operations and safety at intersections can be further improved in a fully-automated environment with advanced CAV trajectory control strategies. Dresner and Stone (2008 and 2004) have developed a multi-agent reservation-based intersection control approach under 100% CAV market penetration rate. They have shown that a signal-free intersection can reduce the average delay at the intersection up to 99.7% compared to a fixed-time intersection control. Shahidi (2010) has shown that a delayed response policy control can further reduce the intersection's average delay by 35% in comparison with the first-come-first-serve framework developed by Dresner and Stone (2008). Lee and Park (2012) have proposed a cooperative intersection control to minimize the total length of overlapped trajectories of CAVs at the intersection. Solving the problem using Genetic Algorithm on a four-way intersection shows the reduction of stop delay and total travel time by 99% and 33% compared to fully-actuated signal control, respectively. Mirheli et al. (2018) have utilized a stochastic look-ahead technique based on the Monte Carlo tree search algorithm (similar to Mirheli and Hajibabai (2019)) to find the near-optimal collision-free trajectories at a signal-head-free intersection with 100% CAV penetration rate. Their numerical results indicate that the proposed algorithm reduces the total travel time at the intersection by 59.4%-83.7% compared to fixed-time and fully-actuated signal control strategies. Wu and Jiang (2023) have used a mixed-integer linear programming (MILP) model to jointly optimize the autonomous intersection management and trajectory smoothing design. The objective of their research is to improve traffic efficiency, driving comfort, and fuel economy simultaneously. They have used a rolling horizon framework to solve the proposed model.

Vitale et al. (2022) have developed a framework for CAV trajectory optimization at signal free intersections while considering uncertainty in CAV locations. They have modeled the uncertainty as ellipses around the barycenters of vehicles using linear-Gaussian motion models. The proposed framework then selects a set of control actions in a way to avoid the ellipses from intersecting. They have presented two different approaches, namely user optimum and system optimum to solve the trajectory optimization model from user and system perspectives, respectively. Their numerical experiments confirm the capability of their methodology of providing real-time near-optimal set of trajectories with probabilistic collision avoidance guarantees.

The effectiveness of automated intersection control is observed more significantly under very high traffic volumes at the intersection. Mirheli et al. (2019) have developed a consensus-based distributed algorithm by decomposing the optimization problem into vehicle-level MINLPs and finding the collision-free trajectory of each CAV in a signal-free intersection. They have tested the effect of removing signal heads on high traffic demands up to 1500 vehicle/hour/lane at an isolated intersection with eight lanes. Their results indicate that their proposed control logic is able to improve the total travel time, intersection throughput, and average speed up to 70.5%, 115.6%, and 400%, respectively compared to optimized fully-actuated signal control. Wu et al. (2019) have modeled the sequential CAV movements through signal-head-free intersections as a Markov decision process to minimize the intersection delay under collision-free constraints. This study decomposes the state space of CAVs into independent and coordinated components and incorporates a reinforcement learning technique to solve the problem in real-time. They have tested the effectiveness of their methodology on a 4-way 6-lane intersection with 2300 vehicle/hour/lane traffic demand for major through movements. Their results show that the proposed approach reduces intersection delay by 51.5%, 63.8%, and 20.6% compared to Webster's signal control, first-come-first-serve, and longest-queue-first based logics, respectively. Yao et al. (2023) have proposed a two-stage optimization model to optimize the schedule and trajectory of CAVs at an isolated autonomous intersection. Their methodology assigns vehicle arrival times at the intersection in the first stage while the second stage optimizes the vehicle trajectories based on the assigned arrival times. They tested their methodology on an isolated four-legged intersection with demand levels as high as 1200 $veh/h/lane$ for through movements. The proposed two-stage methodology could reduce vehicle delay and fuel consumption by up to 89.48% and 46.84%, compared to a first-come-first-serve method. Deng et al. (2023) have developed a vehicle-platoon-aware bi-level optimization algorithm for autonomous intersection management to coordinate the merging of CAVs at unsignalized intersections. Their algorithm is embedded into a rolling horizon framework to balance the computational and operational efficiencies. The upper level of their algorithm consists of a platoon formation scheme and a scheduling model to find an optimal schedule from systematic perspective. Note that the passing sequence and timeslots of vehicles are jointly optimized with the platoon formation scheme. The lower level generates a set of dynamically-feasible and energy-efficient trajectories to maximize space utilization and prevent spillbacks. They have tested their algorithm on an isolated intersection with arrival flow rates of 720 $veh/h/lane$ – 3600 $veh/h/lane$ and compared it with FIFO-, polling-, and scheduling-based methods. Their proposed algorithm could outperform their benchmark methodologies by up to 24.2% and 34.6% in terms of makespan and maximum delay, respectively. In addition, their case study results show the effectiveness of the proposed cooperative platoon formation scheme in avoiding and reducing spillbacks in undersaturated and saturated traffic states.

2.3. Trajectory optimization at signal-head-free intersections in a mixed traffic environment

As discussed in the previous section, removing signal heads in addition to finding the optimal trajectories of CAVs has shown promising results in improving the traffic operations. However, the signal-free intersections mostly assume 100% compliance rate considering fully-automated environments. Adding a new signal indication to traditional signalized intersections and/or operating the human-driven vehicles (HVs) in a platoon led by CAVs are suggested in a few studies to provide conditions similar to signal-free intersections even under lower CAV penetration rates. Rey and Levin (2018) have introduced a new policy for operating intersections under mixed traffic conditions. They have separated CAVs and legacy vehicles (i.e., HVs) by a dedicated lane for CAVs and proposed a CAV-only signal, a.k.a. “blue phase,” to the existing signal phases. Both CAVs and HVs may enter the intersection during the green signal, however, the blue indication is only designed to operate CAVs, during which, CAVs are controlled to prevent collisions between conflicting vehicles. The blue phase results on a case study network of 25 intersections has shown an improvement over optimized conventional signalized intersections with at least 60% CAV market penetration. However, including CAV-dedicated lanes can dramatically decrease the capacity of intersections when CAV penetration rate is low. Furthermore, stopping all movements to operate CAVs will require a high CAV market penetration rate to outperform existing traffic control systems.

Qian et al. (2014) have developed a priority-based coordination framework to accommodate HVs at an intersection while preventing collisions between conflicting vehicles. In the proposed framework, each vehicle needs to send a request to the intersection manager once they enter the coordination area. The HVs are assumed to be detected by sensors; a virtual request will be sent to the intersection manager after the detection. In this study, the intersection manager prioritizes CAVs in such a way that maximizes their speed in the intersection. An HV can enter the conflicting area in the intersection if (i) it has the highest priority among vehicles behind the conflicting area or (ii) it is assigned to a virtual platoon led by a CAV. Their numerical experiments show improvements in the intersection operations when the CAV penetration rate increases. However, the solutions provided in this study are sub-optimal in high traffic volumes due to the priority-based logic. In addition, incorporating HVs in long platoons reduces the efficiency of the proposed intersection control.

2.4. Summary of the literature

The existing literature mostly focuses on joint signal and trajectory optimization for isolated intersections. They mostly fail to provide solutions in real-time or consider simplifying assumptions, low demand levels, or simplified intersection layouts. Therefore, there is a need for a methodology that solves the joint signal and trajectory optimization problem in real-time for isolated intersections. In addition, proper coordination among intersections of a network can further improve the efficiency of the networks. The coordination process is normally an iterative process that requires the intersection signal and trajectory problem to be solved multiple times within a short period of time to maintain real-time applicability. Hence, a desirable intersection-level joint signal and trajectory optimization framework needs to be efficient enough for that purpose. However, literature fails to address this research gap.

In addition, the existing studies stop vehicles behind the intersection stop line to preserve safety even with a fully CAV fleet. Therefore, they either require a fully CAV fleet to use a signal free intersection control logic or use red and green signal indication and stop vehicles behind a red light for safety purposes. However, it is possible to use CAVs as mobile controllers and preserve the safety of the shared fleet using both signal heads and CAVs as mobile controllers. This can help operate intersections similar to a signal free intersection within a mixed-autonomy environment.

CHAPTER 3: JOINT OPTIMIZATION OF VEHICLE-GROUP TRAJECTORY AND SIGNAL TIMING: INTRODUCING THE WHITE PHASE FOR MIXED-AUTONOMY STREAM

This chapter aims to optimize the trajectory of vehicles through intersections using two control mechanisms: (i) traffic lights as stationary controllers and (ii) CAVs as mobile controllers. A central methodology, formulated as a mixed-integer non-linear program (MINLP), determines the optimal signal indications and continuously optimizes the trajectory of CAVs throughout the study period. The methodology will include a new white phase during which, CHVs must follow their immediate front vehicle (either CAV or another CHV) within a vehicle-group. Each vehicle-group is led by a CAV during the white phase. The trajectory of CHVs is integrated into the MINLP via a customized linear car-following model based on Helly (1959). Our customized car-following model accounts for all signal timing variables, including all indications. The proposed MINLP minimizes total travel time of all vehicles at the intersection subject to vehicle dynamics constraints that update all vehicles' states based on the optimal acceleration rates, constraints that prevent collisions between vehicle-groups during the white signal indication, and signal timing constraints. Our hypothesis is that these two control mechanisms can provide safe and efficient vehicle movements through intersections under various CAV market penetration rates and outperform optimized fully-actuated signal control systems. The proposed MINLP formulation includes non-linear terms and a large number of binary decision variables. We linearize the non-linear constraints and incorporate them into a receding horizon framework to tackle the complexities. This framework observes the state of the system at each time step, optimizes the decision variables over a prediction horizon, implements the optimal control decisions in the next time step, and continues this process over the entire study period.

3.1. Research gaps and contributions

Traditional signal control strategies limit the performance of signalized intersections. Signal-free control logics are proposed to utilize the control lost times towards more efficient traffic operations. The existing literature, yet, mostly addresses fully-automated environments. This chapter utilizes a new "white" signal indication to control CHVs led by CAVs (see Figure 3-1). We believe that optimizing the trajectory of sufficiently-penetrated CAVs in the traffic stream leads to promising traffic operations and safety results as CHV groups are to fully follow the CAV leaders, during the white signal, to avoid conflicts. A mathematical formulation is developed to guarantee optimal signal phases and timing plans that utilizes the highest capacity of the intersection under various CAV penetration rates. In contrast with previous studies, the proposed problem formulation works under all CAV penetration rates and is not restricted to assumptions such as splitting CAVs and other vehicle types or operating under priority-based logics.

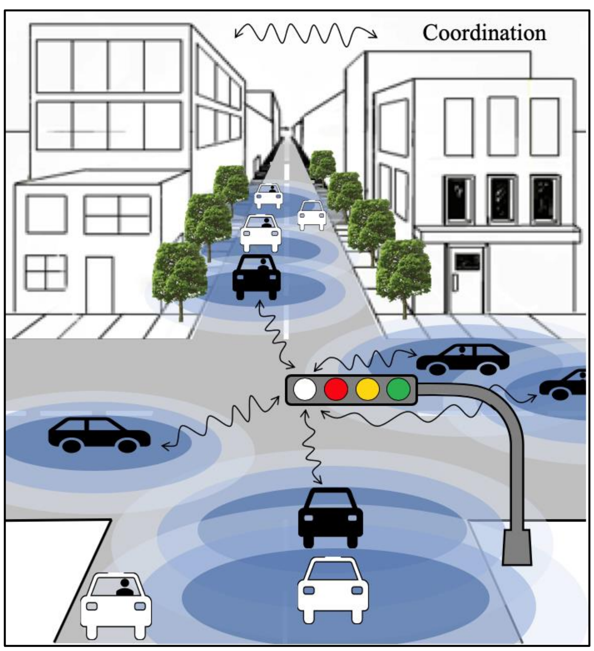

Figure 3-1: Coordination among CAVs, CHVs, and intersection controller.

3.2. Problem formulation

This section introduces a mathematical program to operate intersections in a mixed-autonomy traffic stream, considering both CAVs and CHVs. We assume all vehicles are connected and their speed and location (a.k.a. state) can be obtained in real-time to optimize signal timing plans. Moreover, the trajectory of CAVs are optimized to safely control the movement of all vehicles via the addition of the white signal phase. Decision variables in this study are vehicle acceleration rates and traffic light status for signal timing (i.e., green and white). The sets, parameters, decision variables, and other variables used to formulate the problem are listed in Table 3-1. Furthermore, Figure 3-2 illustrates some defined variables and parameters in the layout of an isolated intersection.

Table 3-1: The sets, parameters, variables, and decision variables used in the problem formulation.

Sets	
L	Set of all lanes
T	Set of all time steps for trajectory updates
$\hat{T}$	Set of all time steps for signal timing updates
I_l	Set of all vehicles on lane $l \in L$
$I_l{}'$	Set of all CAVs on lane $l \in L$
$\hat{I}_l$	Set of all CHVs on lane $l \in L$
C_l	Set of all conflicting lanes with lane $l \in L$
P_l	Set of vehicle-groups on lane $l \in L$
Decision Variables	
a_{il}^t	Acceleration of vehicle $i \in I_l$ on lane $l \in L$ at time $t \in T$
g_l^n	Binary decision variable; 1 if signal for lane $l \in L$ at time step $n \in \hat{T}$ is green, 0 otherwise
w_l^n	Binary decision variable; 1 if signal for lane $l \in L$ at time step $n \in \hat{T}$ is white, 0 otherwise
Other Variables	
x_{il}^t	The location of vehicle $i \in I_l$ on lane $l \in L$ at time $t \in T$
v_{il}^t	The speed of vehicle $i \in I_l$ on lane $l \in L$ at time $t \in T$
γ_{il}^t	1 if vehicle $i \in I_l$on lane $l \in L$ has passed intersection by $t \in T$ or 0 otherwise.
h_{ql}^t	The head location of vehicle-group $q \in P_l$ on lane $l \in L$ at time $t \in T$
e_{ql}^t	The tail location of vehicle-group $q \in P_l$ on lane $l \in L$ at time $t \in T$
ζ_{ql}^t	The length of vehicle-group $q \in P_l$ on lane $l \in L$ at time $t \in T$

Table 3-1 (continued)

${a'}_{il}^{t}$ and d_{il}^{t}	Auxiliary variables for vehicle $i \in I_l$ on lane $l \in L$ at time $t \in T$
${\varphi^{+}}_{jl}^{tk}, {\varphi^{-}}_{jl}^{tk}, {\phi^{+}}_{jl}^{tk}, {\phi^{-}}_{jl}^{tk}$, ϑ_{jl}^{tk}, and θ_{jl}^{tk}	Auxiliary variables for vehicle group $k \in P_j$ on lanes $j \in L$ and $l \in C_j$ at time $t \in T$
Parameters	
$\underline{a}$ and $\overline{a}$	Lower and upper bounds for acceleration
$\underline{v}$ and $\overline{v}$	Minimum and maximum speeds
L_v	Vehicle length
D	Minimum safety distance between two consecutive vehicles on the same lane
S	Minimum safety distance between vehicles and the intersection stop bar
ρ	Minimum safety distance between vehicle-groups of conflicting lanes
$\hat{\tau}$	Reaction time for CHVs
τ'	Reaction time for CAVs
F_{ij}	The location of conflict point between lane $i \in L$ and lane $j \in L$ based on the coordination of lane i
b_l	The position of intersection in lane $l \in L$
$\underline{G}$ and $\overline{G}$	Minimum and maximum green time
ΔT	Time step size for trajectory updates
$\Delta \hat{T}$	Time step size for signal updates
r_l	The destination location of vehicles on lane $l \in L$
α_1 and α_2	Car-following parameters
AR	Duration of all-red time
ξ_{ql}	The order of the first vehicle of vehicle-group $q \in P_l$ on lane $l \in L$
μ_{ql}	The order of the last vehicle of vehicle-group $q \in P_l$ on lane $l \in L$

3.2.1. Objective function

The proposed problem aims to minimize the distance between the vehicle's location and its pre-defined destination (shown with a green arrow in Figure 3-2) for the entire study period. Note that vehicles will be out of the system after they reach the pre-defined destinations.

$$Z = \min \sum_{t \in T} \sum_{l \in L} \sum_{i \in I_l} (r_l - x_{il}^{t}) \tag{3.1}$$

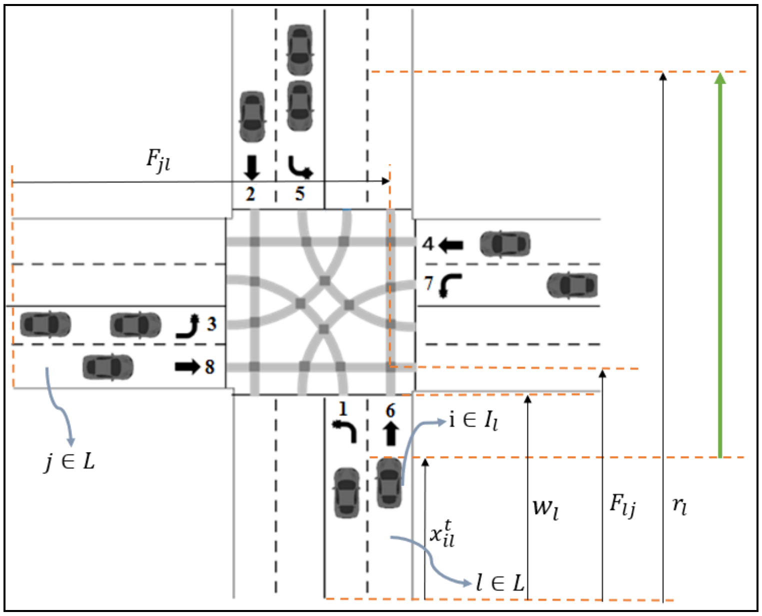

Figure 3-2: An isolated intersection layout including conflict regions and movement notations.

3.2.2. Constraints

We divide the constraints into three categories: (i) vehicle dynamics constraints, (ii) vehicle-group constraints, and (iii) signal timing constraints.

3.2.2.1. Vehicle dynamic constraints

We include car-following model for CHVs and trajectory constraints for CAVs in this category. We update the speed and location of all vehicles based on the optimal acceleration rates, as follows.

$$x_{il}^{t+\Delta T} = x_{il}^{t} + v_{il}^{t}\Delta T + \frac{1}{2}a_{il}^{t}\Delta T^2, \qquad \forall i \in I_l, l \in L, t \in T, \quad (3.2)$$

$$v_{il}^{t+\Delta T} = v_{il}^{t} + a_{il}^{t}\Delta T, \qquad \forall i \in I_l, l \in L, t \in T. \quad (3.3)$$

Optimizing the trajectory of CAVs requires a relatively accurate prediction of future state of CHVs. A linear car-following model, developed by Helly (1959), predicts CHVs' trajectories; i.e., drivers react to both speed difference and distance to vehicle immediately in front of them.

The following constraints show the predicted acceleration rate of CHVs based on the Helly model. The first term presents the difference of speeds between a CHV and its preceding vehicle, while the second term indicates the distance between each CHV and its preceding vehicle excluding a fixed safety distance and driver's reaction time multiplied by the speed of that CHV. The parameters $\alpha_1, \alpha_2 > 0$ are suggested to take values from [0.17, 1.3] and $[\frac{1}{4}\alpha_1, \frac{1}{2}\alpha_1]$, respectively (Askari et al., 2016; Brackstone and McDonald, 1999).

$$a_{il}^t = \alpha_1\left(v_{il}^t - v_{i-1,l}^t\right) + \alpha_2\left((x_{il}^t - x_{i-1,l}^t - L_v) - D - v_{il}^t\hat{\tau}\right), \quad \forall i \in \hat{I}_l, l \in L, t \in T. \quad (3.4)$$

The car-following model is adjusted to react to the traffic light status when a CHV approaches the intersection. We consider a red signal as a virtual preceding vehicle with the speed of zero located at the intersection stop bar. When the signal light turns green or white, the virtual vehicle's speed will be considered as the maximum speed. In addition, the location of the virtual vehicle will be changed to a far distance. The following constraints define the connection between a CHV and a signal light in the car-following model, where binary variable γ_{il}^t for vehicle $i \in I_l$ on lane $l \in L$ at time $t \in T$ relaxes the connection between vehicles and signal light when vehicles pass the intersection stop bar. Relaxing the connection is necessary to ensure that vehicles do not react to the signal indicators after they pass the intersection stop bar.

$$a'^{t}_{il} = \alpha_1\Big((w_l^n + g_l^n)\overline{v} - v_{il}^t\Big) + \alpha_2\Big((Mb_l(w_l^n + g_l^n) + b_l - x_{il}^t) - (1 - w_l^n - g_l^n)S\Big) + M\gamma_{il}^t$$

$$\forall i \in \hat{I}_l, l \in L, t \in T, n \in \hat{T} \quad (3.5)$$

$$\gamma_{il}^t = \begin{cases} 0 & \text{if } x_{il}^t \le b_l \\ 1 & \text{O.W. (intersection stop bar is passed)} \end{cases} \quad \forall i \in I_l, l \in L, t \in T \quad (3.6)$$

We define two updating time intervals, i.e., ΔT and $\Delta\hat{T}$, to (i) update the trajectory of vehicles and (ii) change the status of signal timing variables, respectively. Vehicle trajectories are updated more frequently, i.e., $\Delta\hat{T} > \Delta T$, to capture the uncertainty in driver behavior and prevent any mismatch between vehicles' predicted and actual states. Since the proposed formulation includes both trajectory-related and signal timing variables, we connect the two time indices, as follows.

$$n = \left\lfloor \frac{\Delta T}{\Delta \hat{T}} t \right\rfloor, \qquad \forall t \in T, n \in \hat{T}. \tag{3.7}$$

We re-formulate the linear car-following model as a max-min function to (i) bind the speed and acceleration of CHVs and (ii) account for various situations including cruising with maximum speed in free-flow conditions, following other vehicles, and approaching stationary/non-stationary vehicles and red signal lights, as follows.

$$a_{il}^t = \max \left\{ \underline{a}, \frac{\underline{v} - v_{il}^t}{\Delta T}, \min \left\{ \begin{array}{c} \overline{a}, \\ \frac{\overline{v} - v_{il}^t}{\Delta T}, \\ \alpha_1 \left(v_{il}^t - v_{i-1,l}^t \right) + \alpha_2 \left((x_{il}^t - x_{i-1,l}^t - L_v) - D - v_{il}^t \hat{\tau} \right), \\ \alpha_1 \left((w_l^n + g_l^n) \overline{v} - v_{il}^t \right) + \alpha_2 \left((b_l - x_{il}^t) - (1 - w_l^n - g_l^n) S \right) + M \gamma_{il}^t, \end{array} \right\} \right\}$$

$$\forall i \in \hat{I}_l, l \in L, t \in T, n \in \hat{T} \tag{3.8}$$

Constraints (3.8) define the CHV acceleration rates as the maximum of three terms: (i) minimum acceleration rate, (ii) acceleration rate leading to minimum speed, and (iii) minimum of maximum acceleration rate, acceleration rate leading to maximum speed, and acceleration rate leading to a safe distance from the preceding vehicle (or intersection stop bar in red-signal conditions) based on the relative speed and distance from the preceding vehicle.

The proposed formulation optimizes CAVs' trajectories when they approach the intersection. We impose upper and lower bounds on the CAVs' accelerations and speeds. Besides, we ensure a safe distance between each CAV and its preceding vehicle as a function of pre-defined safe distance D, vehicle length L_v, and distance traveled during the reaction time $\tau' v_{il}^t$, as follows.

$$\underline{a} \leq a_{il}^{t} \leq \overline{a}, \qquad \forall i \in I_l', l \in L, t \in T, \quad (3.9)$$

$$\underline{v} \leq v_{il}^{t} \leq \overline{v}, \qquad \forall i \in I_l', l \in L, t \in T, \quad (3.10)$$

$$x_{i-1,l}^{t} - x_{il}^{t} \geq D + L_v + \tau' v_{il}^{t}, \qquad \forall i \in I_l', l \in L, t \in T. \quad (3.11)$$

To prevent CAVs from entering the intersection during the red signal, CAV's distance to the stop bar shall exceed safety distance S and CAV's distance traveled during time step ΔT. Note that constraints (3.12) will not be activated for (i) green or white signal indications or (ii) CAVs that have already passed the intersection stop bar before the beginning of time $t \in T$.

$$b_l - x_{il}^{t} \geq S + \Delta T v_{il}^{t} - (g_l^n + w_l^n)M - \gamma_{il}^{t} M, \qquad \forall i \in I_l', l \in L, t \in T, n \in \hat{T}. \quad (3.12)$$

We define a CHV vehicle-group led by a CAV to safely pass the intersection during white phases, as follows. To enforce a set of constraints that connect vehicle-level and vehicle-group-level variables, we define the vehicle-group's head location h_{ql}^{t}, tail location e_{ql}^{t}, and length ζ_{ql}^{t}, as shown in Figure 3-3. Besides, ξ_{ql} and μ_{ql} respectively denote the order of first and last vehicles in the vehicle-group $q \in P_l$ on lane $l \in L$. Hence, the location of each vehicle-group's head is captured by the location of the first vehicle in that vehicle-group. Similarly, the location of each vehicle-group's tail is obtained by the location of the last vehicle in that vehicle-group, excluding its length L_v. Finally, the length of each vehicle-group (i.e., ζ_{ql}^{t} that incorporates at least one vehicle's length) is calculated based on it's head and tail locations, i.e., h_{ql}^{t} and e_{ql}^{t}, respectively.

$$h_{ql}^{t} = x_{\xi_{ql} l}^{t}, \qquad \forall\, q \in P_l, l \in L, t \in T, \quad (3.13)$$

$$\mathrm{e}_{ql}^{t} = x_{\mu_{ql} l}^{t} - L_v, \qquad \forall\, q \in P_l, l \in L, t \in T, \quad (3.14)$$

$$\zeta_{ql}^{t} = h_{ql}^{t} - e_{ql}^{t}, \qquad \forall\, q \in P_l, l \in L, t \in T. \quad (3.15)$$

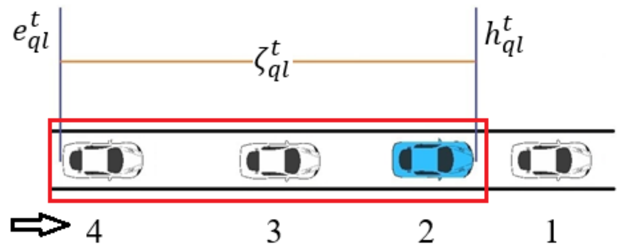

Figure 3-3: Head location, tail location, and the length of vehicle-groups.

Let F_{jl} denote the location of conflict point between lanes $j \in L$ and $l \in C_j$, from lane j. Similarly, we define F_{lj} as the location of conflict point between lanes j and l, from lane l. We define five scenarios with their associated safety constraints and remedial actions, based on the position of each pair of conflicting vehicle-groups in the intersection zone, as shown in Figure 3-4.

(i) The first scenario, shown in Figure 3-4 (a), indicates that none of the two vehicle-groups has reached to the conflicting point, therefore the total distance of both vehicle-groups' head locations to the conflicting points F_{lj} and F_{jl} shall be greater than the safety distance ρ to prevent collision.

(ii) The second scenario, shown in Figure 3-4 (b), indicates a case where the leader passes the conflicting point but not the remainder of the vehicle-group $p \in P_l$. The distance between head location of vehicle-group $q \in P_j$ and conflicting point F_{jl} shall exceed the safety distance.

(iii) Figure 3-4 (c) shows the third scenario, where the last vehicle of vehicle-group p passes the conflict point. In this case, total distance of vehicle-group p's tail location to the conflicting point F_{lj} and vehicle-group q's head location to the conflicting point F_{jl} shall exceed the safety distance ρ.

(iv) In Figure 3-4 (d), the fourth scenario, vehicle-group q's leader passes the conflicting point but not the following vehicle. Therefore, the distance between the tail location of vehicle-group p and the conflicting point F_{lj} shall exceed ρ.

(v) The fifth scenario, illustrated in Figure 3-4 (e), details the case where the following vehicles of both vehicle-groups pass the conflicting point. Hence, the total distance of both vehicle-groups' tail locations to the conflicting points F_{lj} and F_{jl} shall exceed ρ to ensure safety.

The following constraints incorporate the aforementioned scenarios to ensure safety of vehicle-groups in conflicting lanes $j, l \in L$.

$$\left|h_{kj}^{t} - F_{jl}\right| + \left|e_{kj}^{t} - F_{jl}\right| + \left|h_{ql}^{t} - F_{lj}\right| + \left|e_{ql}^{t} - F_{lj}\right| \geq \zeta_{kj}^{t} + \zeta_{ql}^{t} + 2\rho + M\left(w_{l}^{n} + w_{j}^{n} - 2\right)$$

$$\forall k \in P_j, j \in L, q \in P_l, l \in C_j, t \in T, n \in \hat{T} \quad (3.16)$$

where the left-hand side of constraints (3.16) respectively presents the distances from the head and tail of vehicle-group $k \in P_j$ to conflict point F_{jl} in the first two terms, i.e., $\left|h_{kj}^{t} - F_{jl}\right| + \left|e_{kj}^{t} - F_{jl}\right|$. Similarly, the third and fourth terms respectively denote the distances from the head and tail of vehicle-group $q \in P_l$ to conflict point F_{lj}, i.e., $\left|h_{ql}^{t} - F_{lj}\right| + \left|e_{ql}^{t} - F_{lj}\right|$.

The constraints ensure safety between conflicting vehicle-groups $k \in P_j$ and $q \in P_l$ if total distances, i.e., the left-hand side, exceeds 2ρ when both conflicting movements receive the white signal; otherwise (in case of non-white status), there is no need to hold the safety distance between two conflicting vehicle-groups, which reflects the reason to add $M(w_l^n + w_j^n - 2)$ to the constraints. In other words, when each intersection lane receives traditional red or green signal, the safety will be maintained through signal timing constraints, not the CAV control strategy.

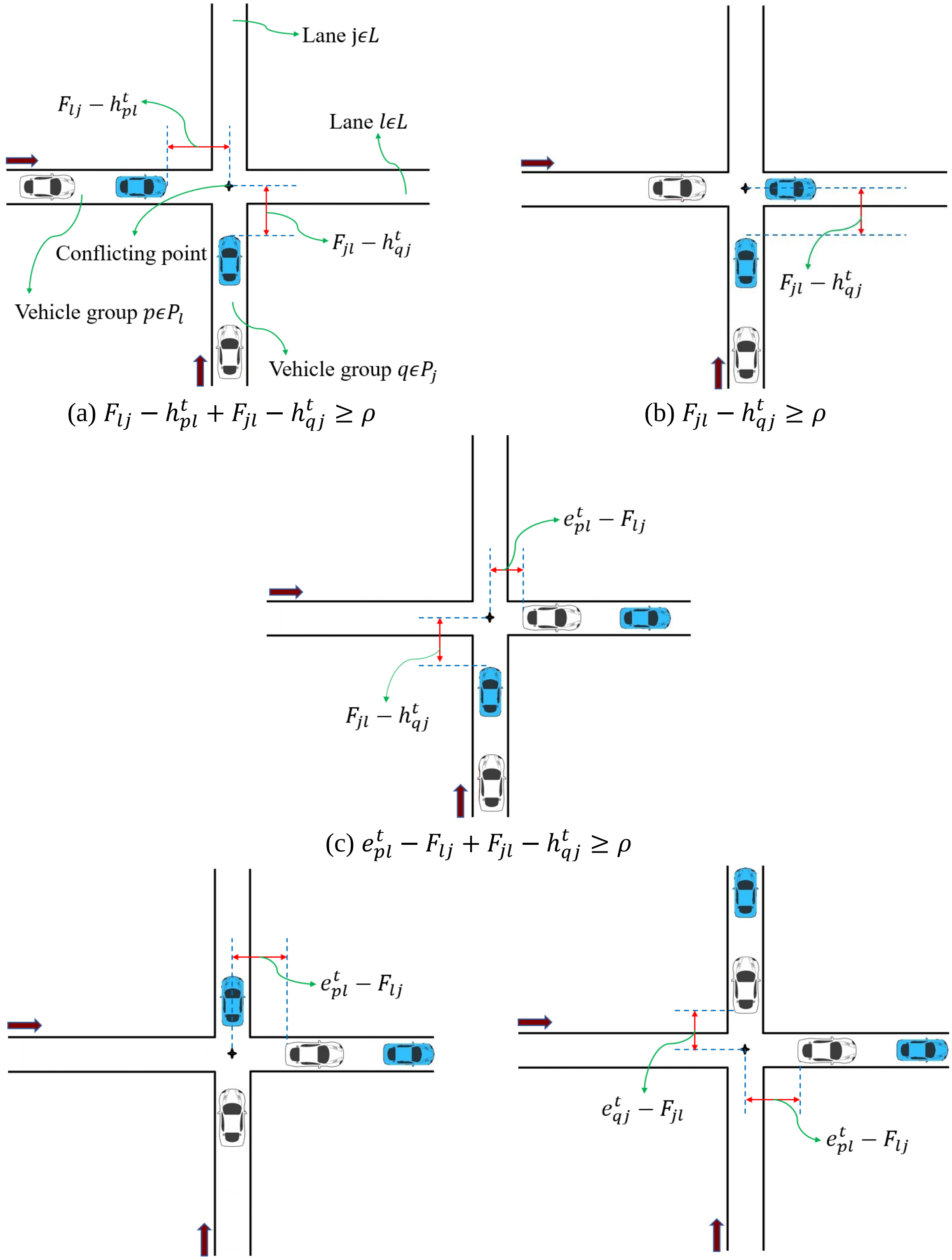

(a) $F_{lj} - h_{pl}^{t} + F_{jl} - h_{qj}^{t} \geq \rho$ (b) $F_{jl} - h_{qj}^{t} \geq \rho$

(c) $e_{pl}^{t} - F_{lj} + F_{jl} - h_{qj}^{t} \geq \rho$

(d) $e_{pl}^{t} - F_{lj} \geq \rho$ (e) $e_{pl}^{t} - F_{lj} + e_{qj}^{t} - F_{jl} \geq \rho$

Figure 3-4: Possible scenarios for the interaction of two vehicle-groups in conflicting lanes.

We assume that signal timing plans are cycle- and phase-free. Since constraints (3.16) are only valid when the signal status for both conflicting movements is white, we prevent green status for a lane-group when its conflicting lane-group receives either green or white indication, as follows.

$$g_l^n + g_{l'}^n + w_{l'}^n \leq 1, \qquad \forall l \in L, l' \in C_l, n \in \hat{T}, \tag{3.17}$$

where $\boldsymbol{w}$ and $\boldsymbol{g}$ denote binary variables indicating white and green signals. Note that red signal status is activated when both green and white variables are zero.

Furthermore, we ensure that a lane-group will not receive a green status longer than the maximum green time. We also impose a lower bound on the green time for each lane-group.

$$\sum_{z=n}^{n+\overline{G}} g_l^z \leq \overline{G}, \qquad \forall l \in L, n \in \hat{T}, \tag{3.18}$$

$$\sum_{z=n+1}^{n+\underline{G}} g_l^z \geq (g_l^{n+1} - g_l^n)\underline{G}, \qquad \forall l \in L\,, n \in \hat{T}. \tag{3.19}$$

The following constraints impose all-red indication after green and white phases to ensure vehicles have cleared the intersection before switching the signal to active movements.

$$\sum_{z=n}^{n+AR-1}(g_l^z + g_{l'}^z + w_l^z + w_{l'}^z) - 2ARg_l^n + 2ARg_l^{n-1} \leq 2AR, \qquad \forall l \in L, l' \in C_l, n \in \hat{T}, \tag{3.20}$$

$$\sum_{z=n}^{n+AR-1}(g_l^z + g_{l'}^z + w_l^z + w_{l'}^z) - 2ARg_l^n - 2ARw_l^n + 2ARw_l^{n-1} \leq 2AR, \qquad \forall l \in L, l' \in C_l, n \in \hat{T}. \tag{3.21}$$

Note that vehicle-groups are led by CAVs and can only be operated during the white phase. Therefore, constraints (3.22) initiate white phases only when the first vehicle behind the intersection stop bar is a CAV, not a CHV; otherwise, a traditional signal (i.e., green) controls the movements. Note that the intersection controller can continue the white signal even if the first vehicle behind the stop bar is a CHV. As it is shown in Figure 3-5, the term $\gamma_{i-1,l}^{t} - \gamma_{il}^{t}$ for vehicle $i \in \hat{I}_l$ is equal to 1 if it is the first vehicle behind the intersection stop bar on lane $l \in L$ at time $t \in T$. In addition, the term w_l^{n-1} is added to the right-hand-side of the constraints to let the intersection controller select white indication at time n if the signal status for time $n-1$ has been white, even if the first vehicle behind the stop bar is not a CAV.

$$w_l^n \leq 1 - \left(\gamma_{i-1,l}^{t} - \gamma_{il}^{t}\right) + w_l^{n-1} \qquad \forall i \in \hat{I}_l, l \in L, n \in \hat{T}, t \in T \quad (3.22)$$

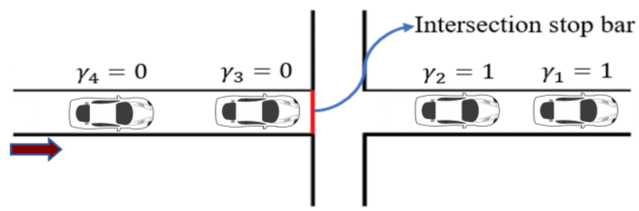

Figure 3-5: The relative location of vehicles in reference to the intersection stop bar.

3.3. Methodology

The proposed MINLP in (3.1)-(3.3), (3.6), and (3.8)-(3.22), described in Section 3.2, is interactable due to non-linear terms and large number of binary decision variables. This section introduces a methodology including a (i) linearization strategy and (ii) receding horizon control approach to reduce the complexities and solve the problem efficiently (Al Islam and Hajbabaie, 2017; Mohebifard et al., 2019).

3.3.1. Linearization

Constraints (3.6) identify the location of vehicle $i \in I_l$ on lane $l \in L$ at time $t \in T$, i.e., before or after the intersection stop bar, which are non-linear. We re-write the constraints in the following linear forms.

$$x_{il}^t - b_l \leq M\gamma_{il}^t, \qquad \forall i \in I_l, l \in L, t \in T, \tag{3.23}$$

$$x_{il}^t - b_l \geq M(\gamma_{il}^t - 1), \qquad \forall i \in I_l, l \in L, t \in T, \tag{3.24}$$

where $\gamma_{il}^t = 0$ is enforced when vehicle $i \in I_l$ is located before the intersection stop bar, i.e., constraints (3.23), or $\gamma_{il}^t = 1$ otherwise, i.e., constraints (3.24).

In addition, car-following constraints (3.8) are non-linear due to the presence of the max-min function. We introduce an auxiliary variable $d_{il}^t \in R^n$ to linearize the min and max functions of the constraints separately. Note that d_{il}^t has the same unit as the acceleration variable.

$$d_{il}^t \leq \overline{a}, \qquad \forall i \in \hat{I}_l, l \in L, t \in T, \tag{3.25}$$

$$d_{il}^t \leq \frac{\overline{v} - v_{il}^t}{\Delta T}, \qquad \forall i \in \hat{I}_l, l \in L, t \in T, \tag{3.26}$$

$$d_{il}^t \leq \alpha_1\left(v_{il}^t - v_{i-1,l}^t\right) + \alpha_2\left((x_{il}^t - x_{i-1,l}^t - L_v) - D - v_{il}^t\hat{\tau}\right), \qquad \forall i \in \hat{I}_l, l \in L, t \in T, \tag{3.27}$$

$$d_{il}^t \leq \alpha_1\left(\left(w_l^n + g_l^n\right)\overline{v} - v_{il}^t\right) + \alpha_2\left((b_l - x_{il}^t) - \left(1 - w_l^n - g_l^n\right)S\right) + M\gamma_{il}^t, \qquad \forall i \in \hat{I}_l, l \in L, t \in T, n \in \hat{T}, \tag{3.28}$$

$$a_{il}^t \geq d_{il}^t, \qquad \forall i \in \hat{I}_l, l \in L, t \in T, \tag{3.29}$$

$$a_{il}^t \geq \frac{\underline{v} - v_{il}^t}{\Delta T}, \qquad \forall i \in \hat{I}_l, l \in L, t \in T, \tag{3.30}$$

$$a_{il}^t \geq \underline{a}, \qquad \forall i \in \hat{I}_l, l \in L, t \in T. \tag{3.31}$$

Although car-following model (3.8) is linearized with inequality constraints (3.25)-(3.31), its linearized form is not equivalent to the original car-following model since the acceleration variable is free to take any value within the inequality bounds. Thus, we penalize the term $a_{il}^t - d_{il}^t \geq 0$ with a big coefficient in the objective function to push the acceleration values in the linearized formulation towards the exact value of the car-following model (3.8). The objective function is updated as shown below.

$$Z = \min_{\boldsymbol{a},\boldsymbol{g},\boldsymbol{w}} \sum_{t\in T} \sum_{l\in L} \sum_{i\in I_l} ((r_l - x_{il}^t) + M(a_{il}^t - d_{il}^t)) \tag{3.32}$$

Constraints (3.16) are also non-linear due to the presence of four absolute value functions. We linearize the constraints through the definition of two non-negative auxiliary variables $\boldsymbol{\varphi}$ and $\boldsymbol{\phi}$, associated with the absolute value functions of the head and tail of each vehicle-group, as presented below.

$$h_{kj}^t - F_{jl} = {\varphi^+}_{jl}^{tk} - {\varphi^-}_{jl}^{tk}, \qquad \forall k \in P_j, j \in L, l \in C_j, t \in T, \tag{3.33}$$

$${\varphi^+}_{jl}^{tk} \leq M\vartheta_{jl}^{tk}, \qquad \forall k \in P_j, j \in L, l \in C_j, t \in T, \tag{3.34}$$

$${\varphi^-}_{jl}^{tk} \leq M\left(1 - \vartheta_{jl}^{tk}\right), \qquad \forall k \in P_j, j \in L, l \in C_j, t \in T, \tag{3.35}$$

$$e_{kj}^t - F_{jl} = {\phi^+}_{jl}^{tk} - {\phi^-}_{jl}^{tk}, \qquad \forall k \in P_j, j \in L, l \in C_j, t \in T, \tag{3.36}$$

$${\phi^+}_{jl}^{tk} \leq M\theta_{jl}^{tk}, \qquad \forall k \in P_j, j \in L, l \in C_j, t \in T, \tag{3.37}$$

$${\phi^-}_{jl}^{tk} \leq M\left(1 - \theta_{jl}^{tk}\right), \qquad \forall k \in P_j, j \in L, l \in C_j, t \in T, \tag{3.38}$$

$$\vartheta_{jl}^{tk}, \theta_{jl}^{tk} \epsilon \{0, 1\}, \qquad \forall k \in P_j, j \in L, l \in C_j, t \in T, \tag{3.39}$$

$${\varphi^+}_{jl}^{tk}, {\varphi^-}_{jl}^{tk}, {\phi^+}_{jl}^{tk}, {\phi^-}_{jl}^{tk} \geq 0, \qquad \forall k \in P_j, j \in L, l \in C_j, t \in T. \tag{3.40}$$

As constraints (3.33) indicate, the difference between the head of vehicle-group $k \in P_j$ at lane $j \in L$ and the conflicting point with lane $l \in C_j$ is equal to the difference of auxiliary variables ${\varphi^+}_{jl}^{tk}$ and ${\varphi^-}_{jl}^{tk}$. Hence, we linearize the absolute value function by enforcing one of the auxiliary variables to take the value of zero in constraints (3.34) and (3.35) using the binary variable ϑ_{jl}^{tk}

and big-M method. Note that the absolute value term will be ${\varphi^+}_{jl}^{tk} + {\varphi^-}_{jl}^{tk}$ if either of the auxiliary variables is zero. The same approach is used to linearize the absolute value functions regarding the distance from the tail of vehicle-groups to the conflicting point through constraints (3.36)-(3.38).

Finally, we rewrite non-linear constraints (3.16) with a linearized form by replacing each of the absolute value functions with the summation of corresponding non-negative auxiliary variables, as follows.

$$
\begin{aligned}
&{\varphi^+}_{jl}^{tk} + {\varphi^-}_{jl}^{tk} + {\phi^+}_{jl}^{tk} + {\phi^-}_{jl}^{tk} + {\varphi^+}_{lj}^{tq} + {\varphi^-}_{lj}^{tq} + {\phi^+}_{lj}^{tq} + {\phi^-}_{lj}^{tq} \geq \zeta_{kj}^t + \zeta_{ql}^t + 2\rho + \\
&M\left(w_l^n + w_j^n - 2\right), \\
&\forall k \in P_j, j \in L, l \in C_j, q \in P_l, t \in T, n \in \hat{T} \qquad (3.41)
\end{aligned}
$$

3.3.2. Receding horizon framework

The proposed MINLP is embedded in a receding horizon control scheme with a finite planning horizon $\hat{N}$. The proposed receding horizon control represents a similar framework to model predictive control (e.g., Mehrabipour and Hajbabaie (2017) and Mohebifard and Hajbabaie (2018)). The initial states are defined as the (i) current vehicle $i \in I_l$'s location $x_{il}^{t_0}$ and speed $v_{il}^{t_0}$ on lane $l \in L$ at time $t_0 \in T$ and (ii) current signal status, i.e., green $g_l^{n_0}$ or white $w_l^{n_0}$, on lane $l \in L$ at time $n_0 \in \hat{T}$. Due to different updating intervals for signal timing and trajectory decisions, the algorithm solves either joint signal and trajectory optimization or only the trajectory optimization with input signal timing parameters over the planning horizon $\hat{N}$. In the joint signal timing and trajectory optimization problem, we find the optimal signal parameters including green and white times during time $n \in [n_0, n_0 + \hat{N}/\Delta\hat{T}]$ based on the current and predicted states of CAVs and

CHVs. In addition, the optimal trajectory of CAVs are found during time $t \in [t_0, t_0 + \hat{N}/\Delta T]$. If only trajectory optimization problem is solved, the signal timing parameters are considered as inputs during time $n \in [n_0, n_0 + \hat{N}/\Delta\hat{T}]$ and only trajectory of CAVs are optimized for $\hat{N}/\Delta T$ trajectory time steps. Note that the future trajectory of CHVs are estimated by the proposed car-following model (3.8).

After solving the optimization problem, actions for the first time step will be implemented. Particularly, the acceleration a_{il}^{t} at time step $t_0 + 1$ will be applied to control the movement of vehicle $i \in I_l$ on lane $l \in L$. Furthermore, the signal indicators w_l^n and g_l^n at time step $n_0 + 1$ on lane $l \in L$ will be implemented into the simulation by a signal controller. After updating the states of all vehicles including CAVs and CHVs at time $t_0 + 1$, we repeat the process again to find the optimal signal and trajectory parameters at time $n \in [n_0 + 1, n_0 + 1 + \hat{N}/\Delta\hat{T}]$ and $t \in [t_0 + 1, t_0 + 1 + \hat{N}/\Delta T]$, respectively. The process continues until the study period is over. Figure 3-6 shows the description of the algorithm in details.

3.4. Numerical results

This section first introduces the case study dataset and then presents the numerical results including the sensitivity of the solutions with respect to various CAV penetration rates. The proposed methodology is coded in JAVA and run on a desktop computer with a quad core 3.6 GHz CPU and 24 GB memory. CPLEX 12.6 (CPLEX, 2014) is used to solve the optimization problem. We have also implemented the developed program in Vissim microscopic traffic simulator (PTV Group, 2015) to measure the mobility performance of the solutions obtained from the proposed program. The Vissim Component Object Model (COM) interface is used to exchange the required information between CAVs and signal controller.

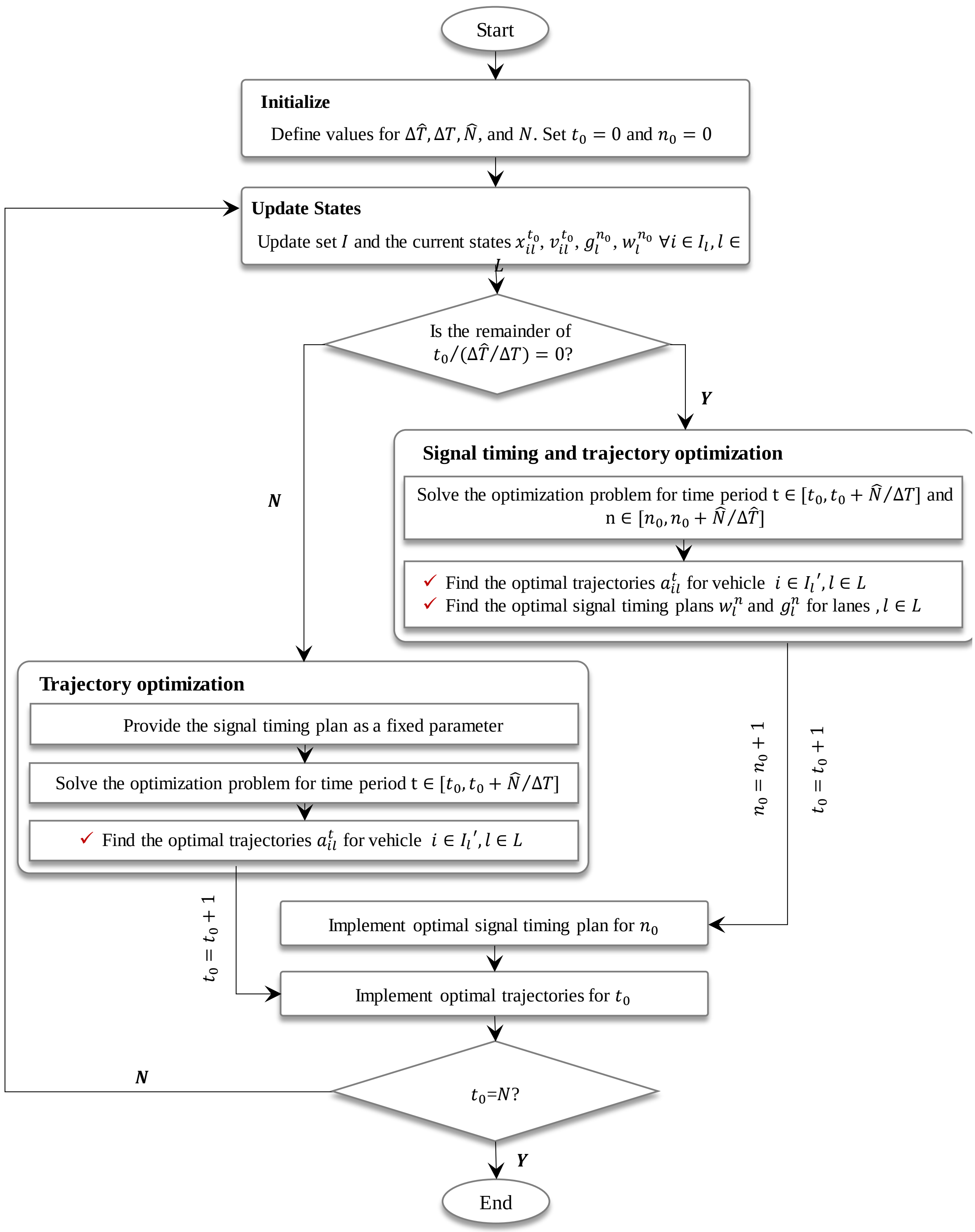

Figure 3-6: Receding horizon general framework.

3.4.1. Case study

We have applied the proposed models (3.1)-(3.22) and solution technique to an isolated four-leg intersection adapted from downtown Springfield, Illinois (Hajbabaie and Benekohal, 2015, 2013) with exclusive through and left-turn lanes. The intersection geometry is shown in Figure 3-2. It is assumed that vehicles are already on their desired lane prior to their arrival to the intersection neighborhood. The communication range between vehicles and infrastructure is set to 200 m, which is within the standard 300 m dedicated short-range communications (DSRC) range. The maximum speed for all vehicles is assumed to be 13 $\mathrm{m/s}$. We update the trajectory of vehicles every $\Delta T = 0.5$ s to frequently capture the dynamic changes in traffic stream and prevent collisions between vehicles during the white phase. Since the signal timing plans in this study are cycle-free, we stabilize the optimal signal timing decisions and prevent frequent changes by updating signal status every two seconds (i.e., $\Delta\hat{T} = 2$ s). In addition, we assume values for the minimum and maximum timings of different signal phases. Table 3-2 provides the details regarding the parameters used in the case study.

The problem is solved for a 5 minute-study period considering three demand patterns, as shown in Table 3-3. Demand for through movements in levels 1 to 3 are 300, 600, and 900 ($\mathrm{veh/h/lane}$), respectively. Demand for turning movements is 8% of the through demand. Eight different CAV market penetration rates are considered for each demand level, ranging from low (0% and 10%), medium (30%, 50%, and 70%), to high (80%, 90%, and 100%), to capture the effects of CAVs on the intersection performance measures.

Table 3-2: Value of the parameters used in the case study.

Parameters	Value
Maximum speed (m/s)	13
Maximum acceleration (m/s^2)	4
Minimum acceleration (m/s^2)	-3.5
Human driver reaction time (s)	1
Automated vehicle reaction time (s)	0.1
Detection range (m)	200
Intersection location (m)	200
Average length of vehicles (m)	4
Safety distance between consecutive vehicles (m)	3.6
Safety distance between CAVs and red signal light (m)	0.3
Safety distance between vehicle-groups of conflicting lane-groups (m)	12.5
Car-following parameter α_1 (s^{-1})	0.95
Car-following parameter α_2 (s^{-2})	0.25
Trajectory updating interval (s)	0.5
Signal status updating interval (s)	2
All red time (s)	2
Minimum green time for through movements (s)	8
Minimum green time for left-turning movements (s)	4
Minimum white time for through movements (s)	6
Maximum green time for through and left-turning movements (s)	60
Planning time horizon (s)	20
Study period (s)	300

Table 3-3: Demand patterns for case studies.

Demand level	Through demand ($veh/h/lane$)	Left-turn demand ($veh/h/lane$)
1	300	24
2	600	48
3	900	72

3.4.2. Results

This section summarizes the mobility and safety performance of the proposed methodology.

3.4.2.1. Mobility

Table 3-4 compares the total delay between the optimized fully-actuated signal timing plan in Vistro (PTV Group, 2015) and the proposed signal timing and trajectory optimization problem with eight levels of CAV penetration rate. The results show that solving the proposed problem with various CAV penetration rates reduces the intersection total delay between 19.6% and 96.2% compared to the optimized fully-actuated signal timing plan from Vistro. Increasing the penetration rates yields more improvements in terms of the intersection delay; two contributing factors include:

(i) CAVs can be operated more efficiently since they adjust their speed to pass the intersection possibly with maximum speed and

(ii) the white phase has a higher chance to get activated in a higher penetration rate of CAVs. As a result, vehicles can join as a vehicle-group and safely pass the intersection during the white phase. As shown in Table 3-4, the reduction in total delay is more significant with 80% CAVs in the traffic stream since the white phase is active more often.

It shall be noted that the traffic volume is very low in demand level 1; thus, the distance between vehicles is long and there is no benefit to operate multiple vehicles in one vehicle group. Therefore, there is no significant difference, in total delay reduction, between various CAV penetration rates of 0%-80% in demand level 1.

Table 3-4: Total delay for three demand levels with different CAV market penetration rates.

Demand level	Fully-actuated signal	Optimal performance with various CAV market penetration rates							
		0%	10%	30%	50%	70%	80%	90%	100%
1	684.4	270.9 (-60.4%)	266.4 (-61.1%)	228.3 (-66.6%)	204.3 (-70.2%)	191.6 (-72.0%)	170.8 (-75.0%)	89.6 (-86.9%)	78.2 (-88.6%)
2	3070.4	2468.8 (-19.6%)	2184.0 (-28.9%)	2000.1 (-34.9%)	1363.2 (-55.6%)	1057.0 (-65.6%)	871.7 (-71.6%)	488.8 (-84.1%)	173.2 (-94.4%)
3	6959.7	4701.6 (-32.4%)	4504.4 (-35.3%)	3510.3 (-49.6%)	2986.1 (-57.1%)	2100.0 (-69.8%)	1136.3 (-83.7%)	1096.9 (-84.2%)	267.1 (-96.2%)

0Figure 3-7 shows the average delay of each vehicle type for different CAV penetration rates in demand level 3. The average delay for CHVs is always higher than CAVs due to their higher reaction time. Another reason is that CHVs' acceleration depends on their relative speed and distance to the preceding vehicle, while CAVs only need to keep a safe distance with their preceding vehicle. Increasing the penetration rate of CAVs decreases the average delay for both types of vehicles. However, the reduction rate is more significant after 70% CAV penetration rate due to activation of white phases. In addition, the difference between average delays of CAVs and CHVs is minimum after 70% CAV penetration rate since CHVs can pass the intersection in vehicle-groups during the white phase.

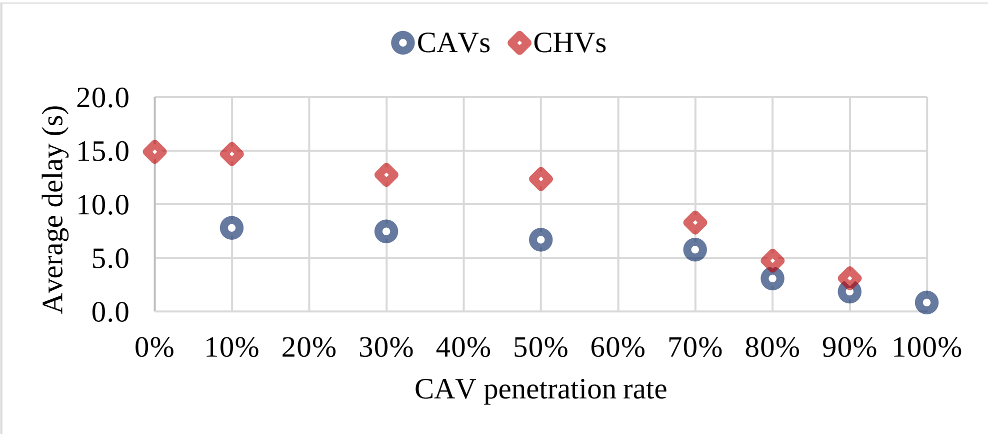

Figure 3-7: Average delay for CAVs and CHVs for demand level 3 with different CAV market penetration rates.

Figure 3-8 shows signal timing plans over time for different approaches of the intersection under six different CAV market penetration rates in demand level 3. Intersection management through white phase activation requires high CAV penetration rates to effectively control CHVs. In other words, when CAV market penetration rate increases, so does the possibility of activating the white phase. As indicated in Figure 3-8, the proposed problem formulation starts giving simultaneous white phases to the conflicting lanes after increasing the CAV penetration rates to 50%. Moreover, the white phase turns out to be the dominant signal status when at least 80% of vehicles are CAVs.

Figure 3-9 shows the trajectory of CAVs and CHVs on Lane 6 (see Figure 3-2) for different CAV penetration rates based on demand level 3. The solid red and blue lines show the trajectory of CHVs and CAVs, respectively. As indicated, vehicles move smoother and fewer vehicles stop when CAV market penetration rate increases. Moreover, vehicles tend to speed up towards the intersection during the white phase to ensure they enter the intersection at their maximum speed to reduce their travel time and exposure to other vehicles.

3.4.2.2. Safety

We have analyzed possible collisions that may occur during different phases of signal timing plans. Crossing and rear-end crashes are considered using the surrogate safety assessment model (SSAM) software (Gettman and Head, 2003). The time to collision (TTC) is considered as the surrogate safety measure. The result of the analysis indicates that there is no near-crash condition for both crossing and rear-end conflicts (assuming a 1.5 s TTC threshold) in different demand levels and various CAV market penetration rates. Figure 3-10 shows the range of rear-end TTC for all rear-end conflicts under TTC threshold of 10 s for different CAV penetration rates with demand level 3. The median of TTC decreases from 0% to 50% CAV market penetration rate and increases afterward. This could be due to the presence of CAVs with a short reaction time in safety constraints (3.11). In addition, the inter-quartile dispersion of TTC increases from 0% to 80% CAV market penetration rate. This could be due to the interactions between CAVs and CHVs in a mixed-autonomy environment. The inter-quartile dispersion of TTC is minimum at extreme points, where all vehicles are either CHV or CAV since less interactions between these two vehicle types exist. No crossing near crash conditions was reported by SSAM, as it does not report any near crash conditions, whose TTC is more than 10 s.

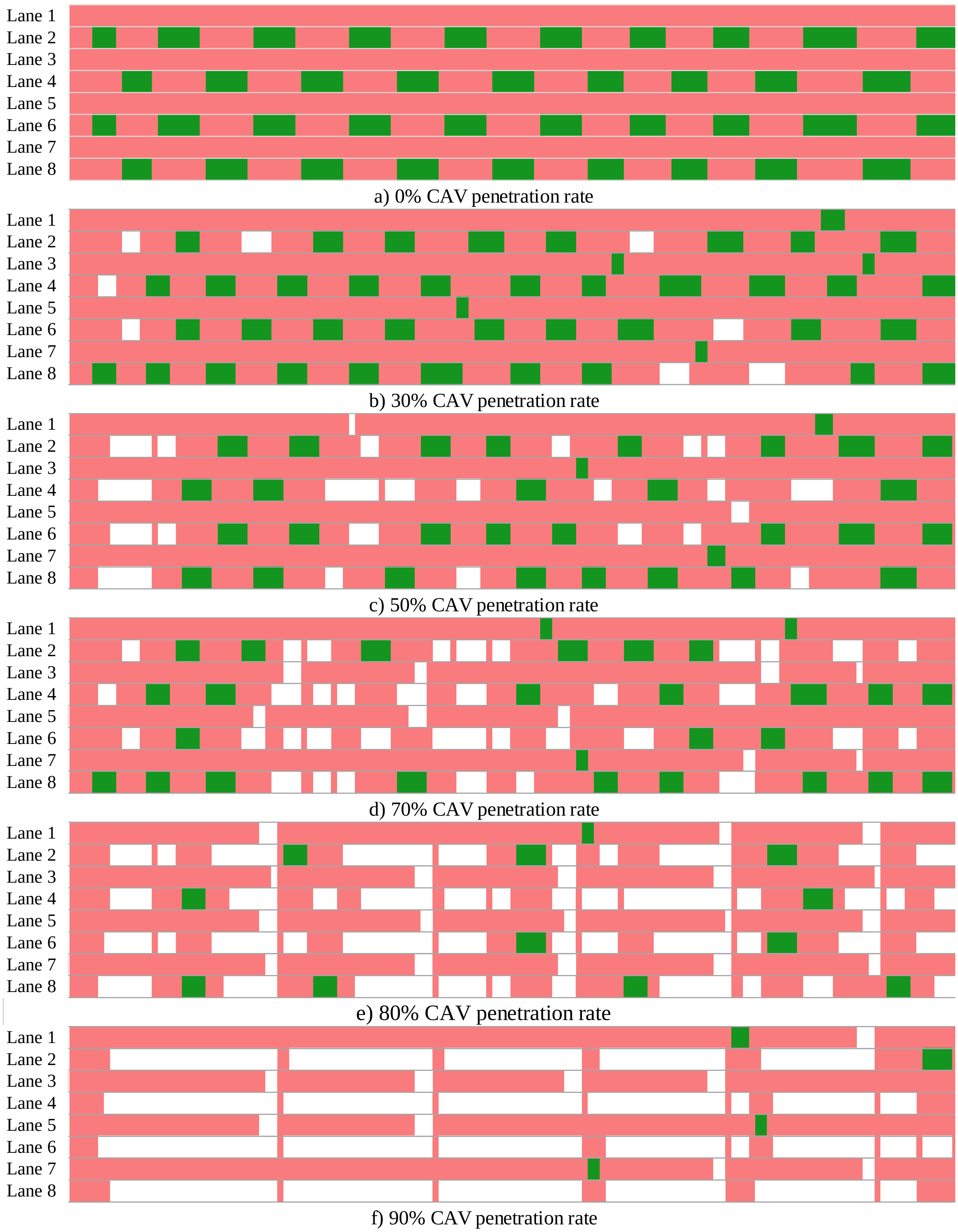

Figure 3-8: Signal timing plans for demand level 3 with different CAV market penetration rates.

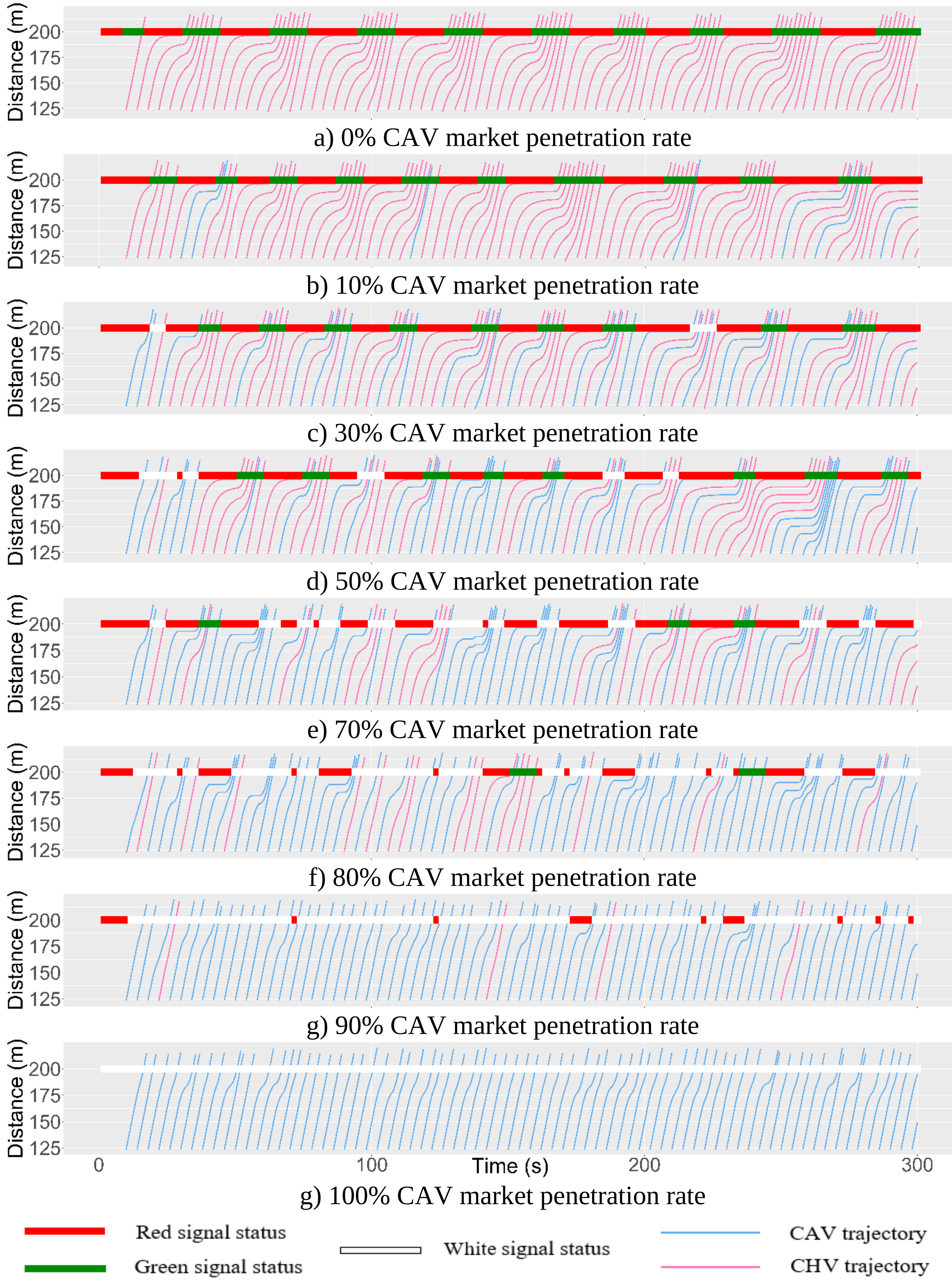

Figure 3-9: Trajectories of vehicles in lane 6 for demand level 3 with different CAV penetration rates.

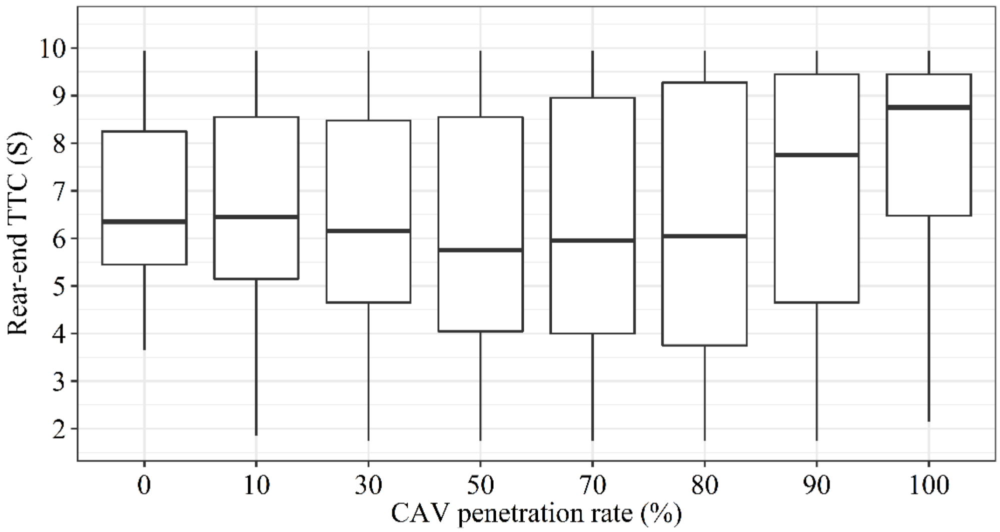

Figure 3-10: Rear-end time to collision for demand level 3 with different CAV market penetration rates.

3.4.2.3. Complexity

Table 3-5 summarizes the computational performance of the proposed approach for three demand levels. The table shows the number of continuous and binary variables, number of constraints, and solution time for each optimization over the planning horizon. The number of variables and constraints are mostly increased as the CAV market penetration rate increases for all demand levels. The solution time, however, increases up to 90% CAV market penetration rate and decreases from 90% to 100% due to (i) less congestion in the intersection neighborhood since CAVs will be processed at a higher rate during white phase, and (ii) no need for changing signal phases, which makes the optimization problem less complex. Note that the reduction of solution time from 90% to 100% CAV market penetration rate is more significant in higher demand levels.

Table 3-5: Complexity parameters for three demand levels with different CAV penetration rates.

Demand level	Parameter	CAV market penetration rates							
		0%	10%	30%	50%	70%	80%	90%	100%
1	# C. V.	1850	4254	7118	6943	14699	13381	15620	15620
	# B. V.	639	1779	3079	2999	6532	5949	6985	6985
	# Cons.	9252	8903	10192	10185	12822	11785	12290	12290
	Run time (ms)	8818	7591	8947	9129	9019	9588	10572	10477
2	# C. V.	3684	6037	10951	15356	27165	26298	28299	31634
	# B. V.	1097	2193	4427	6465	11919	11510	12434	13965
	# Cons.	22504	22584	24585	25319	26562	26985	26949	27836
	Run time (ms)	9084	9117	9101	9392	11600	11412	11508	11464
3	# C. V.	5675	10108	12847	28682	39302	44298	46940	49354
	# B. V.	1595	3621	4883	12122	17069	19374	20586	21689
	# Cons.	17391	32811	47105	53558	52425	53199	54126	55330
	Run time (ms)	10315	10649	10822	11034	13380	67684	115063	60930

C. V.: Number of continuous variables

B. V.: Number of binary variables

Cons.: Number of constraints

3.5. Conclusion

This chapter introduces a novel MINLP to jointly optimize the trajectories of CAVs and signal timings in a mixed CAV and CHV environment. The movements of CHVs are estimated using a customized linear car-following model. A new white indication is added to the conventional signal phases, where CHVs follow their immediate front vehicle and CAVs play the leader role in the vehicle-groups. The proposed formulation ensures safe movements through the intersection, avoiding any collision in conflicting movements. A hybrid technique is employed that include (i) linearization of non-linear constraints and (ii) utilization of a receding horizon approach to tackle the complexities and effectively solve the proposed MINLP. We have applied the proposed methodology to an isolated intersection with eight movements under eight levels of CAV market penetration rate. The results indicate that the solution technique successfully solves the problem and reduces total delay by 19.6%-96.2% compared to fully-actuated signal control. The results further indicate that the white signal status will become the dominant signal indication after the CAV market penetration rate of 80%.

CHAPTER 4: WHITE PHASE INTERSECTION CONTROL THROUGH DISTRIBUTED COORDINATION: A MOBILE CONTROLLER PARADIGM IN A MIXED TRAFFIC STREAM

This chapter first modifies the white phase formulation presented in Chapter 3 to increase the possibility of activation of simultaneous white phases for conflicting movements that can lead to reduction in intersection total delay. Then, presents a vehicle-level distributed coordination strategy that leverages the computational power of each vehicle to address the real-time and scalability requirements of intersection traffic control. Therefore, intersections with more realistic layouts and higher traffic demand levels can be addressed. Each CAV receives the planned trajectory of other CAVs and the estimated trajectory of all CHVs to optimize its own trajectory. To ensure solution feasibility and moving toward system-level optimality, CAVs form agreement on their trajectories. The trajectory of each CHV is estimated using a customized car-following model. Additionally, all vehicles vote on signal timing parameters (i.e., white, green, or red) for all intersection movements based on their planned/estimated trajectories and form an agreement on signal indications to be displayed on signal heads. The vehicles' mixed-integer non-linear programs (MINLPs) are linearized and embedded into a receding horizon control to capture the dynamic nature of signal and trajectory optimizations. The proposed distributed methodology iteratively solves the problem to reach agreement on both signal indications and trajectory plans.

4.1. Research gaps and contributions

Current studies either (1) lead to reductions in intersection capacity at low CAV market penetration rates, (2) must stop vehicles behind the intersection stop bar even with 100% CAVs, and (3) do not scale well with the size of the problem. This chapter enhances the white phase formulation proposed in Chapter 3 to increase the possibility of the white phase activation and develops a vehicle-level agreement-based distributed methodology to solve it. To this end, we assumed that all vehicles are connected and have computational power to solve a simple vehicle-level optimization program. We hypothesize that the approach improves intersection capacity at low CAV market shares, reduces the need to use red phases, and finds solutions in real-time. Each CAV solves an MINLP to plan for its safe passage through the intersection and proposes a signal timing plan for the entire intersection movements. In addition, CHVs estimate their trajectories using a customized car-following model and participate in the voting process by solving an optimization problem with trajectory and signal timing variables. Unlike existing studies, this framework uses the available computational power of vehicles and solves the signal timing and trajectory optimization problem in a distributed manner. Therefore, the framework scales well with the size of the problem and can produce real-time solutions to be implemented in the real world.

4.2. Problem formulation

This section introduces a distributed MINLP for a vehicle-level intersection control with a mixed fleet of CAVs and CHVs. The program aims to jointly optimize the (i) signal timing plan of each intersection and (ii) trajectory of each CAV using shared vehicle states (i.e., vehicle locations and speeds over a planning horizon) in the intersection neighborhood. Furthermore, CHVs are assumed to follow the vehicle immediately in front of them and react to signal indications. Note that each vehicle-level program optimizes/estimates the trajectory of a single vehicle and the solutions for vehicle-level programs do not provide the system-level optimal solutions. Therefore, section 4.3 introduces a coordination scheme where the system-level solutions are achieved by solving vehicle-level optimization programs and coordination via information exchange.

The spatial and temporal elements of the problem are defined as follows. We let T and $\hat{T}$ respectively denote the sets of discrete time steps for making trajectory and signal timing decisions (similar to Niroumand et al. (2020)). Traffic in the intersection is defined by $\mathcal{H}(L, I)$, where L denotes the set of all lanes in the intersection neighborhood and I represents the set of all vehicles. Additionally, $I_l \subset I$ defines the set of all vehicles on lane $l \in L$, where I_l' and $\hat{I}_l$ represent CAVs and CHVs on lane l, respectively. We define C_l as a set of all lanes in conflict with lane $l \in L$ and use P_l to represent the set of all vehicle-groups on lane $l \in L$.

We define two state variables: x_{il}^t represents the location of vehicle $i \in I_l$ on lane $l \in L$ at time $t \in T$ and v_{il}^t denotes the speed of vehicle $i \in I_l$ on lane $l \in L$ at time $t \in T$. State variable x_{il}^t identifies vehicles who pass the intersection stop bar using binary variable γ_{il}^t, where $\gamma_{il}^t = 0$ if $x_{il}^t \leq b$ or 1 otherwise (the intersection stop bar is passed) for all $i \in I_l, t \in T$. We let decision variable a_{il}^t denote the acceleration rate of vehicle $i \in I_l$ on lane $l \in L$ at time $t \in T$. We estimate the movements of CHVs with a given set of signal timing parameters using a customized linear car-following model (Helly, 1959; Niroumand et al., 2020a):

$$a_{il}^t = \max \left\{ \underline{a}, \frac{\underline{v} - v_{il}^t}{\Delta T}, \min \left\{ \begin{array}{c} \overline{a}, \\ \frac{\overline{v} - v_{il}^t}{\Delta T}, \\ \alpha_1 \left(v_{il}^t - v_{i-1,l}^t \right) + \alpha_2 \left((x_{il}^t - x_{i-1,l}^t - L_v) - D - v_{il}^t \hat{\tau} \right), \\ \alpha_1 \left((w_l^n + g_l^n) \overline{v} - v_{il}^t \right) + \alpha_2 \left((b_l - x_{il}^t) - (1 - w_l^n - g_l^n) S \right) + M \gamma_{il}^t, \end{array} \right\} \right\}$$

$$\forall i \in \hat{I}_l, l \in L, t \in T, n \in \hat{T} \tag{4.1}$$

where $M\gamma_{il}^t$ eliminates the connection between signal and vehicles when they pass the intersection stop bar.

We also define decision variables $g_l^n = \{0,1\}$ and $w_l^n = \{0,1\}$ to represent the green and white signal timing decisions for all $l \in L$ and $n \in \hat{T}$, respectively. Table 4-1 defines the remaining variables and parameters used in the proposed formulation. Figure 4-1 shows some defined notations in the layout of an isolated intersection.

Table 4-1: Notations used in the proposed formulation.

Sets	
L	Set of all lanes
T	Set of all time steps for trajectory decisions
$\hat{T}$	Set of all time steps for signal timing decisions
I_l	Set of all vehicles on lane $l \in L$
I_l'	Set of all CAVs on lane $l \in L$
$\hat{I}_l$	Set of all CHVs on lane $l \in L$
C_l	Set of all conflicting lanes with lane $l \in L$
P_l	Set of vehicle-groups on lane $l \in L$
Decision Variables	
a_{il}^t	Acceleration of vehicle $i \in I_l$ on lane $l \in L$ at time $t \in T$
g_l^n	Binary green signal status; 1 if signal for lane $l \in L$ at time $n \in \hat{T}$ is green or 0 otherwise
w_l^n	Binary white signal status; 1 if signal for lane $l \in L$ at time $n \in \hat{T}$ is white or 0 otherwise
y_l^n	Binary white signal status; 1 if signal for lane $l \in L$ at time $n \in \hat{T}$ is yellow or 0 otherwise
Variables	
x_{il}^t	The location of vehicle $i \in I_l$ on lane $l \in L$ at time $t \in T$
v_{il}^t	The speed of vehicle $i \in I_l$ on lane $l \in L$ at time $t \in T$
γ_{il}^t	1 if vehicle $i \in I_l$ on lane $l \in L$ has passed intersection by $t \in T$ or 0 otherwise
h_{ql}^t	The head location of vehicle-group $q \in P_l$ on lane $l \in L$ at time $t \in T$
e_{ql}^t	The tail location of vehicle-group $q \in P_l$ on lane $l \in L$ at time $t \in T$
ζ_{ql}^t	The length of vehicle-group $q \in P_l$ on lane $l \in L$ at time $t \in T$
Parameters	
$\underline{a}, \overline{a}$	Lower and upper bounds for acceleration
$\underline{v}, \overline{v}$	Minimum and maximum speeds
$\mathcal{L}$	Fixed vehicle length
D	Minimum safety distance between two consecutive vehicles on the same lane
S	Minimum distance between vehicles and the intersection stop bar
ρ	Minimum safety distance between vehicle-groups of conflicting lanes
$\hat{\tau}$	Reaction time for CHVs
τ'	Reaction time for CAVs
$F_{kk'}$	The location of conflict point between lane $k \in L$ and lane $k' \in C_k$ based on the coordination of lane k
b	The location of intersection (i.e., the distance of intersection *stop* bar from origin)
$\overline{G}$	Maximum green time
$\underline{G}$	Minimum active time (green plus subsequent white phase)
$\underline{W}$	Minimum white time
Y	Yellow time duration
ΔT	Time step size for trajectory decisions
$\Delta \hat{T}$	Time step size for signal decisions
r_l	The destination location of vehicles on lane $l \in L$
α_1, α_2	Car-following parameters

Table 4-1 (continued).

$\mathcal{R}$	Duration of all-red time
ξ_{ql}	The order of the first vehicle of vehicle-group $q \in P_l$ on lane $l \in L$
μ_{ql}	The order of the last vehicle of vehicle-group $q \in P_l$ on lane $l \in L$
β_{il}^{t}	1 if vehicle $i \in I_l$ on lane $l \in L$ is a member of a vehicle-group or 0 otherwise
$\hat{\gamma}_{jl}^{t}$	Shared input parameter: 1 if vehicle $j \in I_l$ on lane $l \in L$ has passed intersection by $t \in T$ or 0 otherwise
$\hat{x}_{jl}^{t}$	Location of vehicle $j \in I_l$ on lane $l \in L$ as shared input parameter
$\hat{g}_{ljk}^{n}$	Green signal indications on lane $l \in L$ at time $n \in \hat{T}$ voted by vehicle $j \in I_l$ on lane $k \in L$
$\widehat{w}_{ljk}^{n}$	White signal indications on lane $l \in L$ at time $n \in \hat{T}$ voted by vehicle $j \in I_l$ on lane $k \in L$
$\mathcal{T}$	Iteration counter for agreement process
$\bar{\zeta}$	The maximum length of vehicle-groups

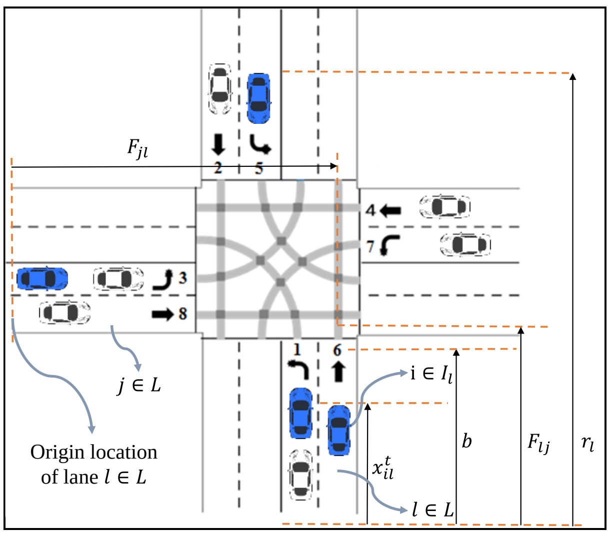

Figure 4-1: An isolated intersection layout including some of the notations

The problem formulation follows. The objective is to minimize the distance between the location of human-driven vehicle $i \in \hat{I}_l$ (or automated vehicle $i \in I_l'$) and its pre-defined destination. A term $\omega|v_{il}^{t+1} - v_{il}^{t}|$ is added to the objective function Z_{il}' of CAVs to minimize the speed variation of vehicle $i \in I_l'$ for driving comfort purposes. Parameter ω is the speed-location conversion factor.

$$\hat{Z}_{il} = \min_{\boldsymbol{a},\boldsymbol{g},\boldsymbol{w}} \sum_{t \in T} (r_l - x_{il}^{t}), \qquad \forall i \in \hat{I}_l, l \in L, \qquad (4.2)$$

$$Z'_{il} = \min_{\boldsymbol{a},\boldsymbol{g},\boldsymbol{w}} \sum_{t\in T}(r_l - x_{il}^t) + \omega\left|v_{il}^{t+1} - v_{il}^t\right|, \qquad \forall i \in I'_l, l \in L. \tag{4.3}$$

Subject to (4.1) and:

$$x_{il}^{t+\Delta T} = x_{il}^t + v_{il}^t \Delta T + \frac{1}{2} a_{il}^t \Delta T^2 \qquad \forall i \in I_l, l \in L, t \in T \tag{4.4}$$

$$v_{il}^{t+\Delta T} = v_{il}^t + a_{il}^t \Delta T, \qquad \forall i \in I_l, l \in L, t \in T, \tag{4.5}$$

$$\underline{a} \le a_{il}^t \le \overline{a}, \qquad \forall i \in I'_l, l \in L, t \in T, \tag{4.6}$$

$$\underline{v} \le v_{il}^t \le \overline{v}, \qquad \forall i \in I'_l, l \in L, t \in T, \tag{4.7}$$

$$\hat{x}_{i-1,l}^t - x_{il}^t \ge D + \mathcal{L} + \tau' v_{il}^t, \qquad \forall i \in I'_l, l \in L, t \in T, \tag{4.8}$$

$$b - x_{il}^t \ge S + \Delta T v_{il}^t - (g_l^n + w_l^n)M - \gamma_{il}^t M \qquad \forall i \in I'_l, l \in L, t \in T, n \in \hat{T} \tag{4.9}$$

$$h_{qj}^t = \hat{x}_{\xi_{qj}j}^t \qquad \forall q \in P_j, j \in C_l, l \in L, t \in T \tag{4.10}$$

$$e_{qj}^t = \hat{x}_{\mu_{qj}j}^t - \mathcal{L} \qquad \forall q \in P_j, j \in C_l, l \in L, t \in T \tag{4.11}$$

$$\zeta_{qj}^t = h_{qj}^t - e_{qj}^t \qquad \forall q \in P_j, j \in C_l, l \in L, t \in T \tag{4.12}$$

$$\left|h_{qj}^t - F_{jl}\right| + \left|e_{qj}^t - F_{jl}\right| + \left|x_{il}^t - F_{lj}\right| + \left|x_{il}^t - \mathcal{L} - F_{lj}\right| \ge \zeta_{qj}^t + \mathcal{L} + 2\rho +$$

$$M(\gamma_{il}^t + \hat{\gamma}_{\xi_{qj}j}^t + w_l^n + w_j^n - 4) \tag{4.13}$$

$$\forall i \in I'_l, l \in L, q \in P_j, j \in C_l, t \in T, n \in \hat{T}$$

$$g_l^n + g_{l'}^n + w_{l'}^n \le 1 \qquad \forall l \in L, l' \in C_l, n \in \hat{T} \tag{4.14}$$

$$\sum_{z=n+1}^{n+\underline{G}} g_l^z + w_l^z \ge (g_l^{n+1} - g_l^n)\underline{G} \qquad \forall l \in L, n \in \hat{T} \tag{4.15}$$

$$\sum_{z=n+1}^{n+\underline{W}} w_l^z \ge (w_l^{n+1} - g_l^n - w_l^n)\underline{W} \qquad \forall l \in L, n \in \hat{T} \tag{4.16}$$

$$\sum_{z=n}^{n+\overline{G}} g_l^z \leq \overline{G}, \qquad \forall l \in L, n \in \hat{T}, \qquad (4.17)$$

$$\sum_{z=n}^{n+Y} y_l^z \leq Y, \qquad \forall l \in L, n \in \hat{T}, \qquad (4.18)$$

$$\sum_{z=n+1}^{n+Y} y_l^z \geq (g_l^n - g_l^{n+1} - w_l^{n+1})Y, \qquad \forall l \in L, n \in \hat{T} \qquad (4.19)$$

$$\sum_{z=n+1}^{n+Y} y_l^z \geq (w_l^n - w_l^{n+1} - g_l^{n+1})Y, \qquad \forall l \in L, n \in \hat{T} \qquad (4.20)$$

$$\sum_{z=n}^{n+\mathcal{R}-1}(g_l^z + g_{l'}^z + w_l^z + w_{l'}^z) - 2\mathcal{R}y_l^n + 2\mathcal{R}y_l^{n-1} \leq 2\mathcal{R} \qquad \forall l \in L, l' \in C_l, n \in \hat{T} \qquad (4.21)$$

$$\sum_{z=n}^{n+\mathcal{R}-1}(w_{l'}^z) - 2\mathcal{R}g_l^n + 2\mathcal{R}g_l^{n-1} \leq 2\mathcal{R} \qquad \forall l \in L, l' \in C_l, n \in \hat{T} \qquad (4.22)$$

$$w_l^n \leq 1 - \left(\hat{\gamma}_{j-1,l}^t - \hat{\gamma}_{jl}^t\right) + w_l^{n-1} \qquad \forall j \in \hat{I}_l, l \in L, n \in \hat{T}, t \in T \qquad (4.23)$$

$$w_l^n \leq 1 - \left(\hat{\gamma}_{j-1,l}^t - \hat{\gamma}_{jl}^t\right) + \beta_{jl}^t \qquad \forall j \in \hat{I}_l, l \in L, n \in \hat{T}, t \in T \qquad (4.24)$$

Constraints (4.4) and (4.5) define fundamental motion equations to update the location $x_{il}^{t+\Delta T}$ and speed $v_{il}^{t+\Delta T}$ of vehicle $i \in I_l$ at time $t + \Delta T$ based on acceleration rate a_{il}^t at time t. Constraints (4.6) and (4.7) ensure that CAVs are enforced to take their acceleration and speed within the threshold of pre-defined minimum and maximum values. Constraints (4.8) ensure the safety of vehicle $i \in I_l'$ on lane $l \in L$ at time $t \in T$ based on its distance from preceding vehicle $i - 1 \in I_l$, where D is a constant safety distance between two consecutive vehicles on the same lane, L_v is the vehicle length, and $\tau' v_{il}^t$ is the distance traveled by the CAV during reaction time τ', given the location of vehicle $i - 1 \in I_l$ on lane l at time t ($\hat{x}_{i-1,l}^t$) that is fed to the optimization program as an input parameter.

Constraints (4.9) will halt CAVs behind the intersection stop bar, keeping a distance S when the signal indication is red. Note that vehicles are allowed to enter the intersection conflicting area during green and white phases. Since the formulation uses discrete time steps, a vehicle can jump from one side of the intersection stop bar to the other side during one time step when the signal is red, therefore, we add the term $\Delta T v_{il}^{t}$ to prevent this jump. Besides, the term $-\gamma_{il}^{t} M$ ensures that CAVs who have already passed the intersection stop bar will not react to any signal indication. Note that S can be as small as zero. Constraints (4.10)-(4.12) define a group of CHVs led by a CAV as a vehicle-group that starts with the CAV and ends with the last CHV in the group, where h_{qj}^{t}, e_{qj}^{t}, and ζ_{qj}^{t} respectively denote the head location, tail location, and length of vehicle-group $q \in P_j$ on lane $j \in C_l$ at time $t \in T$. Each vehicle group starts with a CAV as the vehicle group leader and continues until it reaches the maximum predefined vehicle group length $\bar{\zeta}$ or the next CAV in that lane. For instance, vehicle 1 shown in Figure 4-2 is a vehicle group by itself since both the vehicle and its following vehicle are CAVs. The next vehicle group starts with vehicle 2 as the vehicle group leader and has vehicle 3 as its follower. The third vehicle group starts with vehicle 4 and has vehicle 5 as its follower, however, vehicle 6 is not a member of the third vehicle group since the third vehicle group has reached its maximum predefined length before reaching vehicle 6. Finally, vehicle 7 is a vehicle group by itself since it is a CAV and there is no vehicle after vehicle 7. These constraints aim to connect the vehicle-level variables (i.e., x_{il}^{t}) and vehicle-group-level variables (i.e., h_{qj}^{t}, e_{qj}^{t}, and ζ_{qj}^{t}). Constraints (4.13) enforce collision-free movements based on the topology of conflicting vehicle-groups in the intersection zone when the signal is white (Niroumand et al., 2020a). The additional term $M(\gamma_{il}^{t} + \hat{\gamma}_{\xi_{qj}j}^{t})$ relaxes the constraints when at least one of the vehicle-groups has not entered the conflicting area.

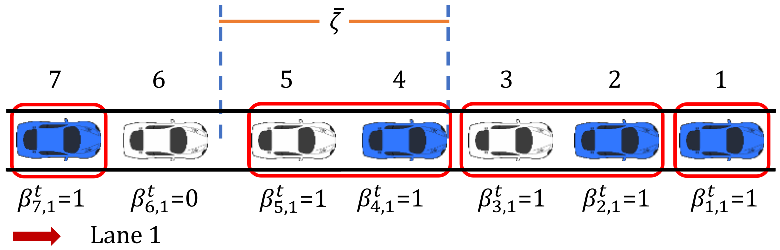

Figure 4-2: Vehicle group formation

Additionally, constraints (4.14) ensure that green-white and green-green signals will not activate simultaneously for conflicting lane-groups (see Figure 4-3). Note that white-white is safe for conflicting lane-groups. However, green and white signal indications can be used for non-conflicting movements simultaneously since they don't share any conflicting points.

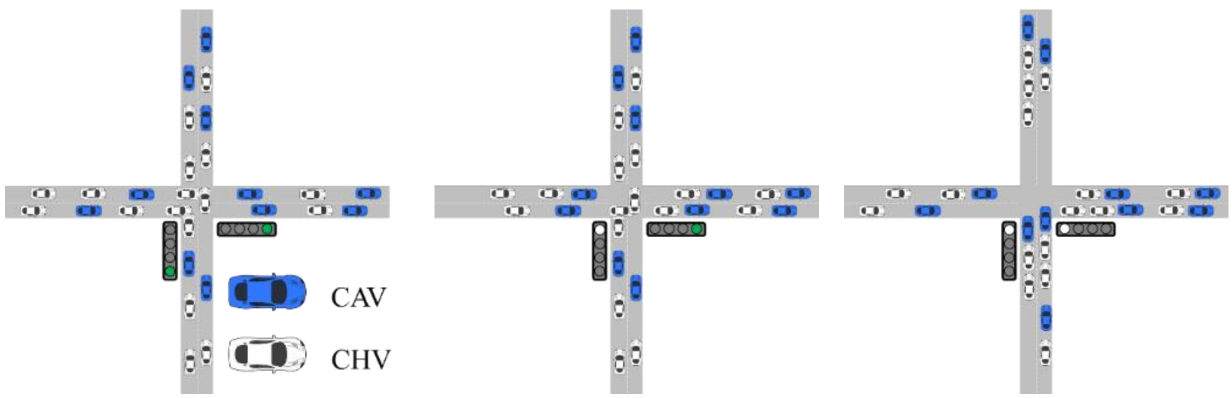

a) green-green ×
b) green-white ×
c) White-white √

Figure 4-3: Different signal combinations for conflicting lane groups

We introduced a set of constraints to impose a lower bound on the minimum green time in the central formulation. This set of constraints state that if a lane group starts receiving green signal indication, it should receive green signal indication for a minimum period $\underline{G}$. However, these constraints can hinder the activation of white phases, which is not beneficial in terms of intersection delay. The first vehicle behind the intersection stop bar of east bound movement shown in Figure 4-4.a is a CHV, therefore, it is not possible to give white indication to east bound movement. The only option to clear the east bound queue is to give green indication to that movement and red indication to the north bound movement. Based on the minimum green constraints, this signal plan should be active for at least $\underline{G}$ minutes. However, if we switch the signal indication from green to white after operating the first vehicle behind the east bound stop bar, we can operate both east bound and north bound movements under simultaneous white phases as shown in Figure 4-4.b. Hence, we replaced the minimum green time constraints by minimum active time constraints presented as constraints (4.15) which imposes a lower bound on the active time (green and following white times) of a lane-group when its signal indication switches from red to green. Similarly, constraints (4.16) impose a minimum duration for the white phase for a lane-group when its signal switches from red to white. constraints (4.17) define an upper bound for the green signal duration of a lane group.

a) Minimum green time   b) Minimum active time

Figure 4-4: Minimum green and active times

Constraints (4.18) define the yellow time duration while constraints (4.19) and (4.20) ensure that signal turns from green to yellow at the end of green and from white to yellow at the end of the white time, respectively. Constraints (4.21) impose all-red indication $\mathcal{R}$ when a lane-group switches from yellow to red. Constraints (4.22) are introduced to clear the intersection conflicting area while switching the signal from green to white. In particular, if the signal is green for lane $l \in L$ at time $n \in \hat{T}$ and the lane is to receive white signal at time $n+1 \in \hat{T}$, constraints (4.22) will prevent conflicting lanes with lane $l \in L$ from receiving white signal for $\mathcal{R}$ duration. Therefore, the last vehicle that entered the intersection conflicting area will clear the intersection before letting the conflicting vehicle-groups enter the conflicting area during white phases.

Constraints (4.23) and (4.24) define the initiation and termination of the white phase. The phase can initiate only when the first vehicle behind the intersection stop bar is a CAV. Additionally, the white phase will be terminated for lane $l \in L$ if the first vehicle behind the intersection stop bar is not a member of a vehicle-group. For instance, the third vehicle shown in Figure 4-5 is the first vehicle behind the intersection stop bar and is not a member of the vehicle-group, therefore, its lane-group cannot receive white.

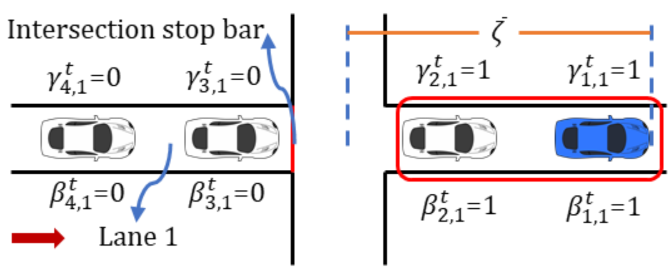

Figure 4-5: The relative location of vehicles in reference to intersection stop bar and vehicle-groups

In summary, CAVs optimize objective function (4.3) subject to constraints (4.4)-(4.24). On the other hand, CHVs estimate their movements using the car-following model (4.1) with a given signal, or optimize objective function (4.2) subject to constraints (4.1), (4.4), (4.5), and (4.14)-(4.24) to estimate their trajectories while finding the optimal signal timing plans for themselves.

4.3. Solution technique

The proposed vehicle-level MINLP contains non-linear terms in the objective function (4.3) and constraints (4.1) and (4.13); and seeks agreement on trajectories among vehicles with conflicting movements. This section first linearizes the aforementioned non-linear terms and then introduces a receding horizon structure over a planning horizon $\widehat{N}$ to capture the dynamics of distributed trajectory and signal timing plans. We first define auxiliary non-negative variables ${\lambda^+}_{il}^{t}$ and ${\lambda^-}_{il}^{t}$ to linearize objective function (4.3) as follows.

$$\tilde{Z}'_{il} = \min_{\boldsymbol{a},\boldsymbol{g},\boldsymbol{w}} \sum_{t\in T}(r_l - x_{il}^t) + \omega({\lambda^+}_{il}^{t+1} + {\lambda^-}_{il}^{t+1}) \qquad \forall i \in I'_l, l \in L \qquad (4.25)$$

$$v_{il}^{t+1} - v_{il}^t = {\lambda^+}_{il}^{t+1} - {\lambda^-}_{il}^{t+1} \qquad \forall i \in I'_l, l \in L, t \in T \qquad (4.26)$$

$${\lambda^+}_{il}^{t+1}, {\lambda^-}_{il}^{t+1} \geq 0 \qquad \forall i \in I'_l, l \in L, t \in T \qquad (4.27)$$

where (4.25) ensures that one of the auxiliary variables gets the value of zero and the other equals the absolute value function. Similar to Niroumand et al. (2020), car-following constraints (4.1) will also be linearized. Additionally, we replace the safety constraints (4.13) by:

$$\begin{aligned} &{\varphi^+}_{jl}^{tq} + {\varphi^-}_{jl}^{tq} + {\phi^+}_{jl}^{tq} + {\phi^-}_{jl}^{tq} + {\varphi^+}_{lj}^{ti} + {\varphi^-}_{lj}^{ti} + {\phi^+}_{lj}^{ti} + {\phi^-}_{lj}^{ti} \geq \zeta_{qj}^t + \mathcal{L} + 2\rho \\ &+M\left(\gamma_{il}^t + \hat{\gamma}_{\xi_{qj}j}^t + w_l^n + w_j^n - 4\right) \qquad (4.28) \\ &\qquad \forall i \in I'_l, l \in L, q \in P_j, j \in C_j, t \in T, n \in \hat{T} \end{aligned}$$

where $\boldsymbol{\varphi}$ and $\boldsymbol{\phi}$ are auxiliary non-negative variables that help linearize the absolute value functions corresponding to the head location and tail location of vehicle-groups, respectively.

Since the proposed optimization program contains binary variables, it is possible to provide some cuts to expedite the solution process of the optimization program. For instance, binary variable γ_{il}^{t} takes the value of one if vehicle $i \in I_l$ on lane $l \in L$ has passed the intersection stop bar by time $t \in T$ and takes the value of zero otherwise. Based on the definition of this variable, we can provide following cuts to reduce the computation time of the problem.

$$\gamma_{il}^{t'} \leq \gamma_{il}^{t}, \qquad \forall i \in I_l, l \in L, t \in T, t' < t, \tag{4.29}$$

$$\gamma_{i'l}^{t} \leq \gamma_{il}^{t}, \qquad \forall i \in I_l, l \in L, t \in T, i' > i, \tag{4.30}$$

$$\gamma_{il}^{t} = 1, \quad if\ x_{il}^{0} \geq b \qquad \forall i \in I_l, l \in L, t \in T, \tag{4.31}$$

Constraints (4.29) state that if vehicle $i \in I_l$ on lane $l \in L$ has not passed the intersection location by time $t \in T$ (i.e., $\gamma_{il}^{t} = 0$), the state variable γ for that vehicle should take the value of zero for time period $t' \in [0, t]$. Similarly, constraints (4.30) indicates that if vehicle $i \in I_l$ on lane $l \in L$ has not passed the intersection location by time $t \in T$, the state variable γ for its following vehicles should take the value of zero at time $t \in T$. Finally, constraints (4.30) states that if a vehicle has already passed the intersection location (i.e., $x_{il}^{0} \geq b$) the state variable γ for that vehicle should take the value of one for the entire planning horizon. Note that x_{il}^{0} is the current location of the vehicle $i \in I_l$ on lane $l \in L$ which is a parameter. Although these constraints seem primitive, they can reduce the computation time by pruning unnecessary branches in the branch and cut process used by CPLEX. Similar cuts are also introduced for the binary variables used for linearizing the safety constraints (4.13).

4.3.1. Receding horizon technique

A receding horizon control is implemented to solve the proposed formulation over a finite planning horizon $\widehat{N}$. We first initialize the state variables $x_{il}^{t_0}$ and $v_{il}^{t_0}$ of vehicle $i \in I_l$ on lane $l \in$

L at time $t_0 \in T$. We also capture the current signal status, i.e., green $g_l^{n_0}$ and white $w_l^{n_0}$ on lane $l \in L$ at time $n_0 \in \hat{T}$. The algorithm proceeds iteratively to form agreement among all vehicles on trajectories as well as signal timing plans. Since the update time steps for trajectory and signal timing plans are different (following sets T and $\hat{T}$, respectively), the algorithm reaches agreement on either (i) trajectories with given signal timing plans at time $t \in [t_0, t_0 + \widehat{N}/\Delta T]$ or (ii) both signal timing plans and trajectories at times $n \in [n_0, n_0 + \widehat{N}/\Delta\hat{T}]$ and $t \in [t_0, t_0 + \widehat{N}/\Delta T]$. Post agreement, the selected actions in the first time step that are (1) acceleration rate a_{il}^t of CAV $i \in I_l'$ on lane $l \in L$ at time $t_0 + 1$ and (2) signal indications w_l^n and g_l^n on lane $l \in L$ at time $n_0 + 1$ will be implemented. Note that the trajectories of CHVs are updated by Vissim and the car-following model (4.1) is only used to estimate the trajectories of the CHVs to be used in the trajectory optimization of CAVs. Tis mismatch between the estimated and implemented trajectories for CHVs results in a stochastic error which is captured using the receding horizon framework. After updating the acceleration rates and signal indications, the same process is repeated to reach agreement on signal timing plans and CAV trajectories at times $n \in [n_0 + 1, n_0 + 1 + \widehat{N}/\Delta\hat{T}]$ and $t \in [t_0 + 1, t_0 + 1 + \widehat{N}/\Delta T]$. The same process is repeated until the end of the study period. The proposed framework is detailed in Figure 4-6.

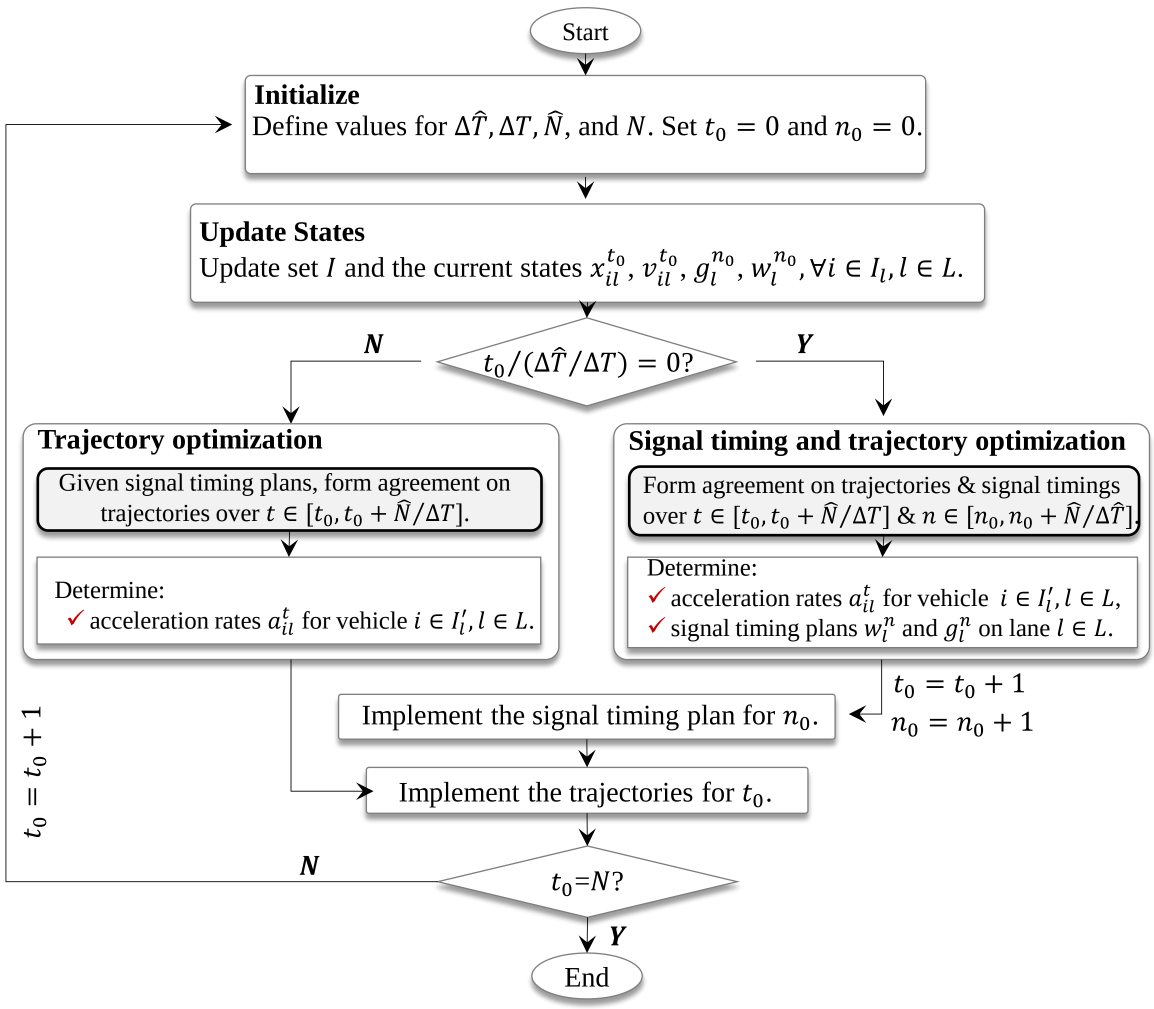

Figure 4-6: Receding horizon framework.

4.3.2. Agreement

Each vehicle optimizes/estimates its own trajectory and proposes a signal timing plan for all intersection lane-groups based on the shared information obtained from the rest of the vehicles in the intersection neighborhood. The decision variables of the vehicle-level optimization programs are the acceleration rate of the vehicle a and green g and white w signal statuses for the lane groups. As a result, each vehicle chooses signal statuses in a way to maximize its own objective function. The value of the signal timing variables optimized by each vehicle is considered as its vote on signal statuses. Note that there is no need for CHVs to be assigned to a vehicle-group to be able to vote on signal timing parameters. Vehicle movements are subject to safety constraints (4.28) during white phases to avoid conflicting vehicle-groups. Therefore, vehicles tend to vote for a green signal for their lane-groups. Hence, vehicle-level objective functions incentivize voting for white signals. We also relax constraints (4.28) by introducing slack variable δ_{il}^{tqj} in the CAVs' objective function with a big coefficient ψ to promote high coordination levels among CAVs. Therefore, objective functions $\hat{Z}_{il}$ and $\tilde{Z}'_{il}$ are rewritten as follows.

$$\widehat{Z^c}_{il} = \min_{\boldsymbol{a},\boldsymbol{g},\boldsymbol{w}} \sum_{t\in T}(r_l - x_{il}^t) + M(a_{il}^t - d_{il}^t) - \mu \sum_{n\in\hat{T}} \sum_{j\in L} w_j^n \quad \forall i \in \hat{I}_l, l \in L \tag{4.32}$$

$$\widetilde{Z^c}'_{il} = \min_{\boldsymbol{a},\boldsymbol{g},\boldsymbol{w}} \sum_{t\in T}(r_l - x_{il}^t) + \omega({\lambda^+}_{il}^{t+1} + {\lambda^-}_{il}^{t+1}) - \mu \sum_{n\in\hat{T}} \sum_{j\in L} w_j^n + \psi \sum_{t\in T} \sum_{q\in P_j} \sum_{j\in C_l} \delta_{il}^{tqj} \quad \forall i \in I'_l, l \in L \tag{4.33}$$

Similarly, safety constraints (4.28) are reformulated as:

$$\begin{gathered} {\varphi^+}_{jl}^{tq} + {\varphi^-}_{jl}^{tq} + {\phi^+}_{jl}^{tq} + {\phi^-}_{jl}^{tq} + {\varphi^+}_{lj}^{ti} + {\varphi^-}_{lj}^{ti} + {\phi^+}_{lj}^{ti} + {\phi^-}_{lj}^{ti} + \delta_{il}^{tqj} \geq \zeta_{qj}^t + \mathcal{L} + \\ 2\rho + M\left(\gamma_{il}^t + \hat{\gamma}_{\xi_{qj}j}^t + w_l^n + w_j^n - 4\right), \\ \forall i \in I'_l, l \in L, q \in P_j, j \in C_j, t \in T, n \in \hat{T} \end{gathered} \tag{4.34}$$

We implement the following steps to reach agreement among vehicles on trajectories and signal timing plans.

Step i Update CAV trajectories

Given the signal timing plans, CAVs solve problem $\mathcal{Z}$ with objective (4.33) and constraints (4.4)-(4.12), (4.14)-(4.24), (4.26)-(4.27), and (4.34) to optimize their trajectories at each iteration

$\mathcal{T}$. The trajectory of vehicle $i \in I_l'$ on lane $l \in L$ at time $t \in T$ at iteration $\mathcal{T}+1$ will be updated by averaging (Powell, 2007) the trajectory from iteration $\mathcal{T}$ (i.e., $\hat{x}_{il}^{t\mathcal{T}}$) and the optimized trajectory x_{il}^{t} to push the trajectories toward system-level agreement after a finite number of iterations $\mathcal{T}$. The maximum allowable value for the slack variable $\boldsymbol{\delta}$ is reduced at each iteration to ensure feasible trajectories.

$$\hat{x}_{il}^{t,\mathcal{T}+1} = \left(1 - \frac{1}{\mathcal{T}}\right)\hat{x}_{il}^{t\mathcal{T}} + \left(\frac{1}{\mathcal{T}}\right)x_{il}^{t}|z \qquad \forall i \in I_l', l \in L, t \in T \qquad (4.35)$$

Step ii Update CHV trajectories

CHVs use car-following model (4.1) to estimate their trajectories based on given signal timing plans and shared information from the rest of the fleet. Note that, the trajectories of CHVs are not averaged since human drivers do not use the exchanged information among vehicles and only react to the implemented trajectories of CAVs. Therefore, the trajectory of vehicle $i \in \hat{I}_l$ on lane $l \in L$ at time $t \in T$ at iteration $\mathcal{T}+1$ is updated only based on the obtained trajectories as follows.

$$\hat{x}_{il}^{t,\mathcal{T}+1} = x_{il}^{t}|z', \qquad \forall i \in \hat{I}_l, l \in L, t \in T. \qquad (4.36)$$

Step iii Share trajectory data

All vehicles share their updated trajectory $\hat{x}_{jl}^{t,\mathcal{T}+1}$ with the rest of the vehicles in the intersection neighborhood to be used at iteration $\mathcal{T}+1$.

Step iv Subroutine for trajectory agreement

A trajectory agreement is reached when the trajectory changes at two consecutive iterations do not exceed a pre-defined value ε; i.e.,

$$|\hat{x}_{il}^{t,\mathcal{T}+1} - \hat{x}_{il}^{t,\mathcal{T}}| \leq \varepsilon, \qquad \forall i \in I_l, l \in L, t \in T, \tag{4.37}$$

Step v Subroutine for signal agreement

At time steps t where joint optimization is involved; each vehicle optimizes its own trajectory and proposes a signal timing plan for all lane-groups. To this end, CAVs solve problem z while CHVs solve problem z' with objective (4.32) and constraints (4.1), (4.4)-(4.5), and (4.14)-(4.24). Note that vehicles that have arrived the intersection earlier must clear the conflicting area before their following vehicles can access the intersection. Therefore, we introduce constraints (4.38) and (4.39) to make sure that vehicles respect to the votes proposed by their preceding vehicles. Constraints (4.38) and (4.39) ensure that vehicle $i \in I_l$ on lane $l \in L$ accepts the signal timing plan proposed by its preceding vehicles on the same lane; this guarantees that preceding vehicles have cleared the intersection by the time vehicle $i \in I_l$ enters the intersection. Note that constraints (4.38) and (4.39) are defining priorities only for the vehicles on the same lane group while the negotiation for signal timing parameters happens between conflicting lane groups. Green and white signal indications on lane $j \in L$ at time $n \in \hat{T}$ voted by vehicle $i \in I_l$ on lane $l \in L$ is denoted by $\hat{g}_{ijl}^{n}$ and $\widehat{w}_{ijl}^{n}$. The term $1 - \hat{\gamma}_{jl}^{t}$ will relax the two constraints after vehicle j passes the intersection stop bar. For instance, assume that vehicle 3 shown in Figure 4-5 proposes green signal indication for lane 1 from time $n = 0$ to $n = 10$. In addition, assume that vehicle 3 is planning to cross the intersection stop bar by the time $t = 8$ which leads to $\hat{\gamma}_{3,1}^{8} = 1$. Please note that signal time step $n = 2$ starts at the same time as the trajectory time step $t = 8$ since we update trajectories and signal indications every 0.5 and 2 seconds, respectively. Constraints (4.38) and (4.39) ensure that vehicle 4 proposes the same signal indications that vehicle 3 proposed for lane 1 to ensure that vehicle 3 has cleared the intersection by the time that vehicle 4 enters the intersection. Furthermore, the term $(1-\hat{\gamma}_{jl}^{t})$ is multiplied to the right-hand side of these constraints to relax them after the preceding vehicle has passed the intersection stop bar. Therefore, vehicle 2 should propose green signal indication for lane 1 from time step $n=0$ to time step $n=2$.

$$w_l^n \geq \widehat{w}_{ljl}^n(1-\hat{\gamma}_{jl}^t), \qquad j<i, l\in L, n\in\hat{T}, t\in T, \tag{4.38}$$

$$g_l^n \geq \hat{g}_{ljl}^n(1-\hat{\gamma}_{jl}^t), \qquad \forall j<i, l\in L, n\in\hat{T}, t\in T. \tag{4.39}$$

If the voted signal timing plans remain unchanged in consecutive iterations, each vehicle will solve the following problem to optimize the signal timings. The signal plans are incorporated into the optimization program of vehicles as input parameters for the next iteration. The objective is to find the signal status for each lane-group with the highest vote from vehicles on the same lane-group.

$$\mathbb{Z} = \min_{\boldsymbol{g},\boldsymbol{w}} \sum_{n\in\hat{T}} \sum_{l\in L} \sum_{i\in I_l} (\mathrm{D}_{il}+1)(1-\hat{\gamma}_{il}^t)\left(\left|g_l^n-\hat{g}_{lil}^{n\mathcal{T}}\right|+\left|w_l^n-\widehat{w}_{lil}^{n\mathcal{T}}\right|\right) \tag{4.40}$$

$s.t.$ (4.14) - (4.24), (4.38) - (4.39)

where D_{il} is the delay of vehicle $i\in I_l$ on lane $l\in L$, obtained from Vissim (PTV Group, 2015) as an input parameter, which imposes greater weight to vehicles with higher delay. For instance, if the delay of vehicle $i\in I_l$ on lane $l\in L$ is 1, its vote will be multiplied by $\mathrm{D}_{il}+1=2$. Additionally, $\hat{g}_{lil}^{n\mathcal{T}}$ and $\widehat{w}_{lil}^{n\mathcal{T}}$ respectively denote green and white signal indications on lane $l\in L$ at time $n\in\hat{T}$ voted by vehicle $i\in I_l$ on lane $l\in L$ at iteration $\mathcal{T}$. Multiplying $1-\hat{\gamma}_{il}^t$ captures vehicle i's vote as far as it has not passed the intersection stop bar.

We utilize a linearized version of $\mathbb{Z}$ and associated constraints as follows.

$$\widetilde{\mathbb{Z}} = \min_{\boldsymbol{g},\boldsymbol{w}} \sum_{n\in\hat{T}} \sum_{l\in L} \sum_{i\in I_l} (\mathrm{D}_{il}+1)(1-\hat{\gamma}_{il}^t)\left(\mathscr{g}^{+}{}_{lil}^{n\mathcal{T}}+\mathscr{g}^{-}{}_{lil}^{n\mathcal{T}}+\mathrm{w}^{+}{}_{lil}^{n\mathcal{T}}+\mathrm{w}^{-}{}_{lil}^{n\mathcal{T}}\right) \tag{4.41}$$

$$g_l^n - \hat{g}_{lil}^{n\mathcal{T}} = \mathcal{g}^{+n\mathcal{T}}_{lil} - \mathcal{g}^{-n\mathcal{T}}_{lil}, \qquad \forall i \in I_l, l \in L, n \in \hat{T}, \tag{4.42}$$

$$w_l^n - \widehat{w}_{lil}^{n\mathcal{T}} = \mathrm{w}^{+n\mathcal{T}}_{lil} - \mathrm{w}^{-n\mathcal{T}}_{lil}, \qquad \forall i \in I_l, l \in L, n \in \hat{T}, \tag{4.43}$$

$$\mathcal{g}^{+n\mathcal{T}}_{lil}, \mathcal{g}^{-n\mathcal{T}}_{lil}, \mathrm{w}^{+n\mathcal{T}}_{lil}, \mathrm{w}^{-n\mathcal{T}}_{lil} \geq 0, \qquad \forall i \in I_l, l \in L, n \in \hat{T}. \tag{4.44}$$

The agreement subroutine for trajectories and signal timing plans is further detailed in Figure 4-7.

Agreement subroutine
Step 1: Set $\mathcal{T} \leftarrow 1$ $\hat{a}_{il}^{t\mathcal{T}} \leftarrow a_{il}^t \qquad \forall i \in I_l, l \in L, t \in [t_0, t_0 + \widehat{N}/\Delta T]$ $\hat{g}_{lil}^{n\mathcal{T}} \leftarrow g_l^n,\ \widehat{w}_{lil}^{n\mathcal{T}} \leftarrow w_l^n \qquad \forall\, l \in L, n \in [n_0, n_0 + \widehat{N}/\Delta\hat{T}]$ **Step 2: Loop until agreements are reached** 2.1. Optimization 2.1.1. Solve problem $\mathcal{z}$ for CAVs 2.1.2. Solve problem $\mathcal{z}'$ for CHVs 2.2. Update 2.2.1. Update CAV trajectories using equations (4.35) 2.2.2. Update CHV trajectories using equations (4.36) 2.3. Signal Agreement 2.3.1. If signal parameters are fixed go to step 2.4. 2.3.2. If votes on signals do not change solve problem (4.14)-(4.24), (4.38)-(4.39), and (4.41)-(4.44) and fix signal variables 2.3.3. Set $\mathcal{T} \leftarrow \mathcal{T} + 1$ and go to step 2.1. 2.4. Trajectory Agreement 2.4.1. If $\lvert \hat{x}_{il}^{t,\mathcal{T}+1} - \hat{x}_{il}^{t,\mathcal{T}} \rvert \leq \varepsilon \quad \forall i \in I_l, l \in L, t \in T$ end 2.4.2. Set $\mathcal{T} \leftarrow \mathcal{T} + 1$ and go to step 2.1. **End Loop**

Figure 4-7: Agreement formation subroutine

4.4. Numerical results

This section first introduces the case study intersection and then discusses the results including mobility, safety, and convergence performances. The proposed problem framework is run on a desktop computer with a Core i9 CPU and 64 GB of memory. Vissim microscopic traffic simulator (PTV Group, 2015) is used to implement the obtained solutions in order to measure mobility and safety performance measures. We overwrite Vissim's car following logic for CAVs based on the trajectories that our methodology finds. On the other hand, we let the Vissim car-following to update the trajectories of CHVs and use the car-following model (4.1) to only estimate the movements of CHVs.

4.4.1. Case study

The proposed problem methodology is applied to a four-legged isolated intersection with exclusive through and left-turn movements. We assume that vehicles are in their preferred lanes prior to entering the intersection neighborhood and thus, lane changing can be ignored. Please note that each phase is associated with one lane since the intersection has one lane for each movement. The communication range is assumed to be 650 ft which is within the maximum 1000 ft dedicated short-range communication range. The maximum speed for all vehicles is assumed to be 42.5 ft/s. We update trajectories and signal indications every $\Delta T = 0.5\ s$ and $\Delta \hat{T} = 2\ s$, respectively. In addition, the maximum length of vehicles-groups is limited to 360 ft. Table 4-2 summarizes the value of the parameters used in the case studies.

The problem is solved for a 900 s study period and three different demand levels as shown in Figure 4-8. Note that the demand for left-turn movements is 8% of the through movements. Eight different CAV market penetration rates are considered for each demand level, ranging from low (0% and 10), medium (30%, 50%, and 70%), to high (80%, 90%, and 100%) to capture the effects of CAVs on the intersection performance measures.

Table 4-2: Value of the parameters used in the case study.

Parameters	Value
Maximum and minimum speeds (ft/s)	42.5 & 0
Maximum acceleration (ft/s^2)	13
Minimum acceleration (ft/s^2)	-11.5
Human driver reaction time (s)	1
Automated vehicle reaction time (s)	0.1
Detection range (ft)	650
Intersection location (ft)	650
Maximum length of vehicle-groups (ft)	360
Average length of vehicles (ft)	13
Safety distance between consecutive vehicles (ft)	11.8
Safety distance between CAVs and red signal light (ft)	1
Safety distance between vehicle-groups of conflicting lane-groups (ft)	40
Car-following parameter α_1 (s^{-1})	0.95
Car-following parameter α_2 (s^{-2})	0.25
Trajectory updating interval (s)	0.5
Signal status updating interval (s)	2
All red time (s)	2
Yellow time (s)	4
Minimum active (green + following white) time for through movements (s)	12
Minimum active (green + following white) time for left-turns (s)	4
Minimum white duration for through movements (s)	6
Minimum white duration for left-turning movements (s)	4
Maximum green time for through and left-turning movements (s)	60
Planning time horizon (s)	20
Study period (s)	900

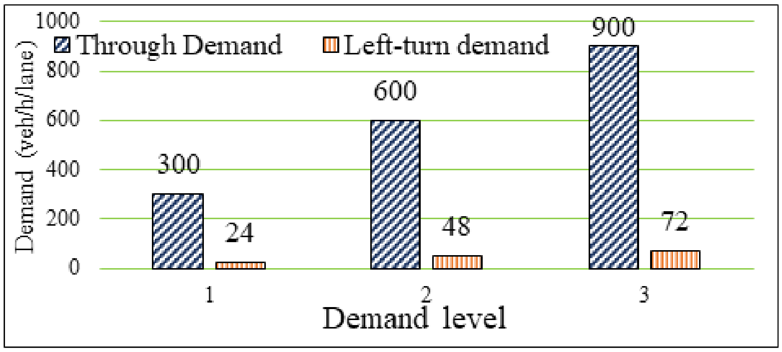

Figure 4-8: Demand levels for case studies.

4.4.2. Results

4.4.2.1. Mobility

Figure 4-9 shows the average delay for the fully-actuated signal timing plan found in Vissim (PTV Group, 2015) and the proposed agreement-based signal timing and trajectory optimization for different demand levels and CAV market penetration rates. The results indicate that the proposed methodology reduces the intersection average delay by 40.2% - 98.9% compared to the fully-actuated signal timing plan for various demand levels and CAV penetrations rates. Increasing the CAV penetration rate contributes to reductions in the average delay in all demand levels. This reduction can be caused by (i) more efficient operation of CAVs and (ii) increasing the possibility of activation of white phases. The significant reduction in intersection average delay from 80% to 90% CAV penetration rate in demand level 3 supports the hypothesis of the effectiveness of the white phase for a mixed autonomy environment. In addition, the difference between average delay for different demand levels decreases as the CAV market penetration rate increases. This can be due to efficient operation of vehicles during white phases which increases the intersection capacity significantly.

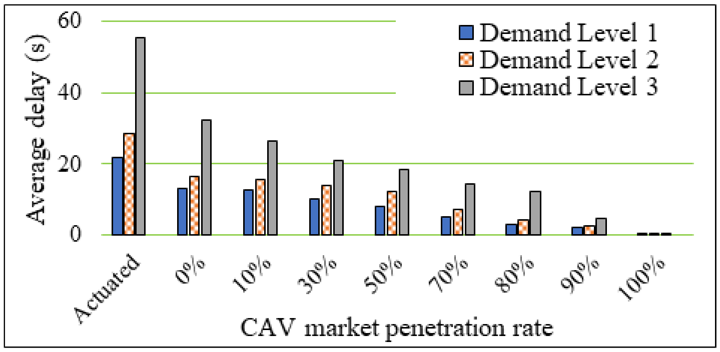

Figure 4-9: Average delay for all demand levels with different CAV market penetration rates.

Figure 4-10 shows the signal timing plans for all lane groups with different CAV market penetration rates in demand level 3. As shown in this figure, white phase activation increases with the CAV market penetration rate. We observe frequent white phase use for conflicting movements when the market penetration rate reaches 50%. The white phase becomes the dominant signal indication when the market share reaches and exceeds 70%; however, red and green signal indications appear even at a 90% CAV penetration rate.

A comparison between the activation rate of white phases with the central formulation proposed by Niroumand et al. (2020a) and the distributed formulation proposed in this study is presented in Figure 4-11. One limitation of the previous work was that the white phase was not activated as frequently as it was expected. As such, in the present study, the formulation was enhanced. As it is shown in this figure, our proposed formulation leads to significantly higher rates of white phase activation than previous formulation for all CAV penetration rates due to the changes made to the formulation. The difference between the white phase activation rates affirms that our proposed formulation could successfully increase the feasible area of the problem.

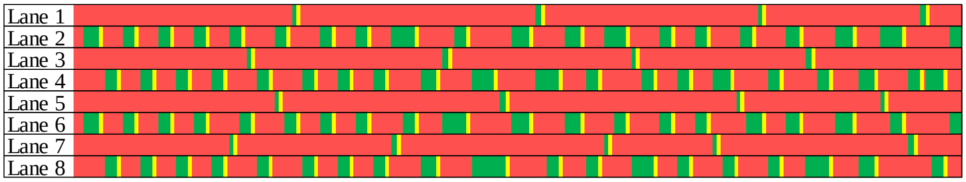

a) 0% CAV market penetration rate

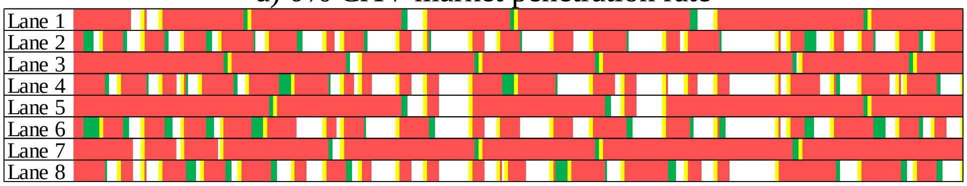

b) 30% CAV market penetration rate

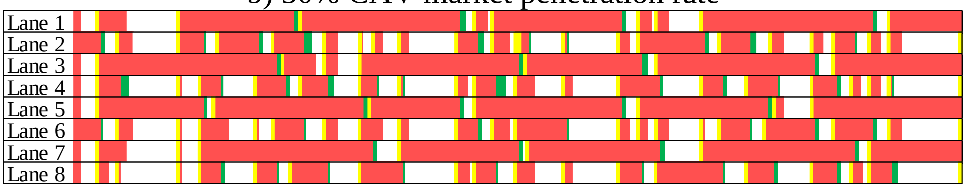

c) 50% CAV market penetration rate

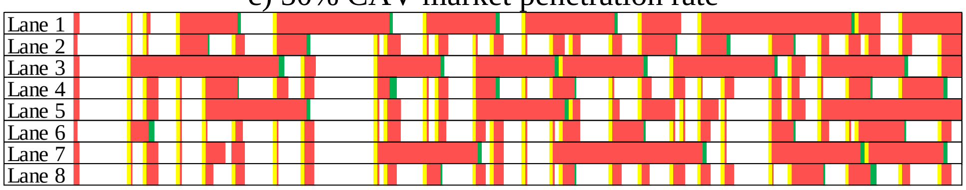

d) 70% CAV market penetration rate

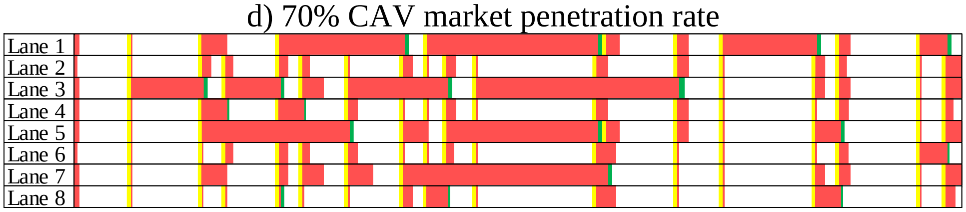

e) 80% CAV market penetration rate

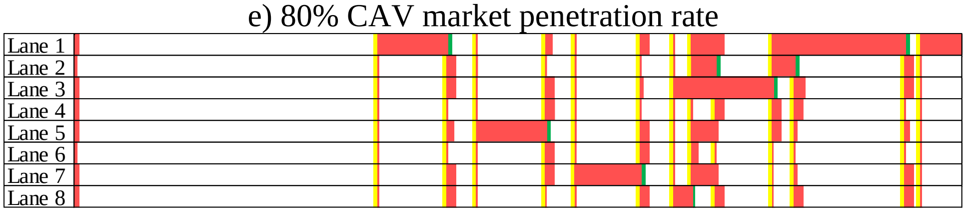

f) 90% CAV market penetration rate

Figure 4-10: Signal timing plans for demand level 3 with different CAV market penetration rates

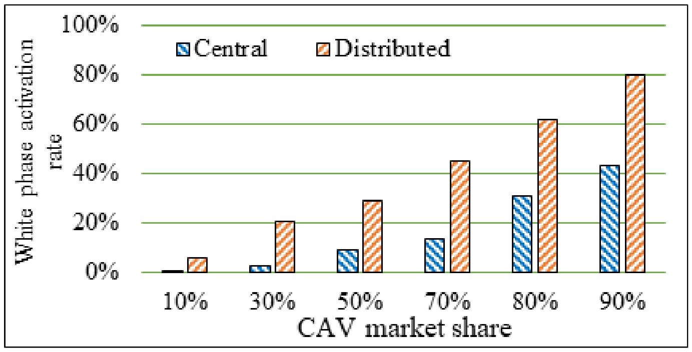

Figure 4-11: White phase activation rate comparison between central and distributed formulations for demand level 3

Table 4-3 compares the average run time and total delay achieved by executing the central (Niroumand et al., 2021, 2020b, 2020a) and distributed methodologies for different CAV penetration rates under demand level 3. The average run time for the distributed methodology is always less than the updating time interval while the run time for the central methodology is much longer than the updating time interval by two orders of magnitude. Furthermore, the distributed methodology yielded shorter total delays than the central methodology when CAV penetration rate is between 50% and 90%. This is because of the higher white phase activation rate in the distributed formulation due to the enhancement we have made in the optimization model used in the central methodology. Note that with 0%, 10%, 30%, and 100% CAV penetration rates the signal timing plans cannot be significantly different between the central and distributed formulations since the possibility of activation of the white phases are low with 0%, 10%, and 30% CAV penetration rates while the white phase is the only phases used with 100% CAV penetration rates. Therefore, the total delay of the distributed methodology is more than the central one due to the decentralized methodology.

Table 4-3: Total delay and average run time comparison between central and distributed methodologies under demand level 3

		Average run time (ms)		Total delay (s)	
		Distributed	Central	Distributed	Central
CAV penetration rate (%)	0	167	10315	4905.7	4701.6
	10	144	10649	3739	3604.4
	30	165	10822	2644	2610.3
	50	161	11034	2374	2436.1
	70	104	13380	1602.6	1800
	80	160	67684	1194	1356.3
	90	128	115063	347.4	362.9
	100	173	60930	85.2	82.31

Figure 4-12 shows the trajectory of CHVs and CAVs on the eastbound lane of the intersection shown in Figure 4-1 with different CAV penetration rates in demand level 3. The trajectory of CHVs and CAVs are shown with solid red and blue lines, respectively. Instead of stopping behind the red light, vehicles adjust their speed during white phases and pass the conflicting zone with a fewer number of stops. Therefore, traffic flow becomes smoother with an increase in the CAV market share.

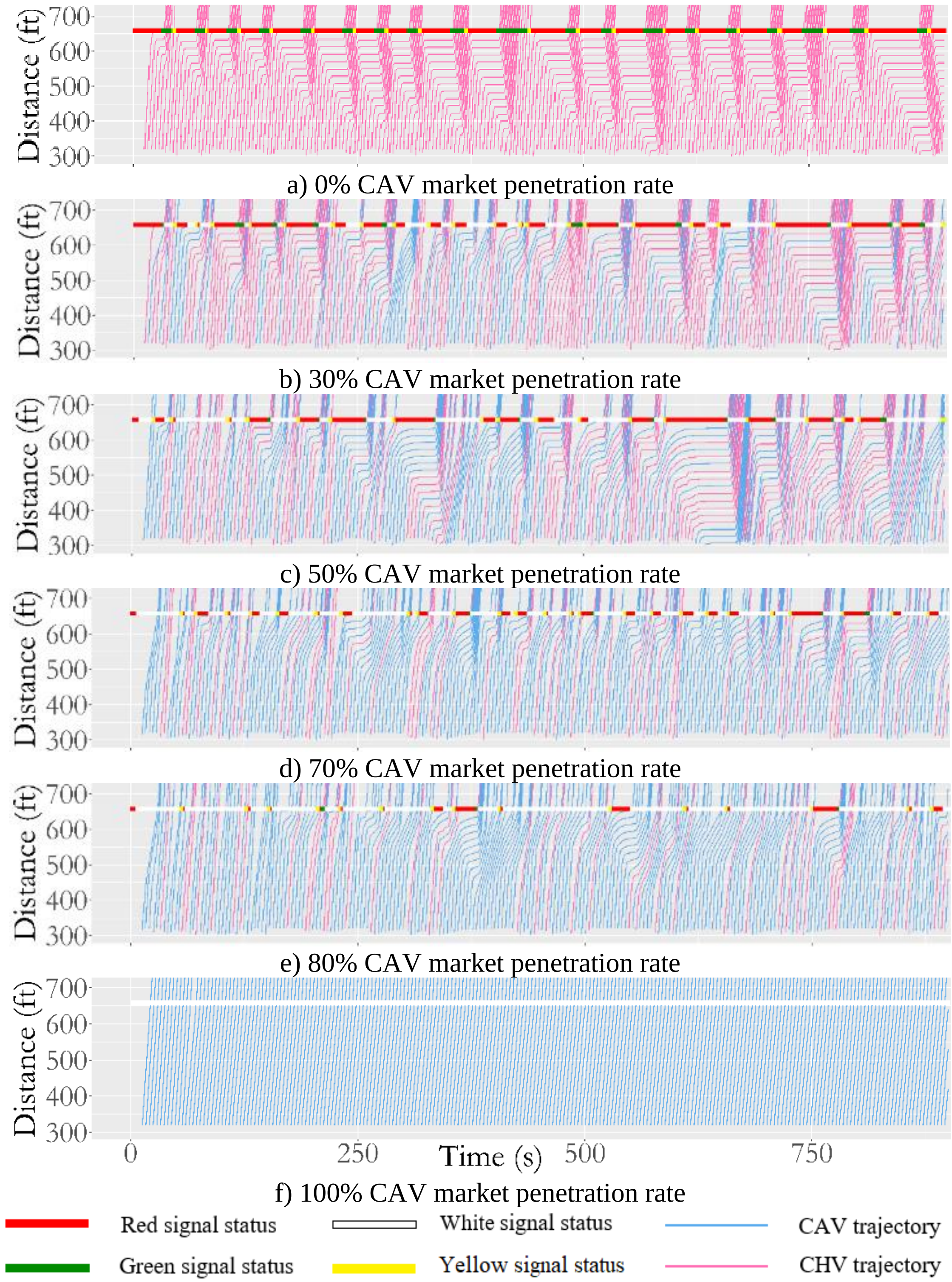

Figure 4-12: Trajectories of vehicles in lane 2 for demand level 3 with different CAV penetration rates

4.4.2.2. Safety

We have analyzed traffic safety considering rear-end and crossing conflicts using the surrogate safety assessment model (SSAM) software (Gettman and Head, 2003). The time to collision (TTC) is used as the surrogate safety assessment measure. The results indicate that there is no near collision case for both considered conflicts with different CAV market penetration rates and demand levels assuming 1.5 s TTC threshold. Figure 4-13 shows the TTC for rear-end conflicts under the TTC threshold of 10 s. The median of TTC shows a decreasing trend by increasing the CAV penetration rate up to 80% due to co-existence of CHVs and CAVs with shorter reaction time. On the other hand, the median of the rear-end TTC decreases from 80% to 100% CAV penetration rates since most of the vehicles are operated during simultaneous white phases which leads to a smaller number of stops compared to green and red phases. On the other hand, interquartile dispersion increases as CAV penetration rate increases up to 80% and decreases from 80% to 100%. This can be due to mixed fleet of CAVs and CHVs and mixed use of green and white signal indications. However, the interquartile dispersion decreases as the fleet and signal indications become uniform in 90% and 100% CAV penetration rates. Note that, no crossing near-crash condition was reported by SSAM.

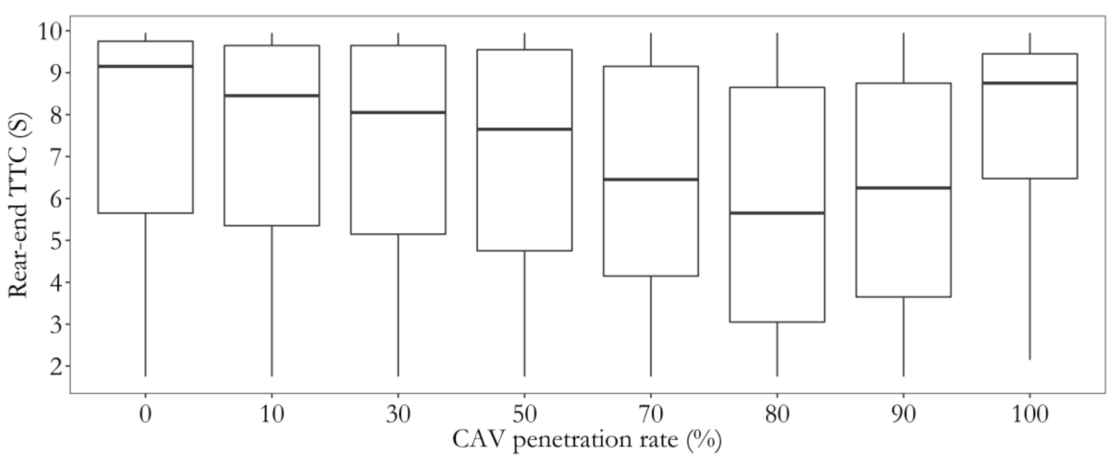

Figure 4-13: Rear-end time to collision for demand level 3 with different CAV penetration rates

4.4.2.3. Rider comfort

Figure 4-14 shows the trajectory, speed, and acceleration profiles of a sample CAV and its following CHV that go through the intersection during the white phase. As it is shown, the CAV reduces its speed to prevent a potential collision with conflicting vehicle-groups. However, it does not need to come to a complete stop to avoid the collision. The following CHV (Figure 4-14. (d), (e), and (f)) goes through the intersection even smoother than the leading CAV since the CAV is responsible for the collision avoidance.

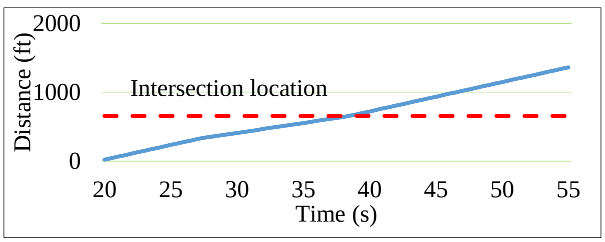

a) CAV trajectory

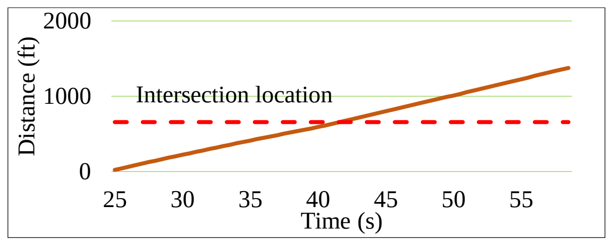

d) CHV trajectory

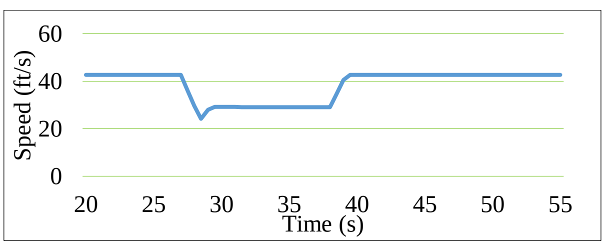

b) CAV speed profile

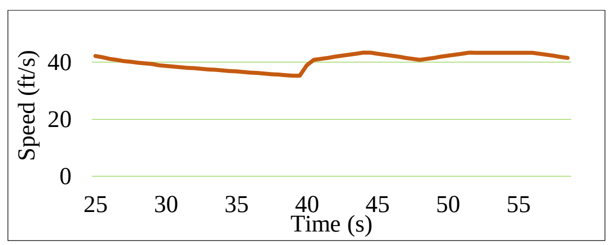

e) CHV speed profile

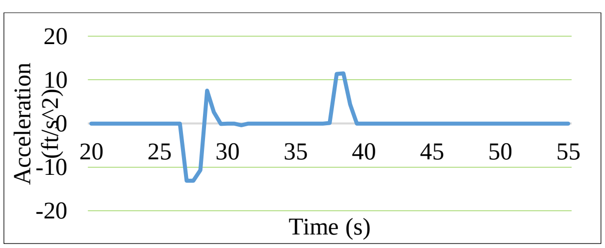

c) CAV acceleration profile

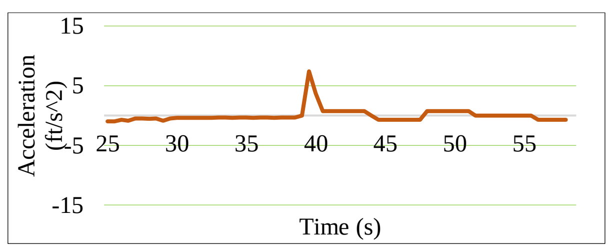

f) CHV acceleration profile

Figure 4-14: Trajectory, speed, and acceleration profiles of a CAV and its following CHV

Table 4-4 summarizes the driving comfort parameters including average and standard deviation of speed, average acceleration and deceleration, average positive and negative jerk. Note that we did not include zero values in our analysis for the positive and negative jerk, acceleration, and deceleration. As shown in the table, the average speed increases for both types of vehicles as the CAV market penetrations rate increases. The average speeds for CAVs are higher than CHVs for all CAV penetration rates since CAVs have smaller reaction times and consider the future states of the signal and other CAVs in their trajectory optimization program. On the other hand, speed variances show a decreasing trend with increasing the CAV penetration rate since the speed difference of CAVs is minimized in their optimization program. Therefore, the speed difference of CAVs is always less than CHVs. In addition, average positive and negative acceleration and jerk are much lower than their maximum and minimum values which shows smooth changes in variations of speed and acceleration rate.

Table 4-4: Driving comfort parameters under demand level 3 and different CAV penetration rates for CAVs and CHVs

Driving Comfort Measure	**CAV Market Share (%)**					
	0	**30**	**50**	**70**	**80**	**100**
CAVs						
Average speed (ft/s)	-	25.66	26.47	28.93	35.68	38.74
Speed standard deviation (ft/s)	-	18.19	17.87	16.69	12.01	5.87
Average acceleration (ft/s^2)	-	3.89	3.80	4.54	5.12	4.98
Acceleration standard deviation (ft/s^2)	-	4.23	4.12	4.49	4.66	4.29
Average deceleration (ft/s^2)	-	-4.03	-3.92	-4.74	-5.34	-7.17
Deceleration standard deviation (ft/s^2)	-	5.07	4.93	5.10	5.29	5.85
Average positive jerk (ft/s^3)	-	3.89	3.98	5.15	7.55	8.31
Positive jerk standard deviation (ft/s^3)	-	5.99	5.91	6.91	8.62	8.14
Average negative jerk (ft/s^3)	-	-3.83	-4.39	-5.20	-7.66	-10.90
Negative jerk standard deviation (ft/s^3)	-	6.04	6.18	7.13	8.82	9.20

Table 4-4 (continued).

CHVs						
Average speed (ft/s)	21.72	24.39	24.97	25.71	31.39	-
Speed standard deviation (ft/s)	19.81	19.08	18.82	18.19	16.52	-
Average acceleration (ft/s^2)	3.39	2.99	3.07	2.84	1.94	-
Acceleration standard deviation (ft/s^2)	4.45	4.17	4.18	4.03	3.27	-
Average deceleration (ft/s^2)	-3.39	-2.45	-2.15	-1.95	-1.29	-
Deceleration standard deviation (ft/s^2)	4.29	3.63	3.27	2.79	1.95	-
Average positive jerk (ft/s^3)	2.33	2.35	2.36	2.08	1.22	-
Positive jerk standard deviation (ft/s^3)	4.25	4.66	4.91	4.72	3.78	-
Average negative jerk (ft/s^3)	-2.52	-2.30	-2.30	-1.91	-1.14	-
Negative jerk standard deviation (ft/s^3)	3.80	4.17	4.38	3.97	2.85	-

4.4.2.4. White phase effect on traffic operations

We study the effects of the white phase on total delay by creating two scenarios of (1) no white phase activation and (2) optimized white phase activation. The no white phase scenario represents joint CAV trajectory and signal optimization. In Figure 4-15 we summarize the results for demand level 3 with 900 vehicle/h/lane on each through lane and 8% left turns. At 0% CAV market penetration rates, the total delays found for each scenario were identical as expected. In fact, the white phase is never activated in either scenario. At 10% CAV market share, we observed the white phase in 6.03% of the study period, which led to a 3.2% reduction in total delay due to reducing the number of phase transitions. With an increase in the CAV market share, the total delay reduction increases because, white phase allows much fewer phase transitions, which leads to less lost time and less delay.

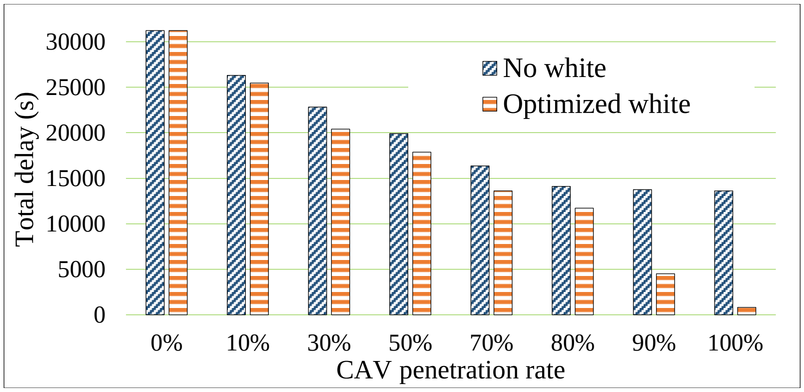

Figure 4-15: No white phase and optimized white phase total delay comparison for demand level 3.

4.4.2.5. Fuel consumption

Figure 4-16 shows the average fuel consumption for different CAV penetration rates and white phase activation scenarios under demand level 3. As it is shown, average fuel consumption strictly decreases as the CAV penetration rate increases for both white phase activation scenarios. In addition, fuel consumption under optimized white phase activation scenario is always lower than no white phase activation scenario due to the presence of simultaneous white phases, which lead to fewer phase transitions and lost time. Average fuel consumption decreases with a relatively high rate from 0% to 30% CAV penetration rates due to higher performances of CAVs. The reduction rate decreases from 30% to 80% and further increases from 80% to 90% due to the dominance of the simultaneous white phases under optimized white phase activation scenario. On the other hand, the reduction in average fuel consumption under no white phase activation scenario is not significant in high CAV penetration rates since vehicles still need to decelerate to stop behind the red signal indications and accelerate to pass the conflicting area during green signals.

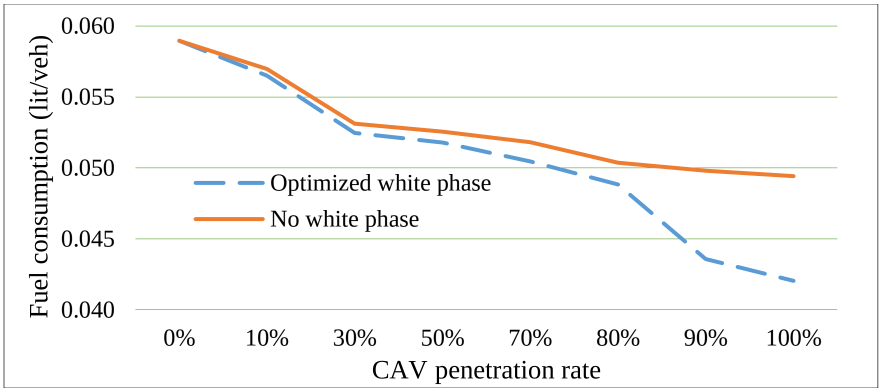

Figure 4-16: No white phase and optimized white phase average fuel consumption comparison for demand level 3

4.4.2.6. Convergence

The convergence of the proposed methodology is studied by comparing the trajectories of vehicles at different iterations. Figure 4-17 shows the trajectory from 180th to 190th second. Note that this vehicle entered the detection area at the 170th second. The vehicle smoothly reduced its speed to enter the conflicting area at the proper time, however, it had to make a minor change in its trajectory prior to entering the conflicting area to avoid collisions. We also observe that the trajectory changes over iterations and the amount of change decreases over iterations until it becomes negligible. This is the point that the agreement is reached among CAVs on their trajectories. Figure 4-18 shows the difference in trajectories between two consecutive iterations. The difference between iterations one and two is large; however, the difference decreases as the algorithm proceeds in iterations. Figure 4-17 and Figure 4-18 show that the trajectory of the vehicle is converged at iteration 7 with no considerable fluctuations. Note that, similar trends are observed for all the vehicles, and we show this trajectory as a sample.

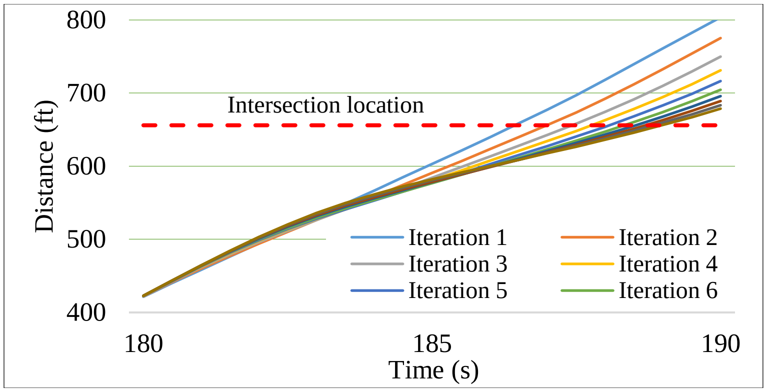

Figure 4-17: Trajectory of a vehicle across different iterations

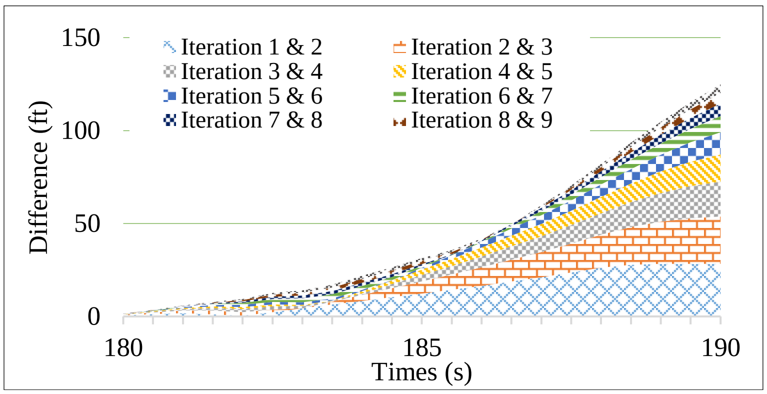

Figure 4-18: The difference of trajectories at consecutive iterations

4.4.2.7. Computation time

Figure 4-19 shows the computation time for demand level 3 with a 100% CAV penetration rate which is the most complicated scenario due to the presence of the highest number of vehicle-groups. As it is displayed, the algorithm converged with less than 0.4 seconds of computation time which represents the possibility of real-world implementation of the proposed methodology considering 0.5 seconds of updating time interval.

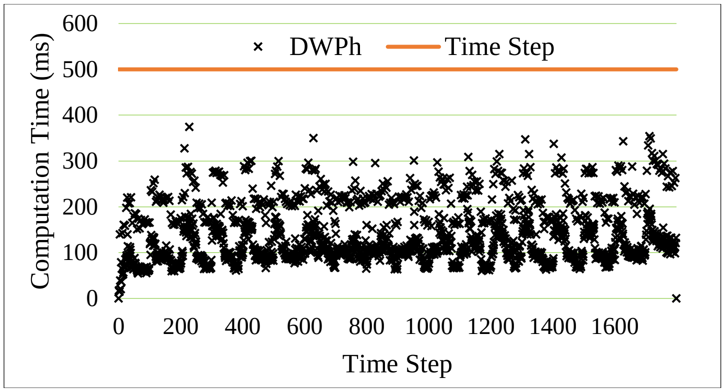

Figure 4-19: Computation time for demand level 3 with 100% CAV penetration rate.

4.5. Conclusion

This paper introduces an agreement-based distributed methodology to control a mixed traffic stream of CAVs and CHVs at signalized intersections. The proposed solution technique aims to design CAV trajectories and signal timings more accurately while reducing the computational complexity of the decision-making process. We have incorporated a new white phase into traffic lights during which, CAVs act as mobile traffic controllers by forming and leading groups of CHVs and navigating through the intersection. The white phase will not be activated when the CAV market penetration rate is not high enough and instead, the green signal indication is utilized. We have formulated the joint signal timing and trajectory optimization problem as vehicle-level MINLPs. To reduce the complexity of the vehicle-level problems, the formulation is first linearized and then embedded into a receding horizon framework. The distributed methodology achieves agreement among all vehicles on vehicles' trajectories and signal timing parameters through an iterative process. Our case study results indicate that the proposed methodology can efficiently solve the problem, where the intersection total delay is reduced by 40.2% - 98.9% compared to a fully-actuated intersection control. In addition, the methodology produces solutions in real-time, which makes it suitable for real-world applications.

Moreover, white phases are occasionally assigned to conflicting movements from a 30% CAV penetration rate and become the dominant signal status from a 70% rate.

CHAPTER 5: REAL-TIME SIGNAL AND TRAJECTORY OPTIMIZATION IN MIXED-AUTONOMY TRAFFIC STREAMS

Previous chapter introduced a real-time framework to solve the joint signal and trajectory optimization program. Although the framework is real-time for an isolated intersection, it is not suitable to be used as a subroutine in network-level signal and trajectory optimization algorithms due to its run time. Therefore, this chapter presents a shooting heuristic-based algorithm that solves the joint signal and trajectory optimization in the order of milliseconds. A bi-level architecture is used to optimize the signal timing plan and optimize/estimate the trajectories of vehicles. The upper level enumerates all the feasible signal timing plans while the lower level uses a shooting heuristic to construct vehicle trajectories for a given signal timing plan. In addition, the proposed problem formulation and solution technique in embedded into a receding horizon framework to further tackle the complexity of the problem and deal with the dynamic nature of the signal and trajectory optimization.

5.1. Research gap and contributions

The existing literature in intersection-level joint signal and trajectory optimization either are not efficient enough to be used in real world or can be solved only one time in real-time. In other words, their run time does not allow them to solve the problem more than one time during each updating time step length. However, network-level signal and trajectory optimization algorithms need to solve the intersection-level problem several times to push the intersection-level solutions toward network-level optima. Therefore, an efficient intersection-level signal and trajectory optimization method is crucial to ensure the real-time applicability of the overall framework. This study presents an efficient bi-level algorithm to solve the joint optimization problem for an isolated intersection in the order of milliseconds. The proposed algorithm enumerates feasible signal timing plans in the upper level and uses a shooting heuristic to construct vehicle trajectories in the lower level.

5.2. Problem formulation

This section introduces a mathematical model to operate a mixed fleet of CAVs and CHVs through a signalized intersection. We assume that all vehicles are connected, and their location and speed are attainable in real-time to be used in signal and trajectory optimization. Decision variables of the formulation are vehicle acceleration rates a_{il}^t for trajectory optimization and green g_l^n traffic signal status for signal timing optimization. We respectively update trajectory and signal timing variables every ΔT and $\Delta\hat{T}$ seconds, where $\Delta\hat{T} > \Delta T$ due the more dynamic nature of vehicle trajectories. We define state variables x_{il}^t and v_{il}^t as the location and speed of vehicle $i \in I_l$ on lane $l \in L$ at time $t \in T$, respectively. Additionally, binary variable γ_{il}^t identifies the vehicles who have passed the intersection stop bar, where $\gamma_{il}^t = 1$ if $x_{il}^t > b_l$ or 0 otherwise. The notations used in the formulation are summarized in Table 5-1.

Table 5-1: The notations used in the problem formulation

Sets	
L	Set of all lanes
T	Set of all time steps for trajectory updates
$\hat{T}$	Set of all time steps for signal timing updates
I_l	Set of all vehicles on lane $l \in L$
I_l'	Set of all CAVs on lane $l \in L$
$\hat{I}_l$	Set of all CHVs on lane $l \in L$
C_l	Set of all conflicting lanes with lane $l \in L$
Decision Variables	
a_{il}^t	Acceleration of vehicle $i \in I_l$ on lane $l \in L$ at time $t \in T$
g_l^n	Binary decision variable; 1 if signal for lane $l \in L$ at time step $n \in \hat{T}$ is green, 0 otherwise
y_l^n	Binary decision variable; 1 if signal for lane $l \in L$ at time step $n \in \hat{T}$ is yellow, 0 otherwise
Other Variables	
x_{il}^t	The location of vehicle $i \in I_l$ on lane $l \in L$ at time $t \in T$
v_{il}^t	The speed of vehicle $i \in I_l$ on lane $l \in L$ at time $t \in T$

Table 5-1 (continued).

γ_{il}^t	1 if vehicle $i \in I_l$ on lane $l \in L$ has passed intersection by $t \in T$ or 0 otherwise.
Parameters	
$\underline{a}$ and $\overline{a}$	Lower and upper bounds for acceleration
$\underline{v}$ and $\overline{v}$	Minimum and maximum speeds
$\mathcal{L}$	Vehicle length
D	Minimum safety distance between two consecutive vehicles on the same lane
S	Minimum safety distance between vehicles and the intersection stop bar
$\hat{\tau}$	Reaction time for CHVs
τ'	Reaction time for CAVs
b_l	The position of intersection in lane $l \in L$
$\underline{G}$ and $\overline{G}$	Minimum and maximum green times
Y	Yellow time duration
ΔT	Time step size for trajectory updates
$\Delta \hat{T}$	Time step size for signal updates
r_l	The destination location of vehicles on lane $l \in L$
α_1 and α_2	Car-following parameters
$\mathcal{R}$	Duration of all-red time

The objective function (5.1) minimizes the distance between each vehicle and its pre-defined destination location. Constraints (5.2) and (5.3) are fundamental equations of motion that respectively update the location and speed of vehicle $i \in I_l$ on lane $l \in L$ at time $t + \Delta T$ based on their optimal acceleration rates at time t. Constraints (5.4) are customized car-following models that estimate the movement of CHV $i \in \hat{I}_l$ on lane $l \in L$ based on the trajectory of its leading vehicle and signal status of lane $l \in L$. Note that the term $M\gamma_{il}^t$ relaxes the connection between signal and vehicles once they pass the intersection stop bar. Constraints (5.5) and (5.6) respectively ensure that the acceleration and speed of vehicles remain within the pre-defined bounds. Constraints (5.7) ensure a safe distance between CAVs and their immediate front vehicles. The safety distance is a function of a constant safety distance D, vehicle length $\mathcal{L}$, and the distance traveled by the following vehicle during its reaction time $\tau' v_{il}^t$. Constraints (5.8) prevent vehicles from red light running by enforcing them to maintain a constant safe distance S from the intersection stop bar when the signal is red. Since time is discretized in this study, vehicles can jump from one side of the intersection stop bar to the other side during one time step without violating any constraints. Therefore, the term $\Delta T v_{il}^{t}$ is added to the right-hand-side of these constraints to prevent vehicles from jumping over the intersection stop bar during red signal phases. In addition, the term $-(g_l^n + y_l^n)M - \gamma_{il}^{t} M$ relaxes these constraints when the signal is not red, or the vehicle has already passed the intersection stop bar. Constraints (5.9) state that no pair of conflicting lane groups can receive non-red (green or yellow) signal indications at the same time. Besides, these constraints prevent the signal status of a lane group to be green and yellow at the same time. Constraints (5.10) and (5.11) respectively define the maximum and minimum green times for each lane group. Constraints (5.12) define the duration of yellow time while constraints (5.13) make sure that lane groups receive yellow signal status after green times. Finally, constraints (5.14) put all-red time after the end of yellow time to clear the intersection before activating other lane groups.

$$Z = \min \sum_{t\in T} \sum_{l\in L} \sum_{i\in I_l} (r_l - x_{il}^{t}) \tag{5.1}$$

$$x_{il}^{t+\Delta T} = x_{il}^{t} + v_{il}^{t}\Delta T + \frac{1}{2} a_{il}^{t} \Delta T^2, \qquad \forall i \in I_l, l \in L, t \in T, \tag{5.2}$$

$$v_{il}^{t+\Delta T} = v_{il}^{t} + a_{il}^{t}\Delta T, \qquad \forall i \in I_l, l \in L, t \in T, \tag{5.3}$$

$$a_{il}^{t} = \max\left\{\underline{a}, \frac{\underline{v}-v_{il}^{t}}{\Delta T}, \min\left\{\begin{matrix}\overline{a}, \\ \frac{\overline{v}-v_{il}^{t}}{\Delta T}, \\ \alpha_1\left(v_{il}^{t} - v_{i-1,l}^{t}\right) + \alpha_2\left((x_{il}^{t} - x_{i-1,l}^{t} - \mathcal{L}) - D - v_{il}^{t}\hat{\tau}\right), \\ \alpha_1\left((y_l^n + g_l^n)\overline{v} - v_{il}^{t}\right) + \alpha_2\left((b_l - x_{il}^{t}) - (1 - y_l^n - g_l^n)S\right) + M\gamma_{il}^{t}, \end{matrix}\right\}\right\}, \tag{5.4}$$

$$\mathcal{L} \qquad \forall i \in \hat{I}_l, l \in L, t \in T, n \in \hat{T},$$

$$\underline{a} \le a_{il}^{t} \le \overline{a}, \qquad \forall i \in I_l{}', l \in L, t \in T, \tag{5.5}$$

$$\underline{v} \le v_{il}^{t} \le \overline{v}, \qquad \forall i \in I_l{}', l \in L, t \in T, \tag{5.6}$$

$$x_{i-1,l}^{t} - x_{il}^{t} \ge D + \mathcal{L} + \tau' v_{il}^{t}, \qquad \forall i \in I_l{}', l \in L, t \in T, \tag{5.7}$$

$$b_l - x_{il}^{t} \ge S + \Delta T v_{il}^{t} - (g_l^n + y_l^n)M - \gamma_{il}^{t} M, \qquad \forall i \in I_l{}', l \in L, t \in T, n \in \hat{T}, \tag{5.8}$$

$$g_l^n + g_{l'}^n + y_l^n + y_{l'}^n \le 1, \qquad \forall l \in L, l' \in C_l, n \in \hat{T}, \tag{5.9}$$

$$\sum_{z=n}^{n+\overline{G}} g_l^z \le \overline{G}, \qquad \forall l \in L, n \in \hat{T}, \tag{5.10}$$

$$\sum_{z=n+1}^{n+\underline{G}} g_l^z \geq (g_l^{n+1} - g_l^n)\underline{G}, \qquad \forall l \in L, n \in \hat{T}, \qquad (5.11)$$
$$\sum_{z=n}^{n+Y} y_l^z \leq Y, \qquad \forall l \in L, n \in \hat{T}, \qquad (5.12)$$
$$\sum_{z=n+1}^{n+Y} y_l^z \geq (g_l^n - g_l^{n+1})Y, \qquad \forall l \in L, n \in \hat{T}, \qquad (5.13)$$
$$\sum_{z=n}^{n+\mathcal{R}-1}(g_l^z + g_{l'}^z + y_l^z + y_{l'}^z) - \mathcal{R}y_l^n + \mathcal{R}y_l^{n-1} \leq \mathcal{R}, \qquad \forall l \in L, l' \in C_l, n \in \hat{T}. \qquad (5.14)$$

5.3. Solution technique

We introduce a framework that uses a bi-level architecture to solve the joint signal and trajectory optimization model. The proposed methodology is also embedded into a receding horizon framework to further decrease the complexity of the problem and be responsive to the dynamic nature of signal and trajectory optimization. Instead of solving the problem over the entire study period N, the problem is solved over a shorter planning horizon period $\widehat{N}$. The proposed receding horizon control first initializes the state of the system by observing the current state of vehicle $i \in I_l$ (i.e. its location $x_{il}^{t_0}$ and speed $v_{il}^{t_0}$) at time $t_0 \in T$ and current status of the intersection's signal, including green $g_l^{n_0}$ and yellow $y_l^{n_0}$ statuses at time $n_0 \in \hat{T}$. Since the trajectory-related variables are updated more frequently than signal timing plans, the algorithm either solves a joint signal and trajectory optimization model or trajectory optimization with a given signal timing plan. At time steps that joint signal and trajectory optimization is involved, the algorithm finds the optimal signal timing plans during time $n \in [n_0, n_0 + \widehat{N}/\Delta\hat{T}]$ along with optimal CAV trajectories during time $t \in [t_0, t_0 + \widehat{N}/\Delta T]$ based on the current and predicted states of the system. Note that the trajectories of CHVs are estimated using the car-following model (5.4). When only the trajectory optimization is involved, the signal timing plans are considered as input parameters during time $n \in [n_0, n_0 + \widehat{N}/\Delta\hat{T}]$ and only the trajectories of CAVs are optimized during time $t \in [t_0, t_0 + \widehat{N}/\Delta T]$. After solving the optimization model, the optimal acceleration rate a_{il}^t at time step $t = t_0 + 1$ will be implemented to control the movement of vehicle $i \in I_l$ on lane $l \in L$. In addition, the signal parameters g_l^n and y_l^n at time step $n = n_0 + 1$ lane $l \in L$ will be implemented to control the signals. After updating the state of the system, the algorithm moves one trajectory time step forward, solves the optimization model, and repeats this process until it reaches the end of the study period N. The general steps of the receding horizon control are shown in Figure 5-1.

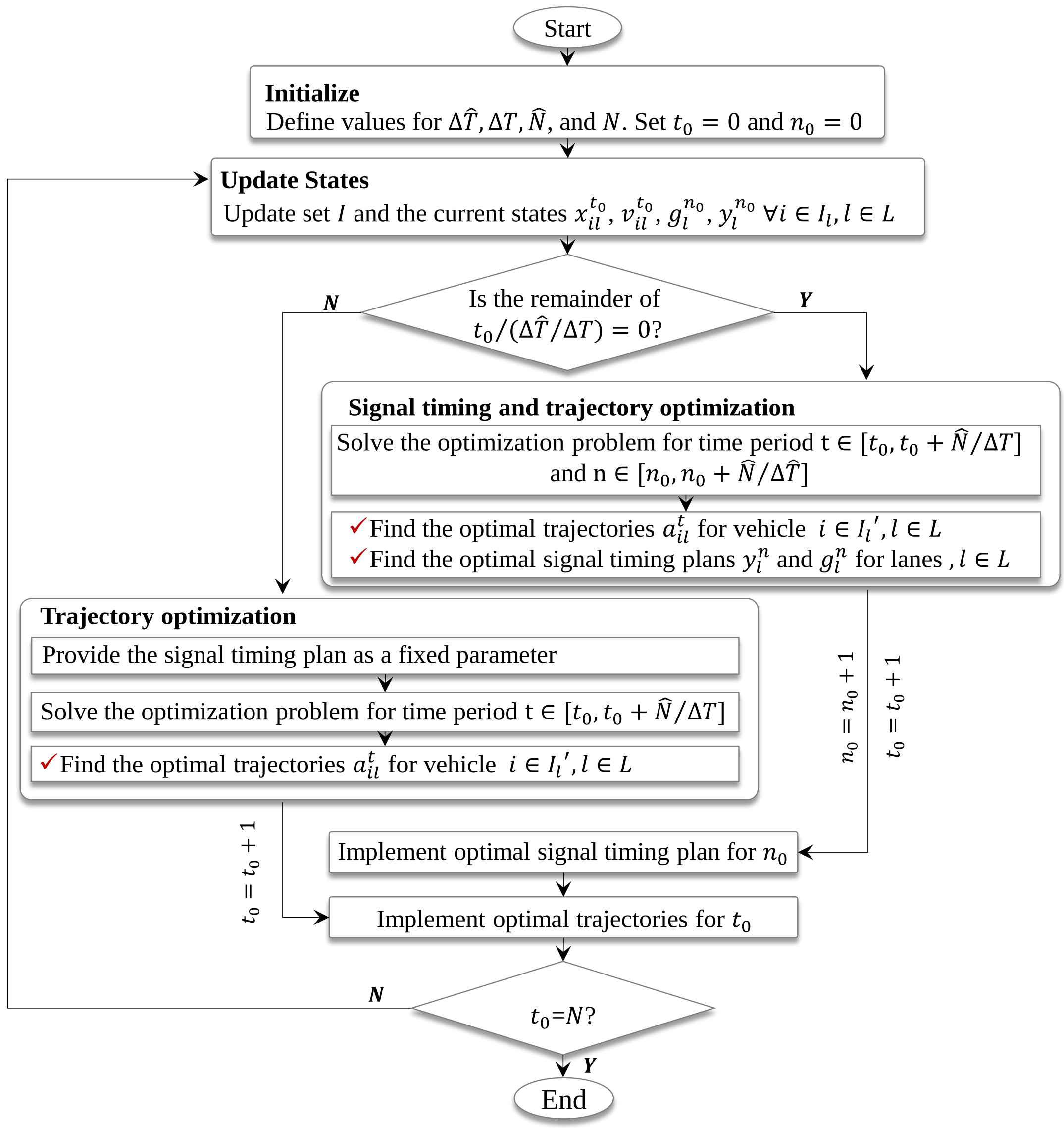

Figure 5-1: Receding horizon control general steps

We introduce a bi-level framework to solve the joint signal and trajectory optimization for an isolated intersection. The upper level enumerates all feasible combinations of signal timing plans in search of the best objective value while the lower level constructs vehicle trajectories for a given set of signal timing parameters using a shooting heuristic. We define four phases as shown in Figure 5-2 with a transition period including yellow time and all-red intervals after each active phase. Note that there is no pair of conflicting movements in a phase, therefore, having only one active phase at a time guarantees constraints (5.9). The upper level of the framework generates all the combinations of different phases, then prunes the ones that either have an active phase for a longer period than the maximum green time $\overline{G}$ or shorter period than the minimum green time $\underline{G}$ to satisfy constraints (5.10) - (5.11), respectively. In addition, it prunes combinations that do not include a transition period (yellow and all-red intervals) before changing the active phase to ensure constraints (5.12) - (5.14). Note that the rest of the constraints (i.e. constraints (5.2) - (5.8)) are satisfied in the different steps of the proposed shooting heuristic at the lower level.

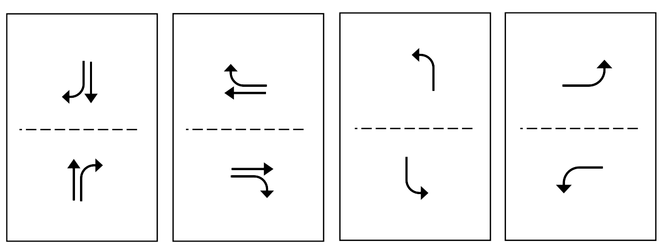

Figure 5-2: Intersection signal phases

The lower level of the proposed framework uses a shooting heuristic to construct the trajectory of each vehicle based on the trajectory of its immediate front vehicle and the signal timing plan of its own lane-group. Therefore, the trajectory construction for each lane can be done in parallel with other lanes while the trajectories of vehicles on the same lane should be constructed in sequence. The algorithm constructs trajectories of vehicles based on their location on the lane as shown in Figure 5-3. The first vehicle that has entered the lane has the highest priority in the trajectory construction process since its trajectory is needed for constructing the next vehicle's trajectory. We use three values for CAV acceleration rates a_{il}^{t}, namely $\overline{a}$ for speeding up, $\underline{a}$ for slowing down, and 0 for cruising with a constant speed, which are within the predefined bounds for acceleration rates based on constraints (5.5). Note that the proposed algorithm works with any number of acceleration rates at the cost of increased run-time. The proposed algorithm updates the state of the vehicles based on fundamental equations of motion (5.2) and (5.3), maintains within the maximum and minimum values of the speed to satisfy constraints (5.6), and continuously checks safety constraints (5.7) and (5.8) to prevent rear-end collisions and red light running. Therefore, the constructed trajectories satisfy vehicle dynamic constraints (5.2) - (5.8).

With a given signal timing plan, we use three steps to construct a trajectory for a CAV. First, initial acceleration step accelerates the CAV to its maximum speed to make sure that the CAV does not lose a green time due to its low speed. Then the algorithm checks for a violation in safety constraints (5.7) and (5.8). If the safety constraints are satisfied, the constructed trajectory is optimal, and the algorithm starts constructing a trajectory for the next vehicle on the lane. Otherwise, the accident prevention step removes positive accelerations prior to the violation time to satisfy the safety constraints. If removing positive acceleration rates could not prevent the violation, deceleration with a value of $\underline{a}$ is used to satisfy the safety constraints. Note that if this step cannot satisfy the safety constraints (5.7) and (5.8), the given signal timing plan is infeasible. Otherwise, the constructed trajectory is feasible, however, it may be sub-optimal. To push the constructed feasible trajectory toward optimality, the third step (speeding up) accelerates the CAV if the acceleration does not cause a safety constraint violation. Then, the algorithm starts to construct a trajectory for the next vehicle on the lane until it reaches the last vehicle on the lane.

Note that the trajectories of CHVs are estimated using car-following model (5.4). The general steps of the proposed shooting heuristic for vehicles on lane $l \in L$ with a given signal timing plan is depicted in Figure 5-4.

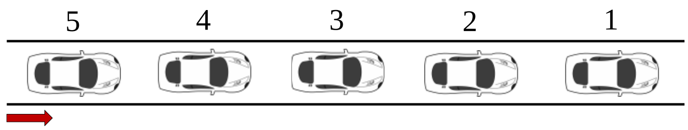

Figure 5-3: Trajectory construction order on a sample lane

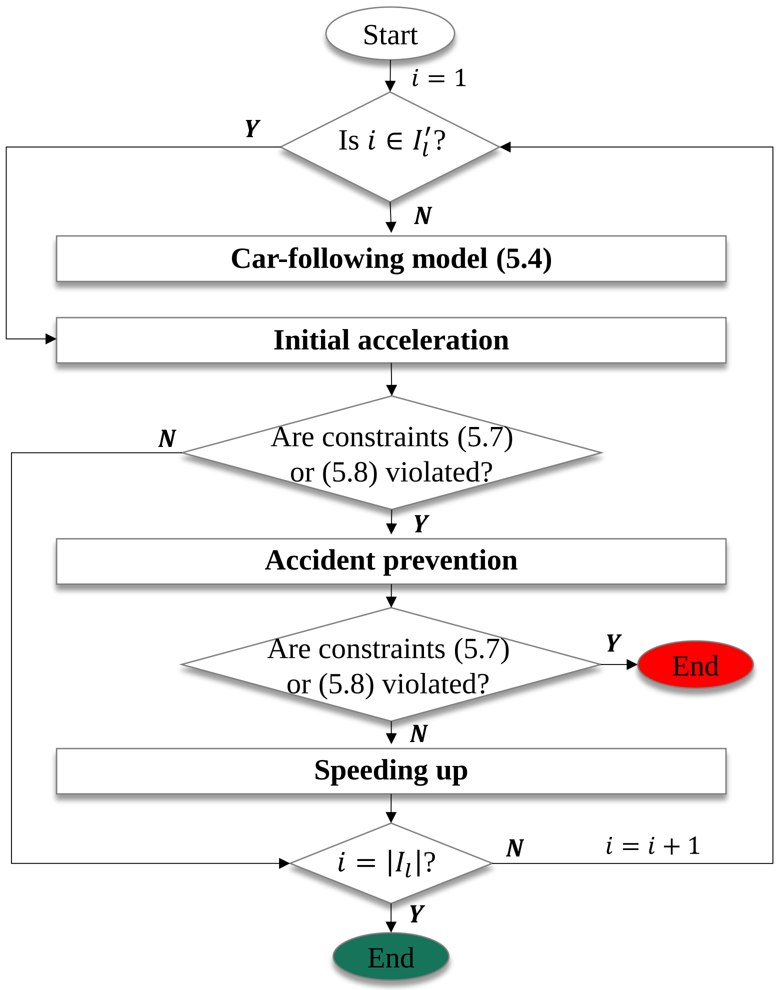

Figure 5-4: General steps of the proposed shooting heuristic for vehicles on lane $l \in L$ with a given signal timing plan.

- Red oval indicates termination caused by infeasibility.
- Green oval indicates successful trajectory construction.

5.3.1. Initial acceleration

Assume CAV i on lane l moving with speed $v_{il}^{t_0} < \bar{V}$ at time t_0. The initial acceleration step accelerates the CAV with a constant value $\bar{a}$ to reach the maximum speed to see if it can pass the intersection stop bar during a green time or not. Note that the CAV may need to stop behind a red light with its current speed while it could pass the intersection if accelerating to the maximum speed. Figure 5-5 shows a CAV trajectory with and without accelerating to the maximum speed. As it can be seen in Figure 5-5.a, keeping the CAV's initial speed traps the CAV behind a red light. However, Figure 5-5.b shows that accelerating to the maximum speed helps the CAV to reach at the intersection stop bar during a green time. After this step, the algorithm checks to see if safety constraints (5.7) and (5.8) are violated or not. If there is no safety constraint violation, the constructed trajectory is optimal. Otherwise, the algorithm moves to the next step as shown in Figure 5-6.

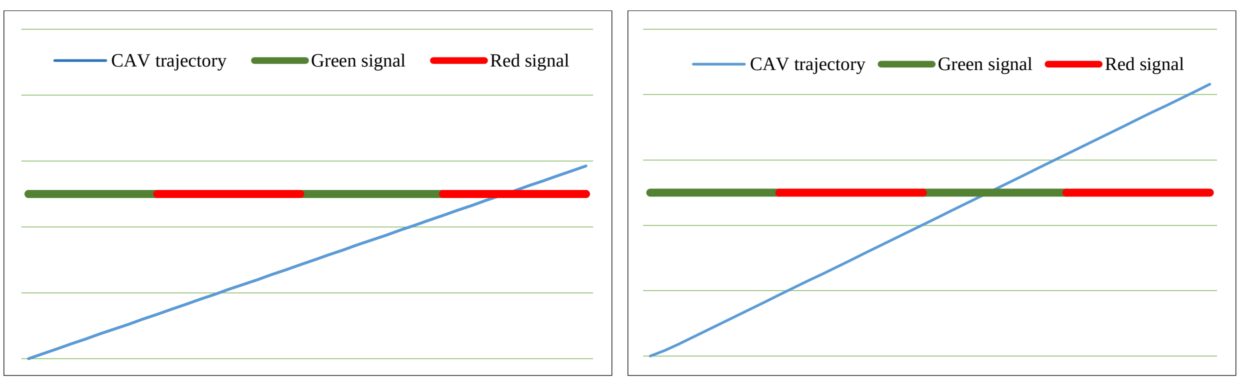

a. Without initial acceleration
b. With initial acceleration

Figure 5-5: A CAV trajectory with and without accelerating to the maximum speed

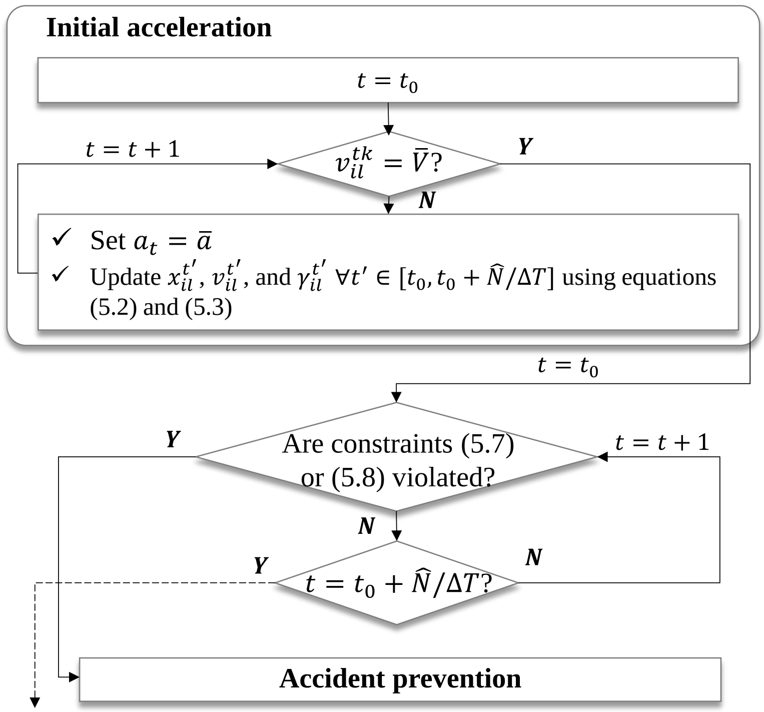

Figure 5-6: Initial acceleration step of the proposed shooting heuristic (Figure 5-4)

5.3.2. Accident prevention

If there is a safety constraint violation after the initial acceleration step, the accident prevention step gets activated to satisfy the safety constraints. Assume that safety constraints (5.7) or (5.8) are violated at time $t \in [t_0, t_0 + \widehat{N}/\Delta T]$. The algorithm moves backward from the violation time t, removes the first positive acceleration rate $\bar{a}$ if exists any, and checks safety constraints (5.7) and (5.8) again. This process continues until either there is no safety constraint violation or no positive acceleration rate before the violation time. If there is no safety constraint violation, the algorithm goes to the speeding up step to increase the CAV speed at any time during the time interval $t \in [t_0, t_0 + \widehat{N}/\Delta T]$ if possible. Otherwise, the algorithm moves backward from the violation time t, finds the first time step with acceleration rate of 0, and sets an acceleration rate of $\underline{a}$ at that time step. Then, checks for a safety constraint violation and goes through the same process until either all the acceleration rates from time $t' = t_0$ to the violation time $t' = t$ are equal to $\underline{a}$ or there is no safety constraint violation. The former scenario is associated with a case where there is a safety constraint violation (either a rear-end collision or red light running) where the CAV cannot satisfy the constraint with the maximum deceleration rate. Therefore, the signal timing plan resulting this trajectory is infeasible. On the other hand, the "speeding up" step is activated if the safety constraint violation is resolved at this step. The detailed steps of the algorithm are shown in Figure 5-7.

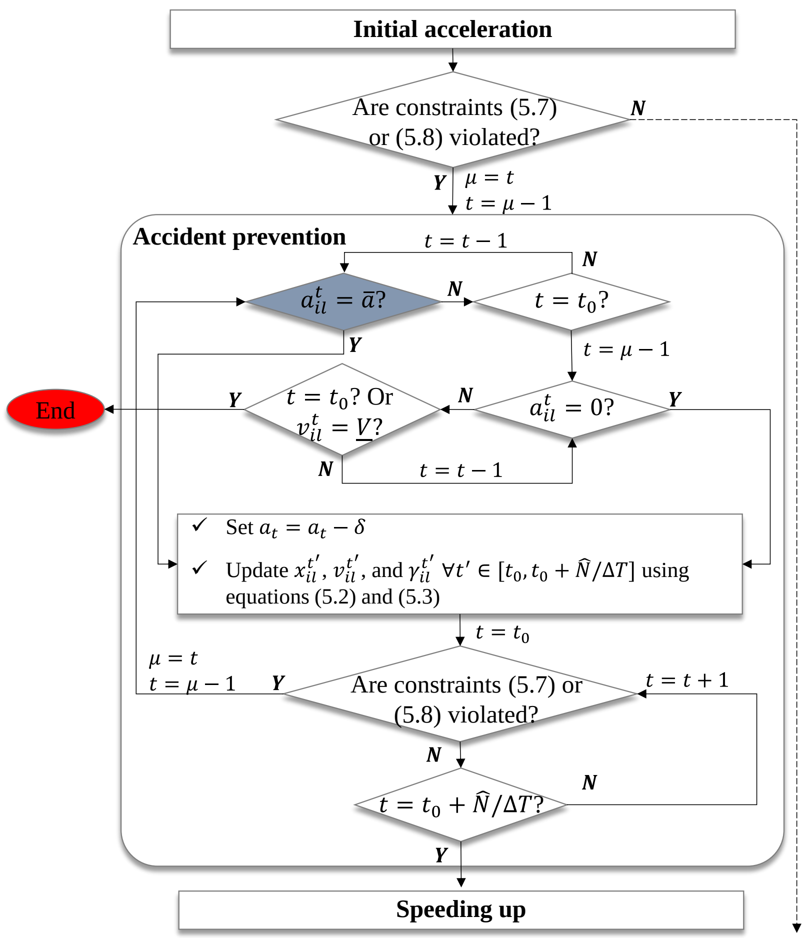

Figure 5-7: Accident prevention step of the proposed shooting heuristic (Figure 5-4)
- Blue tile shows the starting point of this step.

5.3.3. Speeding up

We execute this step if the "initial acceleration" step leads to a safety constraint violation, but the constraints are satisfied at "accident prevention" step. Therefore, there is no safety constraint violations in the current trajectory, which means that the constraints of the proposed MINLP ((5.2) - (5.14)) are satisfied. However, the current trajectory may be far from optimality since the only concern in the previous step was the feasibility of the trajectory. The trajectory of the CAV is pushed toward optimality in this step by speeding up at any time that does not lead to a safety constraint violation. This step starts from time $t = t_0$ and sets $a_{il}^t = \overline{a}$, if $v_{il}^t < \bar{V}$ and $a_{il}^t = 0$, then check the safety constraints (5.7) and (5.8). If there was a safety constraint violation, it sets $a_{il}^{t,k} = 0$ and $t = t + 1$, otherwise, it only updates the time $t = t + 1$. The same process continues until the end of the optimization horizon $t_0 + \widehat{N}/\Delta T$. Note that any acceleration rates with a value of $\underline{a}$ are not changed since they have been set by the previous step to prevent a safety constraint violation. See Figure 5-8 for detailed information about the algorithm.

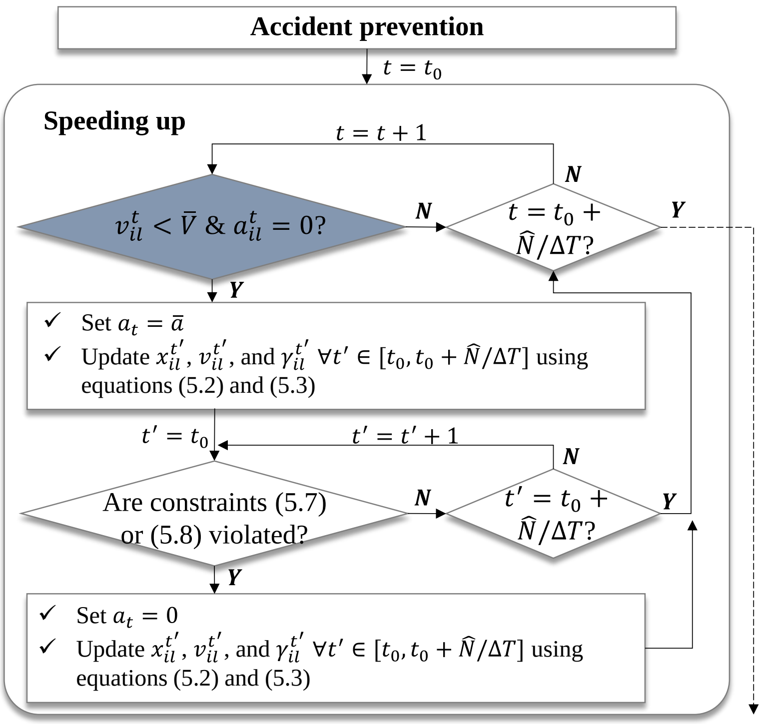

Figure 5-8: Speeding up step of the proposed shooting heuristic (Figure 5-4)

5.3.4. Case study

The case study is an isolated intersection with exclusive left and right turning lanes as shown in Figure 5-9. We assume a single lane for each movement of the intersection and assume that vehicles are in their preferred lanes prior to entering the intersection neighborhood. We tested our framework using four demands levels ranging from 300 $veh/hr/lane$ to 1200 $veh/hr/lane$ at 300 $veh/hr/lane$ increments for through movements. The demand for left and right turning movements are assumed to be 10% and 30% of the through demand, respectively. Demand levels are summarized in Table 5-2. Each demand level is tested with 11 CAV market shares ranging from 0% to 100% at 10% increments. Other parameters used in the case study are summarized in Table 5-3.

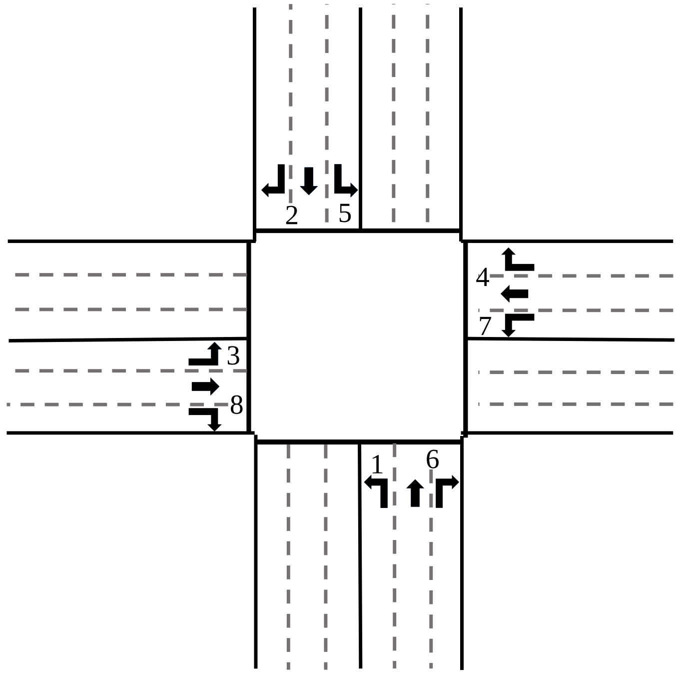

Figure 5-9: Case study intersection.

Table 5-2: The Demand levels for case studies

	Through demand ($veh/hr/lane$)	Right turning demand ($veh/hr/lane$)	Left turning demand ($veh/hr/lane$)
Demand level 1	300	90	30
Demand level 2	600	180	60
Demand level 3	900	270	90
Demand level 4	1200	360	120

Table 5-3: Value of the parameters used in the case study.

Parameters	Value
Maximum speed (ft/s)	39
Maximum acceleration (ft/s^2)	13
Minimum acceleration (ft/s^2)	-13
Human driver reaction time (s)	1
Automated vehicle reaction time (s)	0.1
Average length of vehicles (ft)	13
Safety distance between consecutive vehicles (ft)	11.8
Safety distance between CAVs and red signal light (ft)	1
Car-following parameter α_1 (s^{-1})	0.95
Car-following parameter α_2 (s^{-2})	0.25
Trajectory updating interval (s)	0.5
Signal status updating interval (s)	5

Table 5-3 (continued)

All red time (s)	2
Yellow time (s)	3
Minimum green time for through movements (s)	15
Minimum green time for left-turning movements (s)	5
Planning time horizon (s)	20
Study period (s)	900

5.3.5. Mobility

Table 5-4 summarizes the average delay for different demand levels and CAV market shares. Average delay for all demand levels decreases as the CAV market share increases while the reduction rate increases as the demand increases. This is an indication of successful and efficient operation of CAVs under different demand levels ranging from undersaturated to oversaturated. The changes in average delay are marginal with low demand levels (Demand levels 1 and 2) since the vehicle queues can be completely discharged at each cycle. On the other hand, significant changes in average delay are reported under high demand levels (demand levels 3 and 4) since vehicle queues build up over time with low CAV market shares. As the CAV market share increases, more efficient operation of them helps the entire fleet to clear vehicle queues that leads to significant delay reductions.

Table 5-4: Average delay for different demand levels and CAV market shares in seconds

Demand level	**CAV market share (%)**										
	0	**10**	**20**	**30**	**40**	**50**	**60**	**70**	**80**	**90**	**100**
1	13.14	13.09	13.04	12.91	12.82	12.79	12.72	12.69	12.62	12.51	12.39
2	16.15	15.6	15.38	15.17	15.01	14.82	14.54	14.52	14.38	14.28	14.2
3	34.09	28.55	24.17	20.05	18.03	16.42	15.79	15.67	15.46	15.32	15.21
4	42.15	39.86	36.23	34.79	33.18	29.05	28.55	26.42	25.15	22.84	21.02

Average CAV and CHV delays with different CAV market shares under demand level 4 are shown in Figure 5-10. Average CAV delay is always less than average CHV delay due to their higher performance and advance knowledge of signal timing plans and decisions of other CAVs.

In addition, average delay for both vehicle types decrease as the CAV market share increases. This is due to higher queue discharge rate in presence of CAVs that not only leads to shorter delay times for vehicles on the active lane group but also leaves longer portions of the cycle for the conflicting lane groups.

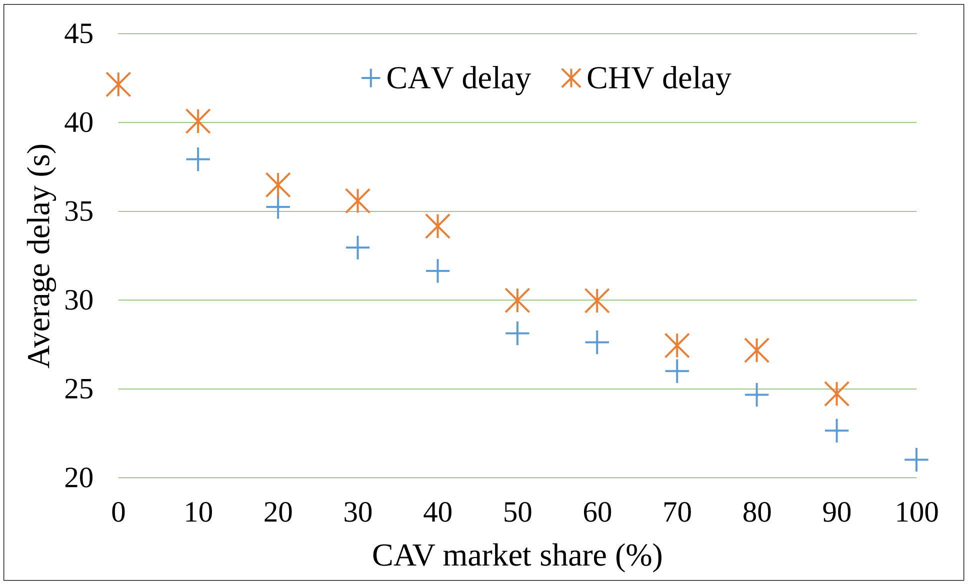

Figure 5-10: Average CAV and CHV delays with different CAV market shares under demand level 4

Figure 5-11 shows the latent demand with different CAV market shares under demand level 4. Latent demand normally happens due to long queues behind the intersection stop bar that prevents vehicles from entering the intersection neighborhood. Latent demand shows a strictly decreasing trend with an increase in CAV market share and becomes zero at 90% CAV market share. CAVs help discharge the queues in a more efficient way by more efficient operation of themselves due to shorter reaction times and advance knowledge of signal timing plans. Hence, they provide more space for their following CHVs to accelerate and clear the queue faster.

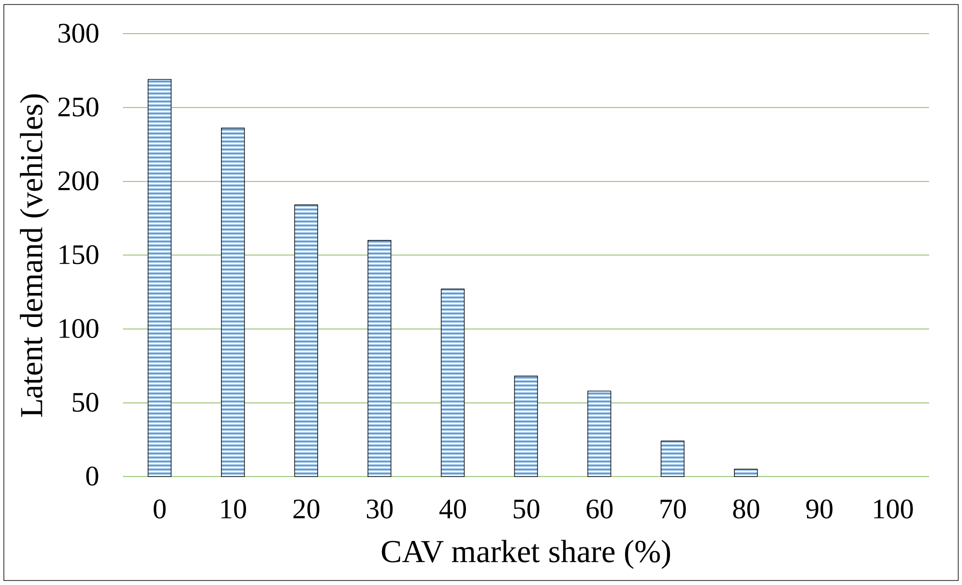

Figure 5-11: Latent demand with different CAV market shares under demand level 4

Figure 5-12 shows intersection signal timing plans for different CAV market shares under demand level 4. The length of green phases decreases as the CAV market share increases. This shows that the more efficient operation of the fleet in presence of higher number of CAVs leads to shorter green times to clear the queue behind the intersection stop bar. As a result, active lane groups are changed more frequently with higher CAV market shares that leads to shorter stopping and delay times.

Figure 5-13 shows vehicle trajectories on eastbound through lane of the intersection under the highest demand level and different CAV market shares. In this figure, blue lines show CAV trajectories while CHV trajectories are shown with pink lines. As it can be seen, vehicles tend to move smoother with a fewer number of stops as the CAV market share increases. In addition, queue length decreases with an increase in CAV market share due to the higher performance of CAVs. CAVs' shorter reaction time and their knowledge of upcoming signal timing plans help them move in a more compact way. Therefore, they can be operated in shorter green time duration that more visible in Figure 5-13.f.

a) 0% CAV market share

b) 20% CAV market share

c) 40% CAV market share

d) 60% CAV market share

e) 80% CAV market share

f) 100% CAV market share

Figure 5-12: Signal timings for different CAV market shares under deman level 4.

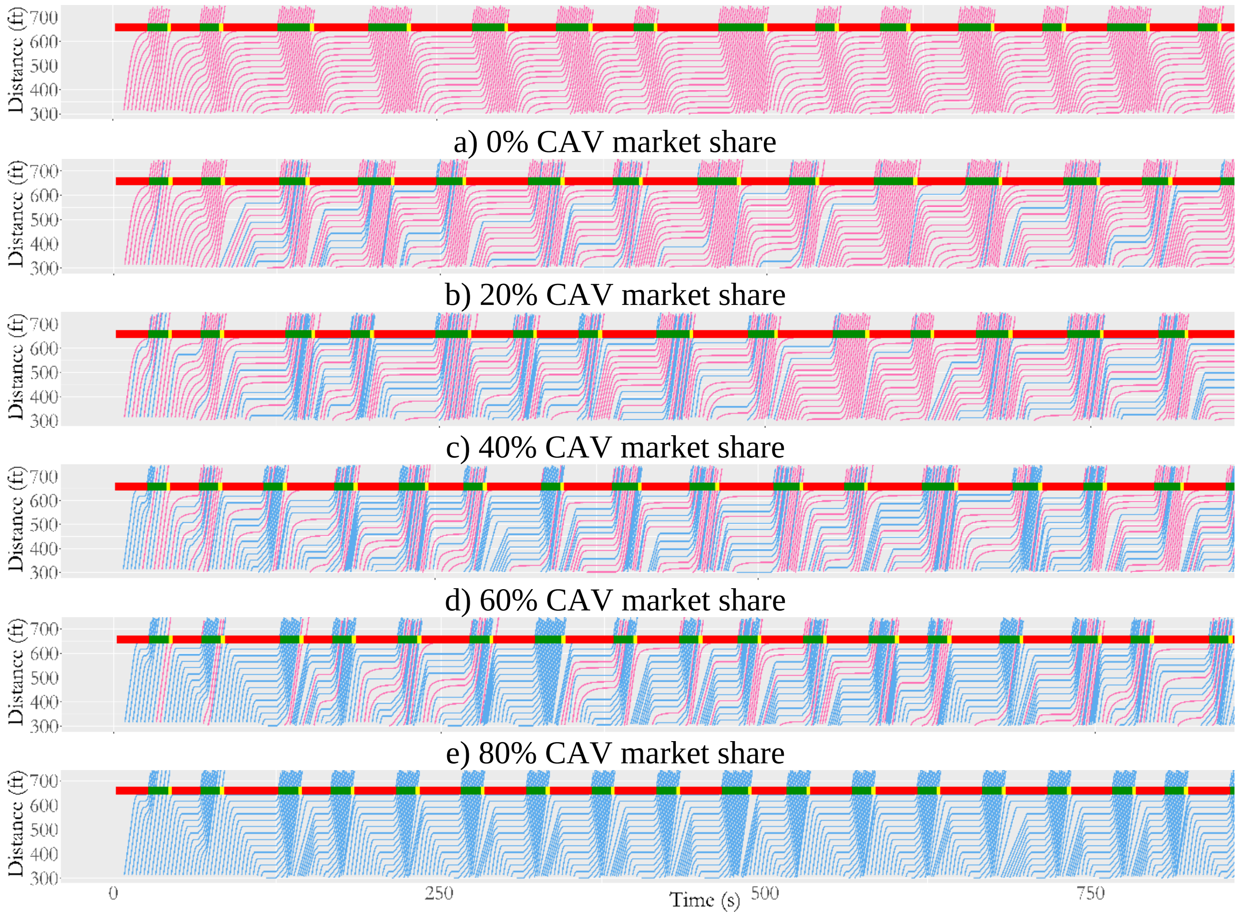

a) 0% CAV market share

b) 20% CAV market share

c) 40% CAV market share

d) 60% CAV market share

e) 80% CAV market share

f) 100% CAV market share

Figure 5-13: Vehicle trajectories for different CAV market shares under deman level 4.

5.3.6. Computation time

Maximum, minimum, average, and standard deviation of the computation times of the proposed framework under the highest demand level and different CAV market shares are shown in Table 5-5. The proposed framework is capable of providing signal timing and vehicle trajectory decisions in at most 39.97 milliseconds, which is twelve times shorter than the 500 millisecond-long time step length. It can be seen that the average run time increases as the CAV market share increases and reaches its maximum value when the CAV market share is 90%. This is due to different ways of constructing trajectories for different vehicle types. CHV trajectories are estimated directly using a customized car-following model, which takes a very short amount of time. On the other hand, CAV trajectories are constructed with an algorithm that requires safety measurements, which takes more time than the car-following model. However, the average run time with a fully CAV fleet is shorter than the case with 90% CAVs. This can be due to more efficient operation of the fleet with a fully CAV fleet that leads to a fewer number of vehicles in the intersection neighborhood.

Table 5-5: Maximum, minimum, average, and standard deviation of the computation times for different demand levels and CAV market shares in milliseconds

	CAV market share (%)										
	0	**10**	**20**	**30**	**40**	**50**	**60**	**70**	**80**	**90**	**100**
Maximum	4.61	27.45	16.82	33.51	24.42	27.45	36.02	32.07	39.97	37.66	28.58
Minimum	0.02	0.08	0.07	0.08	0.09	0.10	0.09	0.09	0.10	0.10	0.09
Average	0.09	0.69	1.08	1.44	1.67	1.77	2.17	2.27	2.46	2.58	2.48
Standard deviation	0.20	1.61	2.24	2.91	3.14	3.24	3.99	4.00	4.33	4.50	4.26

The distribution of the computation time under demand level 4 with 80% CAVs is shown in Figure 5-14. The proposed framework could find the proper signal timing plans and vehicle trajectories for most of the time steps in less than 5 milliseconds. There are only four time steps with a computation time of more than 25 milliseconds.

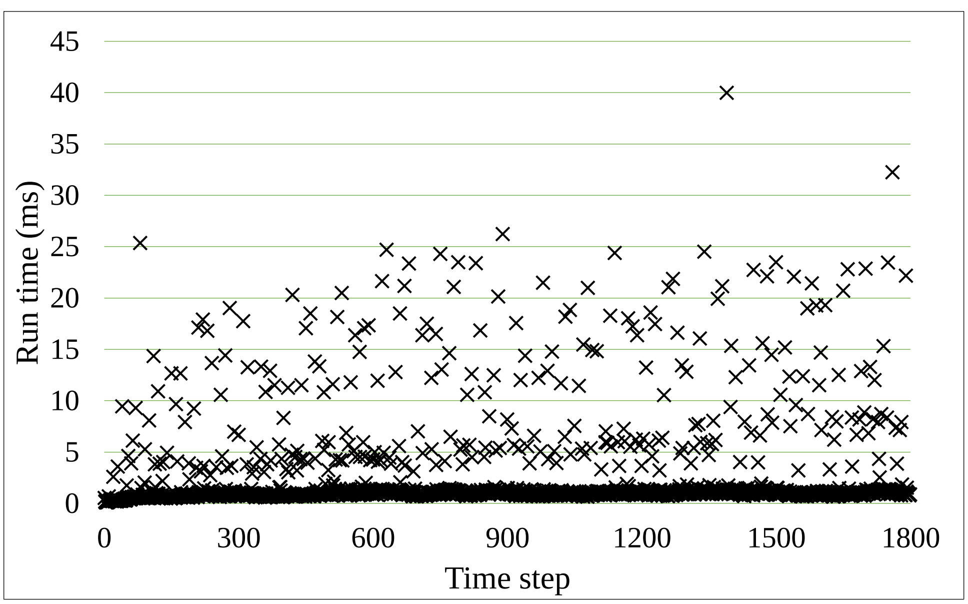

Figure 5-14: Compution time for demand level 4 with 80% CAV market share

5.3.7. Safety

We have used the surrogate safety assessment model (SSAM) software (Gettman and Head, 2003) to analyze possible rear-end and crossing collisions during the study periods considering the time to collision (TTC) as the surrogate safety measure. The results of the analysis show no near crash condition with a TTC of less than 1.5 seconds. In addition, no crossing near crash condition with a TTC of less than 10 seconds is reported by the software. Average rear-end TTC for different demand levels and CAV market shares are shown in Figure 5-15. As it can be seen, average TTC decreases as the CAV market share increases since CAVs have a shorter reactions time than CHVs. In addition, average TTC decreases as the demand increases with a given CAV market share. This is because there are more interactions between vehicles, and they are operated in a more compact way as the demand increases.

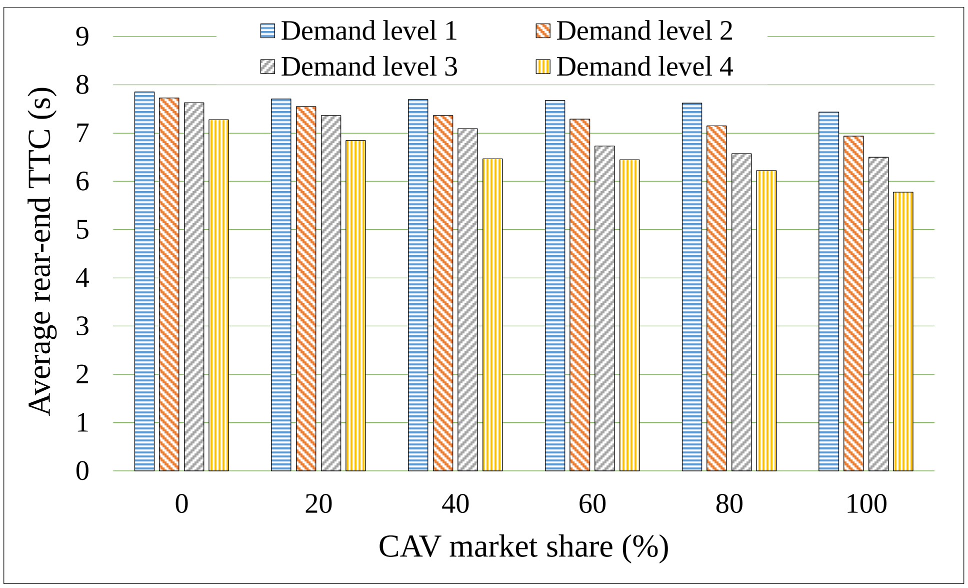

Figure 5-15: Average rear-end TTC for different demand levels and CAV market shares.

5.4. Conclusion

This chapter introduces a shooting heuristic to operate a mixed fleet of CAVs and CHVs through a signalized intersection. Trajectories of CHVs are estimated using a customized car-following model while CAV trajectories are constructed using the proposed shooting heuristic that considers rear-end accident and red light running avoidance constraints. Due to different signal timing and trajectory updating time intervals, the framework either jointly optimizes the signal and trajectory decisions or only optimizes vehicle trajectories with a given signal timing plan. In time steps that joint signal and trajectory optimization is involved, the framework constructs/estimates vehicle trajectories for each feasible signal timing plan and chooses the signal timing plan that leads to the best objective value. The proposed framework is applied to an isolated intersection considering four demand levels and eleven CAV market shares ranging from 0% to 100% at increments of 10%. The case study results show the capability of the proposed framework in providing signal timings and vehicle trajectories in at most 40 milliseconds that is much shorter than the 500 milliseconds-long time step length. In addition, average delay decreases as the CAV market share increases.

CHAPTER 6: REAL-TIME SIGNAL AND TRAJECTORY OPTIMIZATION IN MIXED-AUTONOMY TRAFFIC STREAMS IN PRESENCE OF THE WHITE PHASES

Previous chapter presented an efficient algorithm to operate vehicles through an isolated intersection. The algorithm is fast enough to be used as a subroutine for network-level signal and trajectory optimization algorithms. However, it uses green and red signal indications to control the mixed fleet. Therefore, the intersection controller has to stop vehicles using a red light to ensure the safety of the fleet even within a fully CAV environment. Nevertheless, it is possible to use the white phase concept proposed in Chapter 3 to operate vehicles from conflicting movements simultaneously within mixed-autonomy environments by extending the shooting heuristic-based joint signal and trajectory optimization algorithm proposed in Chapter 5 to accommodate the white phase concept.

6.1. Research gaps and contributions

Existing literature mostly focuses on intersection-level signal and trajectory optimization methods. Hence, they provide real-time solutions for an isolated intersection. However, network-level signal and trajectory optimization algorithms may need to solve the intersection-level optimization model several times to make a proper coordination among intersections. Therefore, an intersection-level signal and trajectory optimization algorithm needs to be fast enough to be executed multiple times within one updating time step length. In addition, most of the available intersection signal control frameworks use only signal heads to control the movements of mixed-autonomy fleets. However, research evidence shows that sufficiently penetrated vehicular fleet can be controlled by using CAVs as mobile controllers (Niroumand et al., 2022, 2021, 2020b, 2020a).

This study builds upon the shooting heuristic-based methodology presented in Chapter 5 and the white phase concept and formulation introduced in Chapter 3. CAVs are used as continuous mobile controllers during a proportion of the cycle indicated as the white phase. The intersection controller can operate the intersection using the traditional green and red signals when there are not enough CAVs in the intersection neighborhood. On the other hand, the intersection controller can operate vehicles from conflicting movements of the intersection during the white phases when the fleet is sufficiently penetrated. Note that the safety of the shared fleet is ensured by controlling the movements of CAVs as mobile controllers. A shooting heuristic-based framework is developed to find proper signal timing plans and construct/estimate vehicle trajectories in real-time.

6.2. Problem formulation

We have introduced an MINLP formulation in our previous studies to process CAVs through an isolated intersection. We revisit the formulation developed in (Niroumand et al., 2020a) as it allows a mixed fleet of CAVs and CHVs. We define two updating time intervals for trajectory and signal timing updates, i.e., ΔT and $\Delta \hat{T}$ and let T and $\hat{T}$ be the set of trajectory update and signal timing update time steps, respectively. The decision variables of this formulation are the acceleration rate a_{il}^{t} of vehicle $i \in I_l$ on lane $l \in L$ at time $t \in T$ for trajectory optimization and green g_l^n and white w_l^n signal indications for lane $l \in L$ at time $n \in \hat{T}$ for signal optimization. Table 6-1 summarizes the notations used in the formulation.

Table 6-1: The notations used in the problem formulation

Sets	
L	Set of all lanes
T	Set of all time steps for trajectory updates
$\hat{T}$	Set of all time steps for signal timing updates
I_l	Set of all vehicles on lane $l \in L$
$I_l{}'$	Set of all CAVs on lane $l \in L$
$\hat{I}_l$	Set of all CHVs on lane $l \in L$
C_l	Set of all conflicting lanes with lane $l \in L$
P_l	Set of vehicle-groups on lane $l \in L$

Table 6-1 (continued).

Decision Variables	
a_{il}^t	Acceleration of vehicle $i \in I_l$ on lane $l \in L$ at time $t \in T$
g_l^n	Binary decision variable; 1 if signal for lane $l \in L$ at time step $n \in \hat{T}$ is green, 0 otherwise
w_l^n	Binary decision variable; 1 if signal for lane $l \in L$ at time step $n \in \hat{T}$ is white, 0 otherwise
y_l^n	Binary decision variable; 1 if signal for lane $l \in L$ at time step $n \in \hat{T}$ is yellow, 0 otherwise
Other Variables	
x_{il}^t	The location of vehicle $i \in I_l$ on lane $l \in L$ at time $t \in T$
v_{il}^t	The speed of vehicle $i \in I_l$ on lane $l \in L$ at time $t \in T$
γ_{il}^t	1 if vehicle $i \in I_l$on lane $l \in L$ has passed intersection by $t \in T$ or 0 otherwise.
h_{ql}^t	The head location of vehicle-group $q \in P_l$ on lane $l \in L$ at time $t \in T$
e_{ql}^t	The tail location of vehicle-group $q \in P_l$ on lane $l \in L$ at time $t \in T$
ζ_{ql}^t	The length of vehicle-group $q \in P_l$ on lane $l \in L$ at time $t \in T$
Parameters	
$\underline{a}$ and $\overline{a}$	Lower and upper bounds for acceleration
$\underline{v}$ and $\overline{v}$	Minimum and maximum speeds
$\mathcal{L}$	Vehicle length
D	Minimum safety distance between two consecutive vehicles on the same lane
S	Minimum safety distance between vehicles and the intersection stop bar
$\hat{\tau}$	Reaction time for CHVs
τ'	Reaction time for CAVs
$F_{kk'}$	The location of conflict point between lane $k \in L$ and lane $k' \in C_k$ based on the coordination of lane k
b_l	The position of intersection in lane $l \in L$
$\underline{G}$ and $\overline{G}$	Minimum and maximum green times
$\underline{W}$	Minimum white time
Y	Yellow time duration
ΔT	Time step size for trajectory updates
$\Delta \hat{T}$	Time step size for signal updates
r_l	The destination location of vehicles on lane $l \in L$
α_1 and α_2	Car-following parameters
$\mathcal{R}$	Duration of all-red time
ξ_{ql}	The order of the first vehicle of vehicle-group $q \in P_l$ on lane $l \in L$
μ_{ql}	The order of the last vehicle of vehicle-group $q \in P_l$ on lane $l \in L$

The objective function of the mathematical program aims to minimize the relative distance between a vehicle's location and its predefined destination (r_l) as shown in (6.1). The location and speed of vehicle $i \in I_l$ on lane $l \in L$ are updated based on acceleration rates at time step $t \in T$ as shown in Equations (6.2) and (6.3), respectively. Constraints (6.4) are customized based on Helly's linear car-following model to estimate the movements of CHVs. Based on these constraints, human drivers react to speed and distance differences relative to their immediate front vehicle. This car-following model takes into account the drivers' reaction to the status of signal timing indications as well. where $\overline{a}$ and $\underline{a}$ are maximum and minimum acceleration rates, $\overline{v}$ and $\underline{v}$ are maximum and minimum speed, α_1 and α_2 are car-following parameters that are suggested to take values from [0.17, 1.3] and $[\frac{1}{4}\alpha_1, \frac{1}{2}\alpha_1]$, respectively (Askari et al., 2016; Brackstone and McDonald, 1999), $\mathcal{L}$ is the length of vehicles, D is the minimum safety distance between two consecutive vehicles, $\hat{\tau}$ is human driver's reaction time, b_l is the location of intersection stop bar in the coordination of lane $l \in L$, and S is the minimum safety distance between vehicles and intersection stop bar.

Constraints (6.5) and (6.6) respectively define the maximum and minimum acceleration rate and speed for CAV trajectory optimization. Constraints (6.7) prevent rear-end collisions between CAVs and the vehicle directly in front of them by keeping the distance between two consecutive vehicles as a function of minimum safety distance (D), length of vehicles ($\mathcal{L}$), and the distance traveled during the reaction time of CAVs ($\tau' v_{il}^t$), where τ' is the reaction time of CAVs. Constraints (6.8) are used to prevent CAVs from entering the intersection during red phases. Vehicle $i \in I_l'$ on lane $l \in L$ at time step $t \in T$ should stop behind the intersection stop bar with a safe distance S when the signal indication is red. These constraints will be relaxed when the signal indication is green or white or vehicle i has passed the intersection stop bar. Since time steps in this study are not continuous, the term $\Delta T v_{il}^t$ is added to constraints (6.8) to keep vehicles from jumping from the intersection stop bar in one time step without violating these constraints during red phases.

We define a vehicle-group as a group of CHVs led by a CAV during white phases. Figure 6-1 shows such a vehicle group that starts from vehicle 2 and ends with vehicle 4. Constraints (6.9) - (6.11) are used to connect vehicle-level variables and vehicle-group-level variables by defining the head location, tail location, and length of vehicle group $q \in P_l$ on lane $l \in L$ at time $t \in T$, respectively. Note that ξ_{ql} and μ_{ql} are the order of the first and last vehicle in vehicle group $q \in P_l$ on lane $l \in L$, respectively. For example, the first and last vehicles in the vehicle group shown in Figure 6-1 are the second and the fourth vehicles on the lane. Therefore, ξ_{ql} is equal to 2 and μ_{ql} is equal to 4. Constraints (6.12) ensure collision free movement of vehicle group $k \in P_j$ on lane $j \in L$ and vehicle group $q \in P_l$ on lane $l \in C_j$ during the white phase. Note that these constraints are relaxed if at least one of the lane groups is receiving a non-white signal indication.

Constraints (6.13) prevent conflicting lane $l' \in C_l$ from receiving green, white, or yellow signal indications when lane $l \in L$ is receiving green signal status. Constraints (6.14) and (6.15) ensure that the green signal duration for lane $l \in L$ is shorter than a predefined maximum green time ($\overline{G}$) and longer than a predefined minimum green time ($\underline{G}$), respectively. Similarly, constraints (6.16) impose a lower bound on the duration of the white phase for lane $l \in L$. Constraints (6.17) states that lane $l \in L$ should receive yellow signal status for a predefined value Y. Constraints (6.18) and (6.19) ensure that lane $l \in L$ should receive yellow signal indication after end of green and white signal indications, respectively. Constraints (6.20) impose all-red time after end of yellow signal indication before switching the active movements for clearance purpose. Finally, constraints (6.21) state that white signal phase for lane $l \in L$ at time $n \in \hat{T}$ can start only if the first vehicle behind the intersection stop bar is a CAV.

$$Z = \min \textstyle\sum_{t \in T} \sum_{l \in L} \sum_{i \in I_l} (r_l - x_{il}^t) \tag{6.1}$$

$$x_{il}^{t+\Delta T} = x_{il}^t + v_{il}^t \Delta T + \frac{1}{2} a_{il}^t \Delta T^2, \qquad \forall i \in I_l, l \in L, t \in T, \tag{6.2}$$

$$v_{il}^{t+\Delta T} = v_{il}^t + a_{il}^t \Delta T, \qquad \forall i \in I_l, l \in L, t \in T, \tag{6.3}$$

$$a_{il}^t = \max \left\{ \underline{a}, \frac{\underline{v} - v_{il}^t}{\Delta T}, \min \left\{ \begin{array}{c} \overline{a}, \\ \frac{\overline{v} - v_{il}^t}{\Delta T}, \\ \alpha_1 \left(v_{il}^t - v_{i-1,l}^t \right) + \alpha_2 \left((x_{il}^t - x_{i-1,l}^t - \mathcal{L}) - D - v_{il}^t \hat{\tau} \right), \\ \alpha_1 \left((w_l^n + g_l^n) \overline{v} - v_{il}^t \right) + \alpha_2 \left((b_l - x_{il}^t) - (1 - w_l^n - g_l^n) S \right) + M \gamma_{il}^t, \end{array} \right\} \right\}, \tag{6.4}$$

$$\forall i \in \hat{I}_l, l \in L, t \in T, n \in \hat{T},$$

$$\underline{a} \le a_{il}^t \le \overline{a}, \qquad \forall i \in I_l{}', l \in L, t \in T, \tag{6.5}$$

$$\underline{v} \le v_{il}^t \le \overline{v}, \qquad \forall i \in I_l{}', l \in L, t \in T, \tag{6.6}$$

$$x_{i-1,l}^t - x_{il}^t \ge D + \mathcal{L} + \tau' v_{il}^t, \qquad \forall i \in I_l{}', l \in L, t \in T, \tag{6.7}$$

$$b_l - x_{il}^t \ge S + \Delta T v_{il}^t - (g_l^n + y_l^n + w_l^n) M - \gamma_{il}^t M, \qquad \forall i \in I_l{}', l \in L, t \in T, n \in \hat{T}, \tag{6.8}$$

$$h_{qj}^t = x_{\xi_{qj} j}^t, \qquad \forall q \in P_j, j \in C_l, l \in L, t \in T, \tag{6.9}$$

$$e_{qj}^t = x_{\mu_{qj} j}^t - \mathcal{L}, \qquad \forall q \in P_j, j \in C_l, l \in L, t \in T, \tag{6.10}$$

$$\zeta_{qj}^t = h_{qj}^t - e_{qj}^t, \qquad \forall q \in P_j, j \in C_l, l \in L, t \in T, \tag{6.11}$$

$$\left| h_{qj}^t - F_{jl} \right| + \left| e_{qj}^t - F_{jl} \right| + \left| x_{il}^t - F_{lj} \right| + \left| x_{il}^t - \mathcal{L} - F_{lj} \right| \ge \zeta_{qj}^t + \mathcal{L} + 2\rho + M(\gamma_{il}^t + \gamma_{\xi_{qj} j}^t + w_l^n + w_j^n - 4), \tag{6.12}$$

$$\forall i \in I_l', l \in L, q \in P_j, j \in C_l, t \in T, n \in \hat{T},$$

$$g_l^n + g_{l'}^n + y_{l'}^n + w_{l'}^n \le 1, \qquad \forall l \in L, l' \in C_l, n \in \hat{T}, \tag{6.13}$$

$$\sum_{z=n}^{n+\overline{G}} g_l^z \le \overline{G}, \qquad \forall l \in L, n \in \hat{T}, \tag{6.14}$$

$$\sum_{z=n+1}^{n+\underline{G}} g_l^z \ge (g_l^{n+1} - g_l^n) \underline{G}, \qquad \forall l \in L, n \in \hat{T}, \tag{6.15}$$

$$\sum_{z=n+1}^{n+\underline{W}} w_l^z \ge (w_l^{n+1} - w_l^n) \underline{W}, \qquad \forall l \in L, n \in \hat{T}, \tag{6.16}$$

$$\sum_{z=n}^{n+Y} y_l^z \le Y, \qquad \forall l \in L, n \in \hat{T}, \tag{6.17}$$

$$\sum_{z=n+1}^{n+Y} y_l^z \ge (g_l^n - g_l^{n+1}) Y, \qquad \forall l \in L, n \in \hat{T}, \tag{6.18}$$

$$\sum_{z=n+1}^{n+Y} y_l^z \ge (w_l^n - w_l^{n+1}) Y, \qquad \forall l \in L, n \in \hat{T}, \tag{6.19}$$

$$\sum_{z=n}^{n+\mathcal{R}-1} (g_l^z + g_{l'}^z + y_l^z + y_{l'}^z + w_l^z + w_{l'}^z) - \mathcal{R} y_l^n + \mathcal{R} y_l^{n-1} \le \mathcal{R}, \qquad \forall l \in L, l' \in C_l, n \in \hat{T}, \tag{6.20}$$

$$w_l^n \le 1 - \left(\gamma_{i-1,l}^t - \gamma_{il}^t \right) + w_l^{n-1}, \qquad \forall j \in \hat{I}_l, l \in L, n \in \hat{T}, t \in T. \tag{6.21}$$

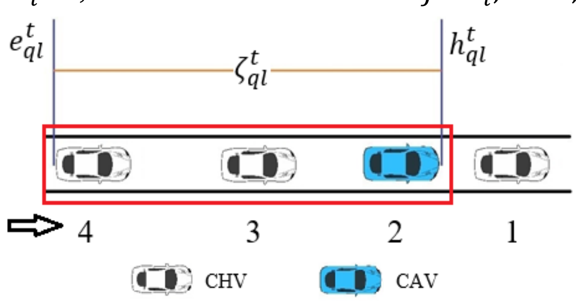

Figure 6-1: Head location, tail location, and length of a vehicle group

6.3. Solution Technique

Similar to the previous chapter, we introduce a bi-level solution technique to solve the joint signal and trajectory optimization model. The proposed problem formulation and solution technique is also embedded in a receding horizon framework to both reduce the complexity of the problem and account for the dynamic nature of it. At each decision time step, the optimization model is solved over a planning time horizon $\widehat{N}$ instead of the entire study period N. This framework first initializes the state of the system consisting of the location $x_{il}^{t_0}$ and speed $v_{il}^{t_0}$ of vehicle $i \in I_l$ on lane $l \in L$ at time $t_0 \in T$ and the current state of the intersection's signal, including green $g_l^{n_0}$, white $w_l^{n_0}$, and yellow $y_l^{n_0}$ statuses for lane $l \in L$ at time $n_0 \in \hat{T}$. Due to the more dynamic nature of the trajectory related variables, the acceleration rates of vehicles are updated more frequently than the signal timing parameters. Therefore, the algorithm either solves a joint signal and trajectory optimization problem or optimizes the trajectories of CAVs with a given set of signal timing plans. At time steps that joint signal and trajectory optimization is involved, the algorithm finds proper signal timing plans during period $n \in [n_0, n_0 + \widehat{N}/\Delta\hat{T}]$ and CAV trajectories during period $t \in [t_0, t_0 + \widehat{N}/\Delta T]$. Otherwise, the signal timing plan is fed to the algorithm and only CAV trajectories are constructed during period $t \in [t_0, t_0 + \widehat{N}/\Delta T]$. Then, the optimal acceleration rate a_{il}^t for vehicle $i \in I_l$ on lane $l \in L$ at time step $t = t_0 + 1$ will be implemented. Furthermore, the optimal signal timing parameters including green g_l^n, white w_l^n, and yellow y_l^n signal indications for lane $l \in L$ at time step $n = n_0 + 1$ will be implemented to control intersection signal. After the implementation step, the algorithm rolls one trajectory time step forward, updates the state of the system, solves the optimization model, and repeats the same process until the end of the study period N. The general steps of the proposed receding horizon framework is shown in Figure 6-2.

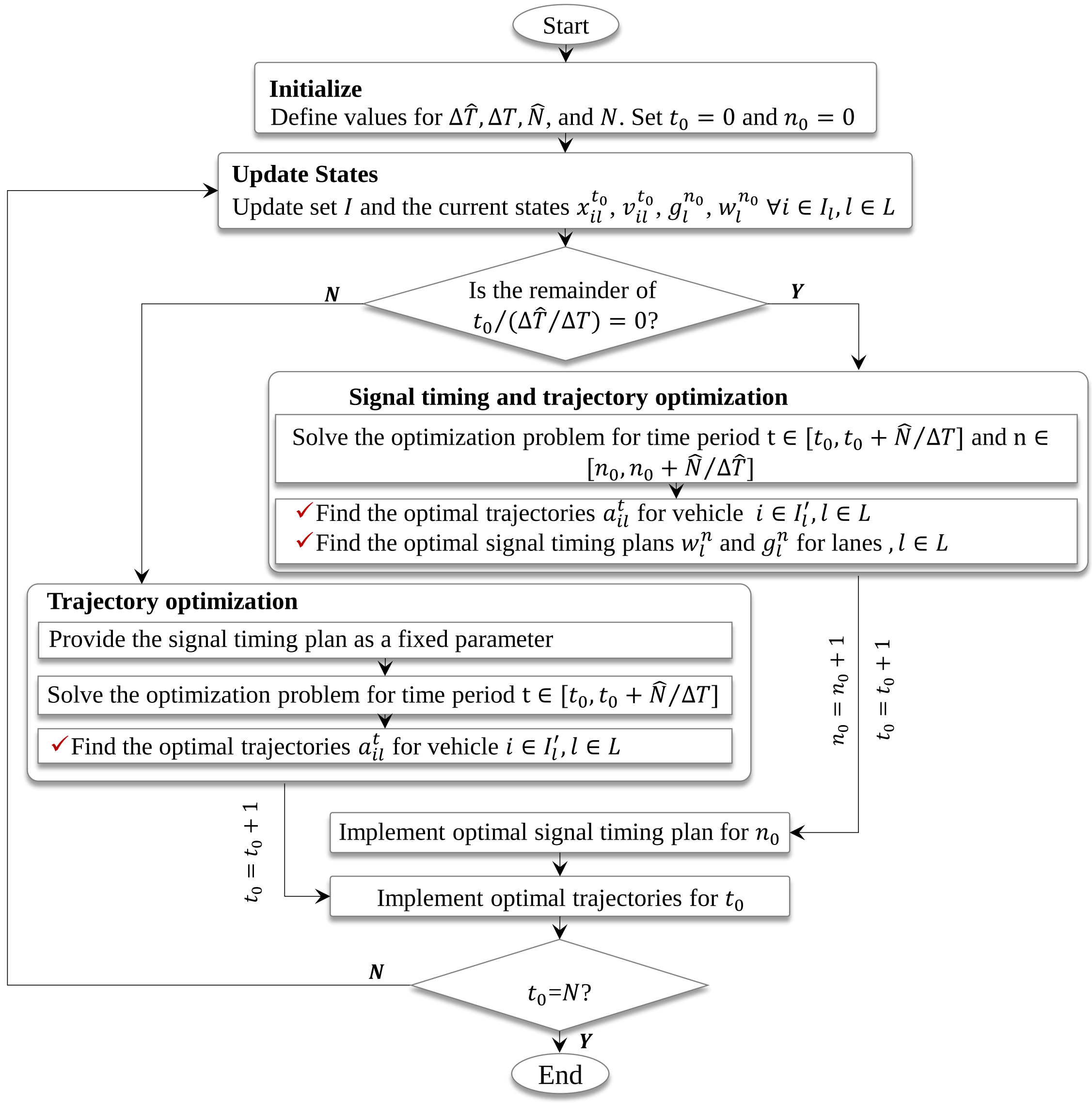

Figure 6-2: Receding horizon control general steps

We introduce a bi-level algorithm to solve the joint intersection signal timing and CAV trajectory optimization problem for an isolated intersection.

6.3.1. Upper level

The upper level of this algorithm enumerates all feasible signal timing plans to find the signal timing plan with the best objective value. The lower level, constructs CAV trajectories and estimates the movements of CHVs for a given set of signal timing plans, then sends the associated objective value to the upper level. We assume six signal phases according to Figure 6-3. Since no lane-group receives either green or white signal indications when its conflicting lane-groups receive a green signal indication, constraints (6.13) are satisfied. The upper level generates all possible combinations of phases, then prunes the ones that violate the minimum and maximum green time constraints (constraints (6.14) and (6.15)), minimum white time constraints (constraints (6.16)), and signal transition constraints (constraints (6.17) - (6.20)). Note that the white phase activation constraints (6.21) will be checked after executing the lower level when the trajectories are constructed.

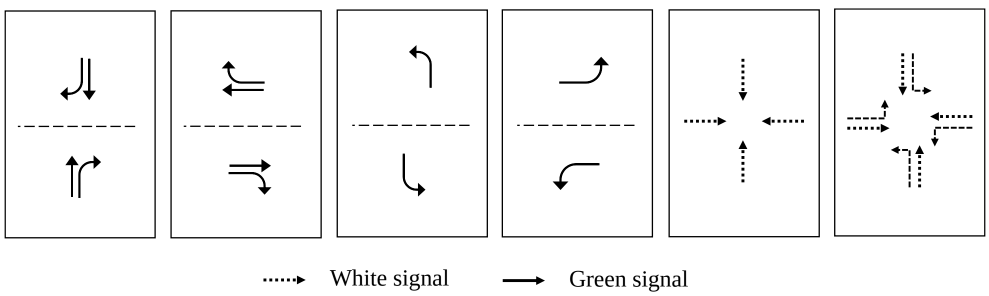

Figure 6-3: Intersection signal phases

6.3.2. Lower level

The lower level of the proposed algorithm uses a shooting heuristic to construct CAV trajectories and estimate the movements of CHVs. Note that the movements of CHVs are directly estimated using car-following model (6.4). We construct CAV trajectories using three acceleration rates a_{il}^t consisting of $\overline{a}$ for speeding up, $\underline{a}$ for slowing down, and 0 for keeping a constant speed, which satisfy the acceleration bounds defined in constraints (6.5). The proposed algorithm updates the location and speed of vehicles using constraints (6.2) and (6.3), maintains the defined bounds for the speed of CAVs in constraints (6.6), and continuously checks the safety constraints (6.7), (6.8), and (6.12). In the following, subsection 6.3.2.1 details the steps of the proposed shooting heuristic to construct trajectories for members of a single vehicle group. Then, subsection 6.3.2.2 provides an algorithm to construct trajectories for all vehicles at the neighborhood of the studied intersection.

6.3.2.1. Shooting heuristic for a single vehicle group

Trajectories of members of vehicle group $q \in P_l$ on lane $l \in L$ is constructed using the algorithm shown in Figure 6-4. This algorithm consists of three steps, namely initial acceleration, accident prevention, and speeding up. The initial acceleration step speeds up the CAV leader of the vehicle group to its maximum speed to not miss any available green time due to a low speed. Note that the trajectories of CHV followers of the vehicle group are estimated using car-following model (6.4) after applying any change to the trajectory of the CAV leader to update vehicle group variables. If the current set of trajectories satisfy safety constraints (6.7), (6.8), and (6.12), the current trajectories are optimal. Otherwise, the accident prevention step is activated to satisfy the safety constraints by removing the positive acceleration rates set by the initial acceleration step. If removing the positive acceleration rates could not prevent the safety constraints violation, deceleration rates with the value of $\underline{a}$ is used to satisfy the constraints. If the accident prevention step cannot satisfy the safety constraints, the current signal timing plan is infeasible, and we move to the next signal timing plan generated by the upper level. Otherwise, the current set of trajectories are feasible, but may be sub-optimal. Therefore, the speeding up steps pushes the trajectories toward optimality by setting positive acceleration rates at any time step that does not lead to a safety constraint violation.

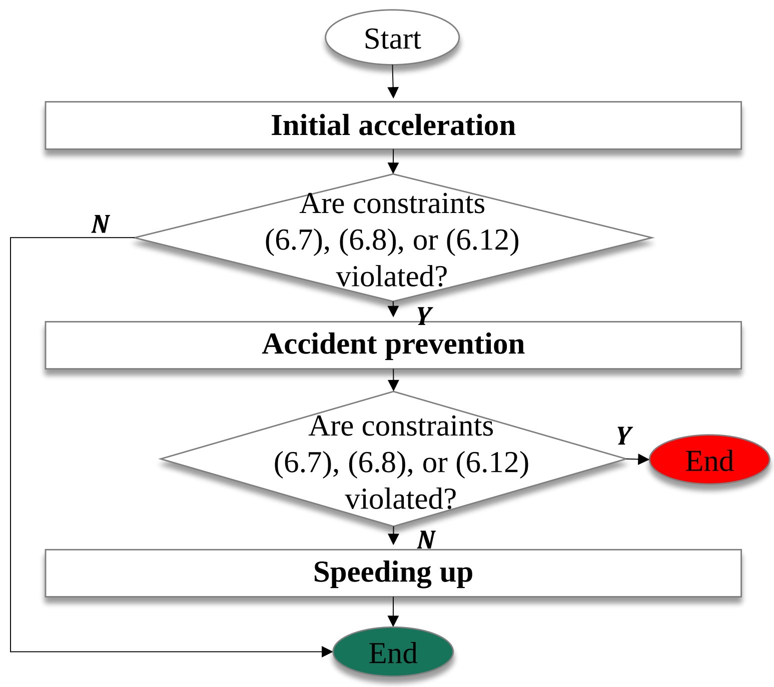

Figure 6-4: General steps of the proposed shooting heuristic for vehicle group $q \in P_l$ on lane $l \in L$ with a given signal timing plan.

- Red oval indicates termination caused by infeasibility.
- Green oval indicates successful trajectory construction.

6.3.2.1.1 Initial acceleration

Assume that a CAV belongs to vehicle group $q \in P_l$ on lane $l \in L$ and is moving with speed $v_{il}^{t_0} < \bar{V}$ at time t_0. The order of this CAV on lane $l \in L$ is defined by ξ_{ql}. In addition, this vehicle group has zero or more CHVs as its followers that can be denoted as $i \in (\xi_{ql}, \mu_{ql}]/\xi_{ql}$. For instance, the value of ξ and μ for the vehicle group shown in Figure 6-1 are 2 and 4. Therefore, the CAV leader of this vehicle group is the second vehicle on the lane and it has CHVs $i \in (2,4]$ as its followers. The initial acceleration step applies acceleration rates of $\bar{a}$ to increase the CAV speed to the maximum speed $\bar{V}$. Then, it uses the car-following model (6.4) to estimate the movements of the CHV followers of the vehicle group, given the trajectory of the leading CAV and signal timing plans. Finally, safety constraints (6.7), (6.8), and (6.12) are checked. If there is no safety constraint violation, the current trajectory is optimal, otherwise, accident prevention step is activated to resolve the safety violation. General steps of the initial acceleration step are depicted in Figure 6-5.

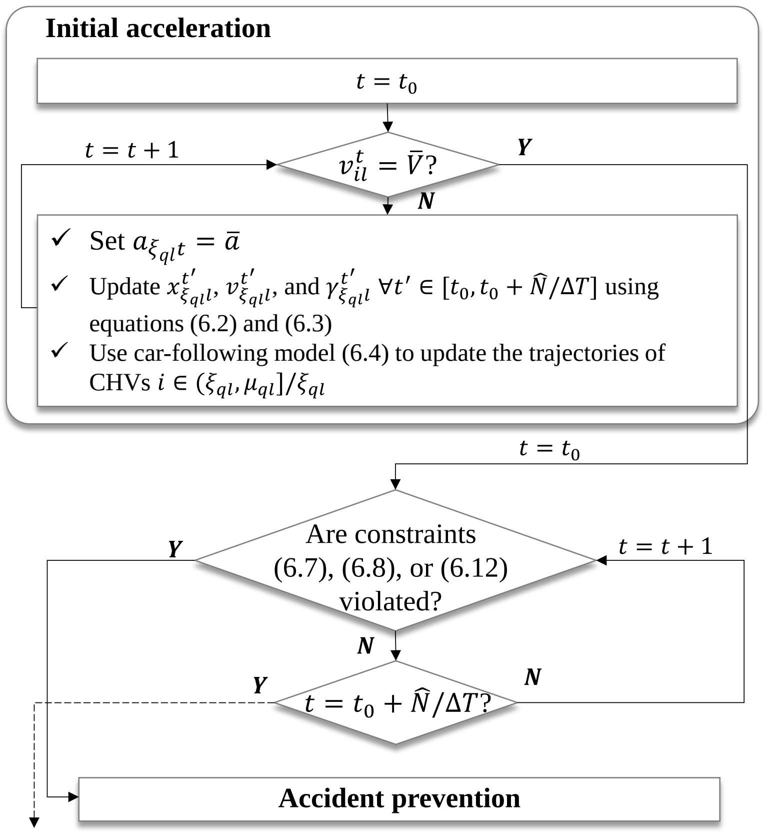

Figure 6-5: Initial acceleration step of the proposed shooting heuristic (Figure 6-4)

6.3.2.1.2 Accident prevention

This step gets activated if there is a safety constraint violation after the initial acceleration step. Assume that there is a safety violation at time $\beta \in [t_0, t_0 + \widehat{N}/\Delta T]$. This step moves backward from the violation time β, removes positive acceleration rates of the CAV one by one, updates the trajectories of CHVs, then checks the safety constraints. The same process is repeated until there is no positive acceleration rate during period $t' \in [t_0, \beta]$ or the safety violation is resolved. If the safety violation is resolved, the algorithm moves to the speeding up step to push the current feasible trajectories toward optimality. Otherwise, the algorithm moves backward from time β and sets acceleration rates of $\underline{a}$ for the CAV to resolve the safety violation by slowing down the CAV leader. Then, the trajectories of CHV followers are updated and safety constraints are checked. The same process continues until $a^{t}_{\xi_{ql}} = \underline{a}$ for the period $t' \in [t_0, \beta]$ or the safety violation is resolved. If the safety violation is resolved at any iteration of this process, the algorithm moves to the speeding up step. Otherwise, the current signal timing plan is infeasible, and we move to the next signal timing plan. Figure 6-6 shows the algorithm with more details.

6.3.2.1.3 Speeding up

Activation of this step means that the previous step could successfully construct a set of feasible trajectories for the members of vehicle group $q \in P_l$ on lane $l \in L$. However, they may be sub-optimal since the only concern of the accident prevention step is to satisfy safety constraints (6.7), (6.8), and (6.12). Therefore, this step is designed to set an acceleration rate of $\bar{a}$ at any time step that does not lead to a safety constraint violation. This step starts from time $t = t_0$ sets an acceleration rate of $a_{\xi_{ql}t} = \bar{a}$ if $v^{t}_{\xi_{ql}l} < \bar{V}$ and $a^{t}_{\xi_{ql}l} = 0$ for CAV $i = \xi_{ql}$ on lane $l \in L$, then updates the trajectories of its following CHVs and checks the safety constraints (6.7), (6.8), and (6.12). If there is a safety constraint violation, it sets $a_{\xi_{ql}t} = \bar{a}$, and $t = t + 1$, otherwise, it only sets $t = t + 1$. The same process continuous until the end of the planning time horizon $t_0 + \widehat{N}/\Delta T$ or reaching the maximum speed $\bar{V}$. See Figure 6-7 for the general steps of the speeding up process.

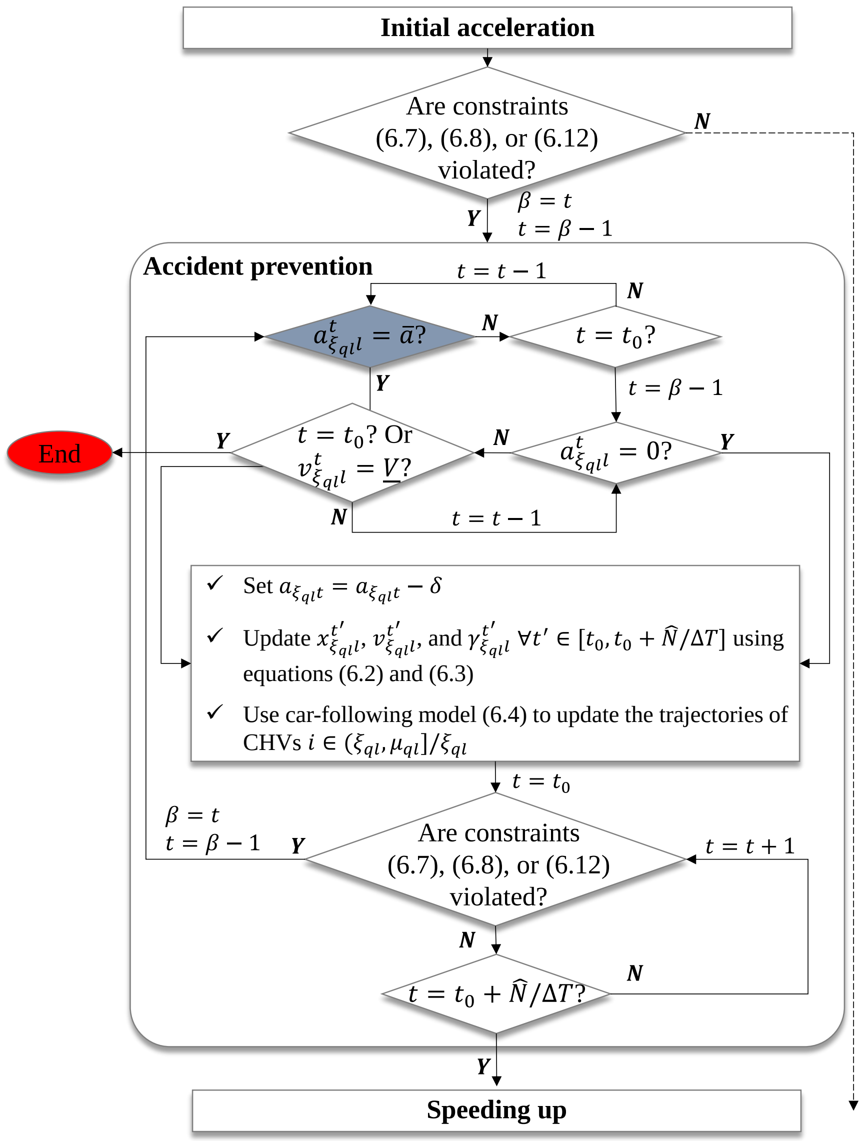

Figure 6-6: Accident prevention step of the proposed shooting heuristic (Figure 6-4)

- Blue tile shows the starting point of this step.

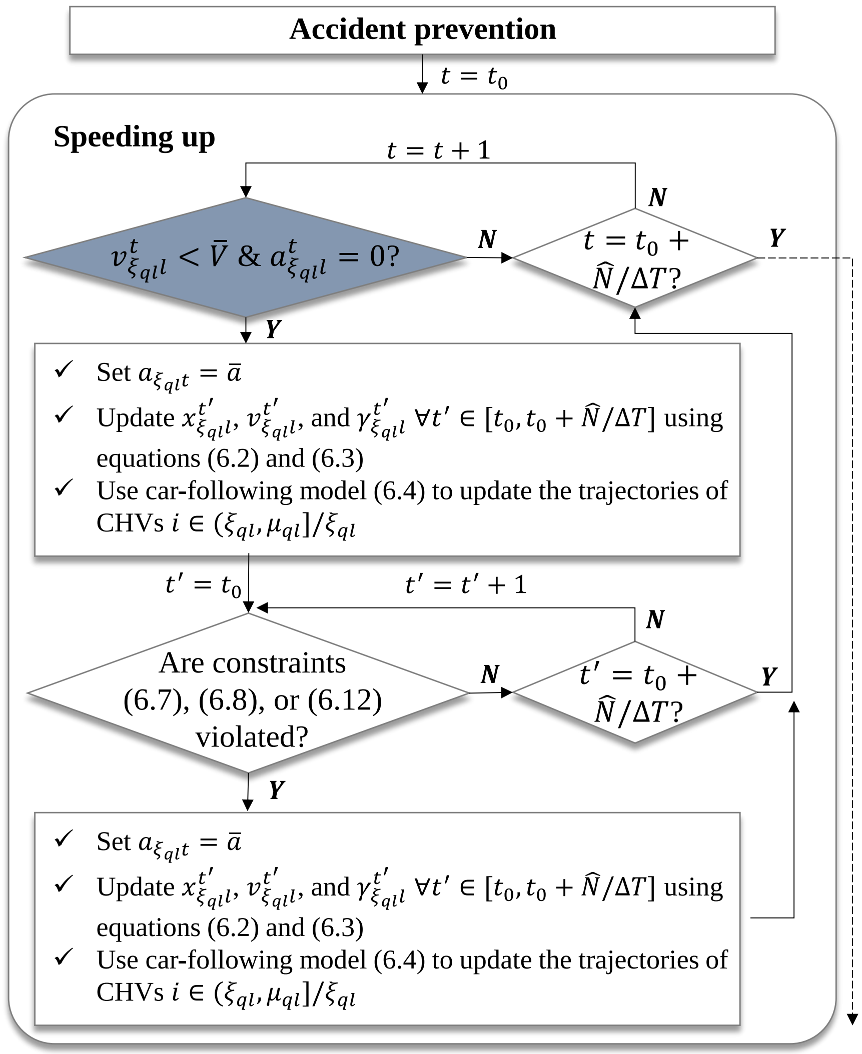

Figure 6-7: Speeding up step of the proposed shooting heuristic (Figure 6-4)

6.3.2.2. Trajectory construction for the entire fleet

We assume that the intersection controller records the time that each vehicle enters the coordination area of the intersection and saves it in variable e_{il} for vehicle $i \in I_l$ on lane $l \in L$. The algorithm finds vehicle $i \in I_l$ on lane $l \in L$ with the least e_{il} value and uses the car-following model (6.4) to estimate its movement if it is a CHV. If it is a CAV, the algorithm finds vehicle group q in a way that $\xi_{ql} = i$, which means that CAV i on lane $l \in L$ is the CAV leader of vehicle group $q \in P_l$. Then it uses the shooting heuristic shown in Figure 6-4 to construct trajectories for that CAV and its following CHVs. If the number of vehicles inside the vehicle group is greater than or equal to the predefined maximum platoon length PS, the algorithm moves forward with the next vehicle with the minimum e value. Otherwise, the algorithm moves forward with vehicle group $q + 1$ on the same lane and constructs trajectories for its members. If the headway between the last vehicle of vehicle group q and the CAV leader of vehicle group $q + 1$ is less than a predefined maximum value δ, the constructed trajectories are kept. Then, the algorithm checks for the maximum platoon length PS considering vehicle groups q and $q + 1$. If the headway between the last vehicle of vehicle group q and the CAV leader of vehicle group $q + 1$ is greater than the predefined maximum value δ, the algorithm disregards the constructed trajectories for vehicle group $q + 1$ and moves forward with the next vehicle with the minimum e value. This process continues until it constructs trajectories for all vehicles in the intersection neighborhood. Then, it checks for the white phase activation constraints (6.21). If these constraints are violated, the signal timing plan is infeasible.

6.4. Results

This section introduces the case study setting and discusses the results. The proposed framework is coded in JAVA and is run on a desktop computer with a core i9 CPU and 64 GB of memory. VISSIM microscopic traffic simulator (PTV Group, 2015) software is used to implement the optimal solutions to measure the performance of the proposed framework.

6.4.1. Case study

We used an isolated four-legged intersection with exclusive left turning lanes as shown in Figure 6-8 to test our proposed methodology. We assume that all vehicles are connected, and their speed and location are acquirable in real-time. In addition, we assume that vehicles are in their preferred lanes prior to entering the intersection neighborhood. We used three demand levels with 600 $veh/hr/lane$, 900 $veh/hr/lane$, and 1200 $veh/hr/lane$ demands for through movements. Demand for left turning movements is assumed to be 8% of the through demand. Demand levels are detailed in Table 6-2. Each demand level is tested using 11 CAV market shares ranging from 0% to 100% at 10% increments. Other parameters used in the case study are summarized in Table 6-3.

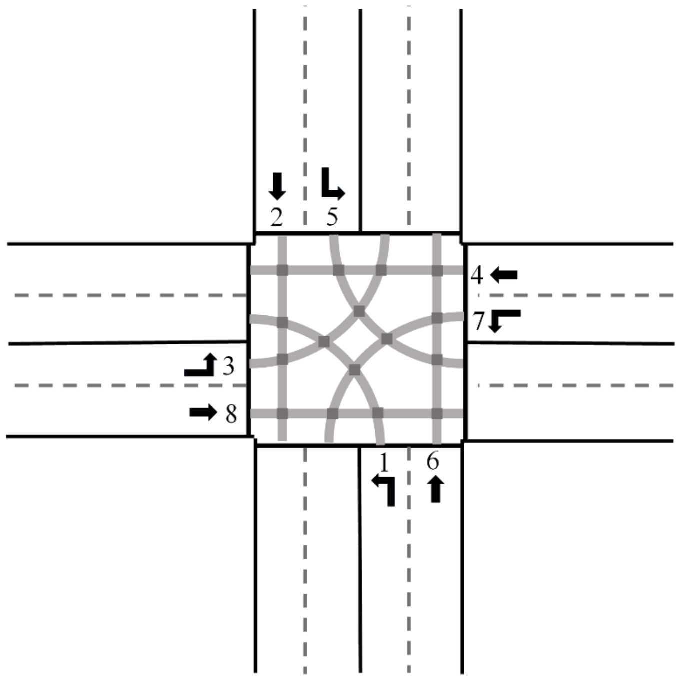

Figure 6-8: Case study intersection.

Table 6-2: Demand levels for case studies

	Through demand ($veh/hr/lane$)	Left turning demand ($veh/hr/lane$)
Demand level 1	600	48
Demand level 2	900	72
Demand level 3	1200	96

Table 6-3: Value of the parameters used in the case study.

Parameters	Value
Maximum speed (ft/s)	39
Maximum acceleration (ft/s^2)	13
Minimum acceleration (ft/s^2)	-13
Human driver reaction time (s)	1
Automated vehicle reaction time (s)	0.1
Detection range (ft)	650
Intersection location (ft)	650
Average length of vehicles (ft)	13
Safety distance between consecutive vehicles (ft)	11.8
Safety distance between CAVs and red signal light (ft)	1
Safety distance between vehicle-groups of conflicting lane-groups (ft)	40
Car-following parameter α_1 (s^{-1})	0.95
Car-following parameter α_2 (s^{-2})	0.25
Trajectory updating interval (s)	0.5
Signal status updating interval (s)	5
All red time (s)	2
Yellow time (s)	3
Minimum green time for through movements (s)	15
Minimum green time for left-turning movements (s)	5
Minimum white time (s)	10
Planning time horizon (s)	20
Study period (s)	900
Maximum headway (s)	1.5
Maximum platoon size	10

6.4.2. Mobility

Average delays for different demand levels and CAV market shares are summarized in Table 6-4. Average delay for all demand levels decreases as the CAV market share increases. This is due to the more efficient operation of CAVs, their awareness of the upcoming signal indications, and more activation rates of the white phases with a higher CAV market share. In addition, average delay for all demand levels experiences a significant drop from 80% to 90% CAV market share since the white phase is the dominant signal phase with 90% CAV market share. Moreover, vehicle groups get shorter as CAV market share increases, which contributes to the more efficient operation of them.

Table 6-4: Average delay for different demand levels and CAV market shares in seconds

Demand level	**CAV market share (%)**										
	0	**10**	**20**	**30**	**40**	**50**	**60**	**70**	**80**	**90**	**100**
1	17.8	17.45	16.83	16.63	15.29	15.21	14.64	12.79	10.16	3.88	1.45
2	33.74	25.58	21	19.91	18.76	17.44	17.29	16.26	14.05	7.04	4.18
3	53.6	46.24	41.93	38.31	36.1	33.58	28.66	27.61	26.02	16.98	8.89

Average CAV and CHV delays with different CAV market shares under demand level 3 are shown in Figure 6-9. As expected, average CAV delay is always less than average CHV delay due to higher operational performance of CAVs. Moreover, average delays for both vehicle types decrease as the CAV market share increases due to higher queue discharge rates and higher white phase activation rates with higher CAV market shares.

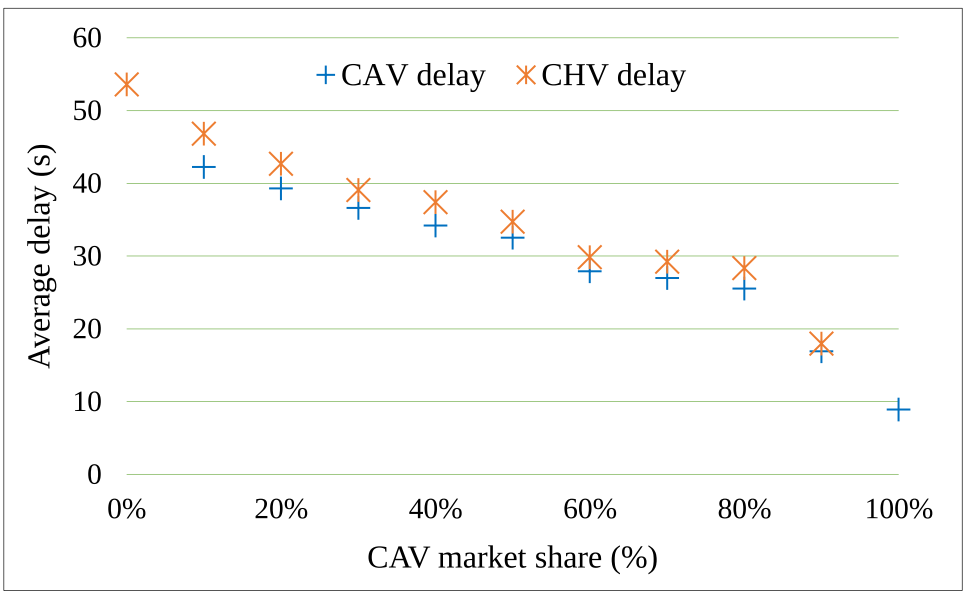

Figure 6-9: Average CAV and CHV delays with different CAV market shares under demand level 3

Figure 6-10 shows intersection signal timing plans for different CAV market shares under demand level 3 based on lane numbering shown in Figure 6-8. The intersection controller only uses green signal indications to operate vehicles when CAV market share is less than 50% since intersection control with white phase requires a relatively high CAV market share to efficiently control CHVs. White phases start to appear with at least 50% CAV market share and are used more frequently as

CAV market share increases. White phase becomes the dominant phase when CAV market share is higher than 70%.

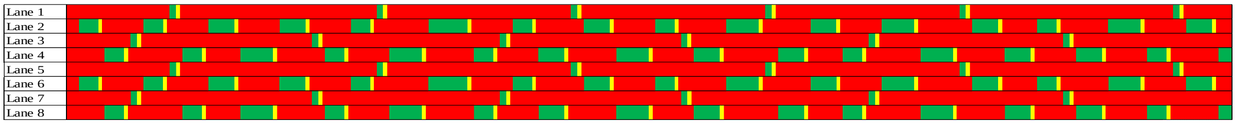

a) 0% CAV market share

b) 20% CAV market share

c) 40% CAV market share

d) 50% CAV market share

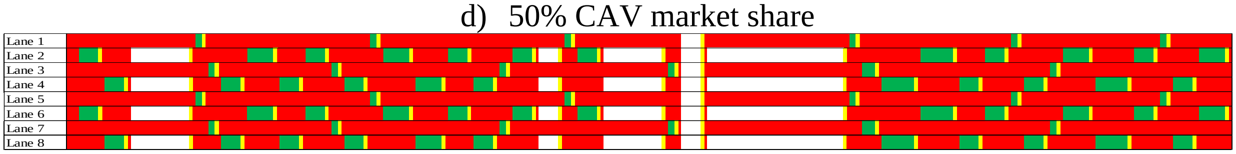

e) 60% CAV market share

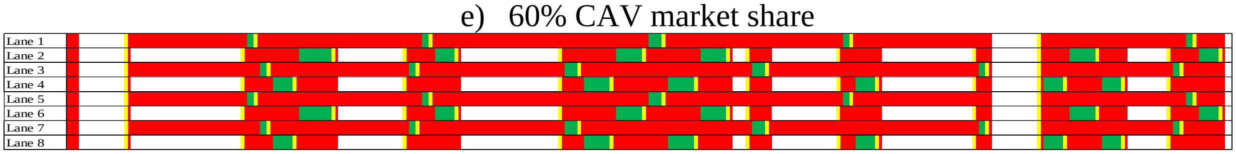

f) 70% CAV market share

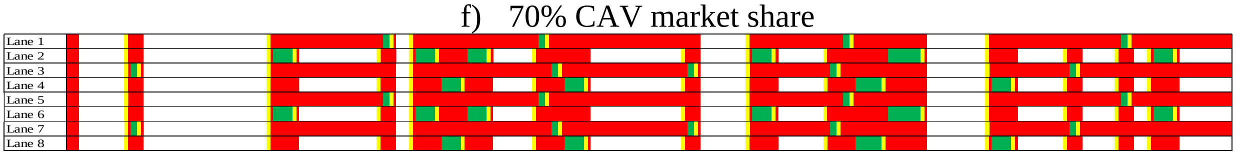

g) 80% CAV market share

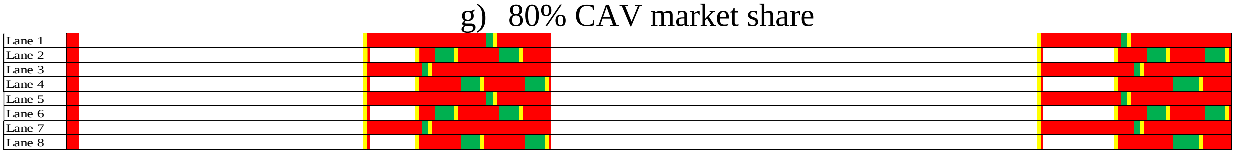

h) 90% CAV market share

Figure 6-10: Signal timings for different CAV market shares under deman level 3.

Figure 6-11 shows vehicle trajectories on lane 6 for various CAV market shares under demand level 3. The red and blue lines depict the trajectory of CHVs and CAVs, respectively. As shown, vehicles tend to move smoother with a fewer number of stops as the CAV market share increases. In addition, shorter queue lengths are observed whit higher CAV market shares. Moreover, vehicles tend to adjust their speeds to pass the intersection without stopping during the white phases. Therefore, not only does the activation of the white phases lead to smoother movements for CAVs, but it also helps smoothing the trajectories of CHVs.

We introduce two white phase activation scenarios, namely optimized-white-phase and no-white-phase to study the effects of white phase on operational and safety performance measures of the intersection. The intersection controller can use a combination of green and white signal indications to operate vehicles under the optimized-white-phase scenario. On the other hand, only green signal indication is used under the no-white-phase scenario. Figure 6-12 shows the average intersection delay for different CAV market shares under demand level 3 with the two white phase activation scenarios. Average delays with both white phase activation scenarios are identical up to 40% CAV market shares since using white phases was not beneficial with low CAV market shares. Average delay under optimized-white-phase scenario is less than average delay under no-white-phase scenario with CAV market shares of 50% and above. In addition, the difference between the two average delays increases as the CAV market share increases due to higher white phase activation rates with higher CAV market shares.

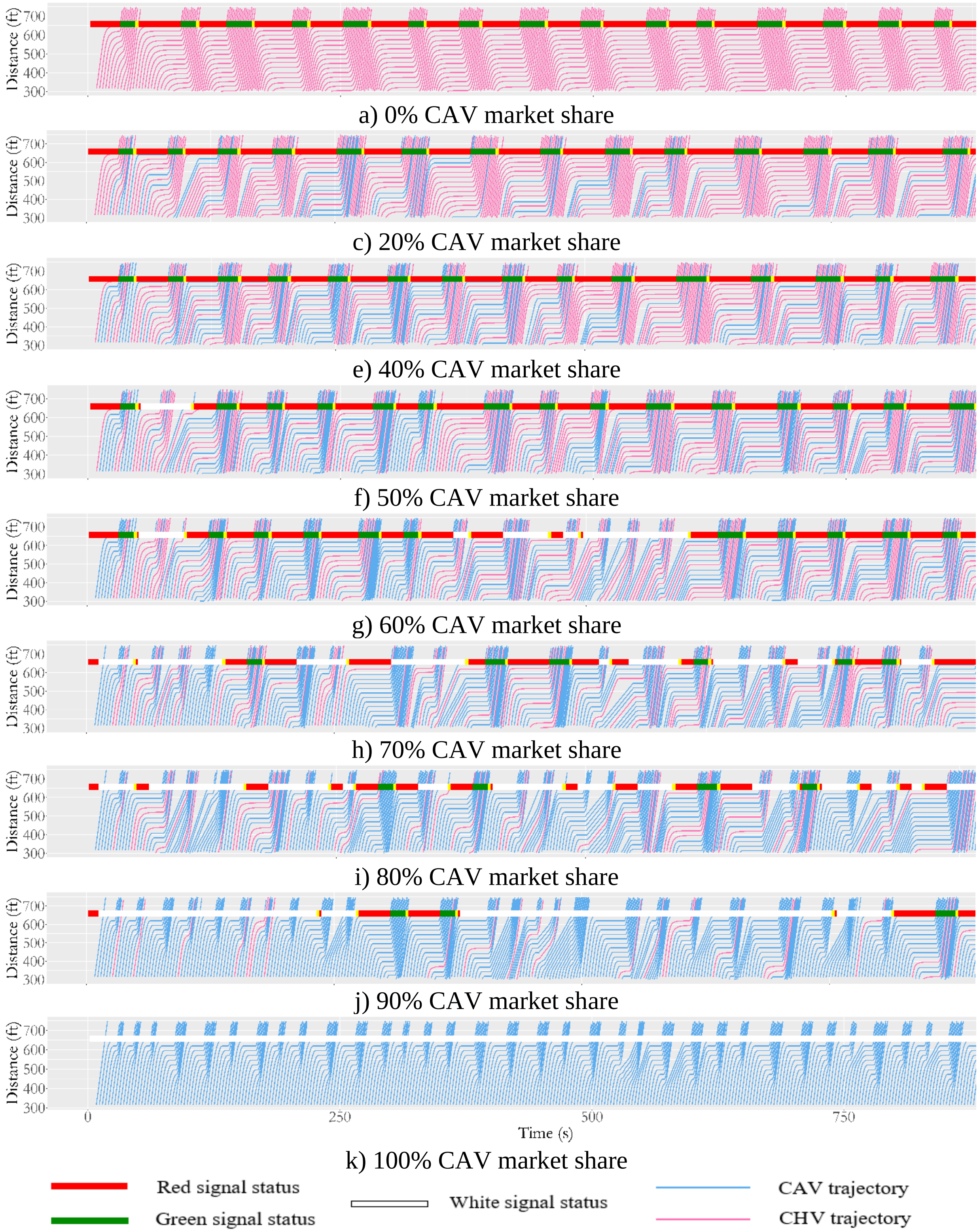

Figure 6-11: Vehicle trajectories for different CAV market shares under deman level 3.

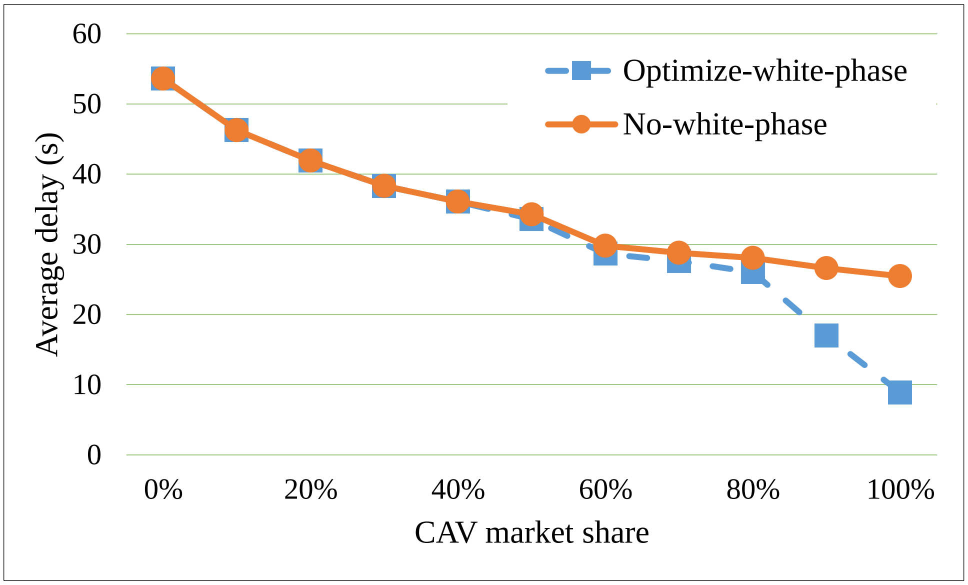

Figure 6-12: Average intersection delay with different CAV market shares under demand level 3 with two white phase activation scenarios

Figure 6-13 shows the latent demand for different CAV market shares under demand level 3 with different white phase activation scenarios. Latent demand happens due to long queues that prevent vehicles from entering the intersection neighborhood. Increasing CAV market share positively contributes to reducing the latent demand under both white phase activation scenarios. Latent demands are identical up to 40% CAV market share. However, latent demand under optimized-white-phase scenario is less than latent demand under no-white-phase scenario. This shows that using the white phase helps us operate more vehicles with less experienced delays. In presence of the white phase, the proposed framework could successfully operate the entire demand with at least a 90% CAV market share. However, the intersection controller failed to accommodate all the incoming vehicles even with a fully CAV fleet without using the white phase.

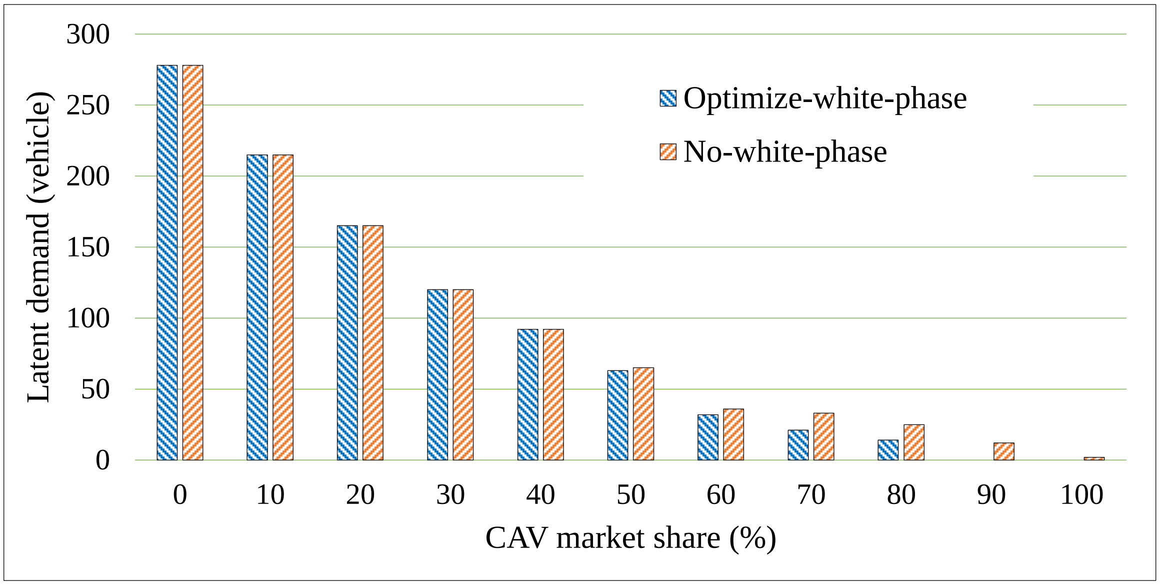

Figure 6-13: Latent demand with different CAV market shares under demand level 3 with two white phase activation scenarios

6.4.2.1. Safety

We have used the surrogate safety assessment model (SSAM) software (Gettman and Head, 2003) to study possible rear-end and crossing collisions. Time to collision (TTC) is considered as the surrogate safety measure. TTC is the time that it would take for a pair of vehicles to collide if they keep their current speed. The results of the analysis indicate that there is no near collision case with a TTC of less than 1.5 seconds. Moreover, no crossing near collision case with a TTC of less than 10 seconds is observed. Average rear-end TTC for different CAV market shares under demand level 3 with the two white phase activation scenarios are shown in Figure 6-14. Average TTCs for different CAV market shares are similar for different CAV market shares. In addition, average TTC under optimized-white-phase scenario is slightly less than of no-white-phase scenario since vehicles are operated within compact groups during white phases.

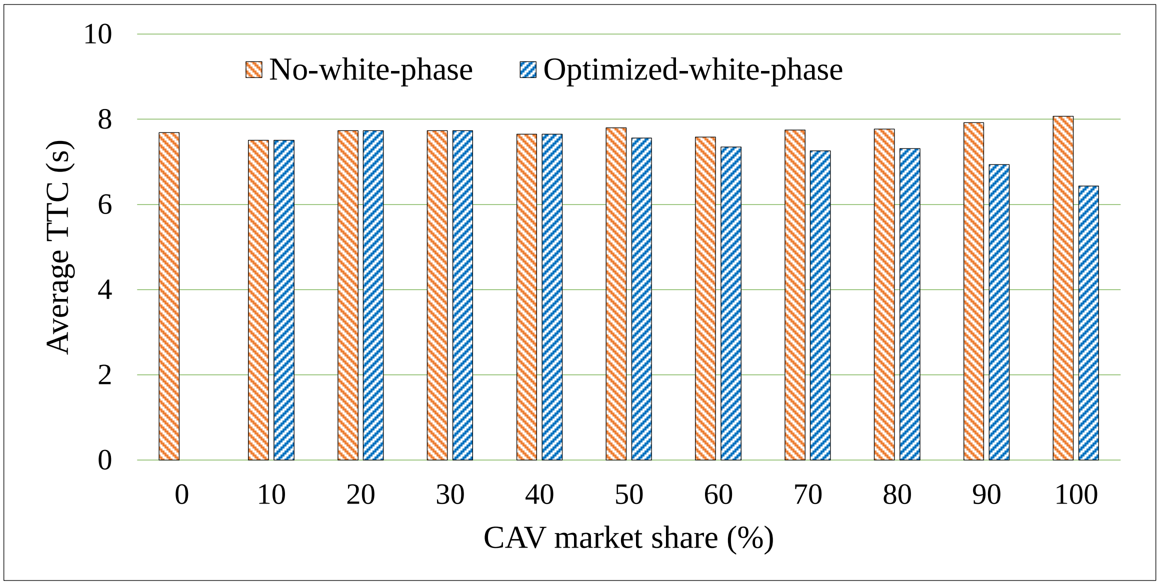

Figure 6-14: Average rear-end TTC with different CAV market shares under demand level 3 with two white phase activation scenarios

6.4.2.2. Computation time

Distribution of computation times under demand level 3 with 100% CAV market share is shown in Figure 6-15. Note that this is the most complex case since each vehicle is a vehicle group by itself. The proposed methodology could successfully provide intersection signal timing plans and CAV trajectories in at most 37 milliseconds that is more than 13 times faster than the 500 milliseconds-long updating time step length.

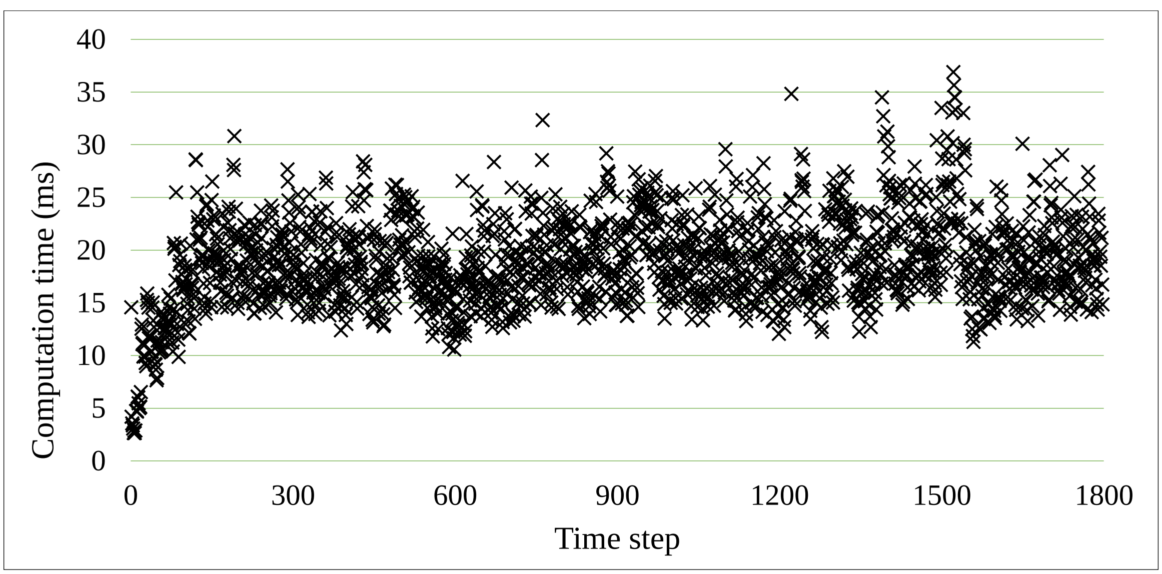

Figure 6-15: Compution time for demand level 3 with 100% CAV market share

6.5. Conclusion

This chapter introduces a bi-level shooting heuristic-based methodology for the joint optimization of CAV trajectory and intersection signal timing plans. A new white phase is added to green and red signal indications that is activated when there are enough CAVs at the intersection vicinity to lead groups of CHVs. During this phase, CAVs act as mobile controllers to lead groups of CHVs through the conflicting area of the intersection while preserving their safety. Note that green and red signal indications are used when there are not enough CAVs to ensure the safety of the entire fleet. The upper level of the proposed framework enumerates all feasible signal timing plans in search of the best objective value. The lower level uses a shooting heuristic to construct CAV trajectories while considering rear-end collision avoidance, red light running avoidance, and vehicle-group safety constraints. A platooning algorithm is also used to operate platoons of vehicles consisting of one or more vehicle groups instead of individual vehicle groups to increase the efficiency of the framework. The case study results show that the proposed framework is able to find solutions in no longer than 37 milliseconds for a scenario with 1200 $veh/h/lane$ demand. This makes the framework suitable as a subroutine in network-level signal and trajectory optimization algorithms. In addition, the introduced white phase reduces the average delay by up to 65%, compared to a joint signal and trajectory optimization with different CAV market shares.

CHAPTER 7: CONCLUSION

7.1. Summary

Emerging CAV technologies offer a great potential to transform traditional traffic control methods in transportation networks. The optimal control of CAV trajectories helps reduce travel time and energy consumption at signalized intersections. Significant improvements in traffic operations are reported when signal timing parameters and CAV trajectories are jointly optimized in a fully automated environment. Moreover, traffic operations will be further improved by replacing traffic lights with a signal-free intersection control when all vehicles are automated. However, there is a need to prepare for the transition from human-driven to self-driving cars as technology, regulation, and safety limitations influence the expansion of CAV market penetration rate for many years to come. This dissertation aimed at developing concepts and frameworks to jointly optimize intersection signal timing plans and CAV trajectories within mixed-autonomy environments.

This research presented a new “white” phase for mixed-autonomy traffic streams, during which CAVs form groups of CHVs and navigate them through the intersection. The joint signal and trajectory optimization problem is formulated as an MINLP. The movements of CHVs are incorporated into the optimization program using a customized car-following model. A hybrid solution technique including: 1) linearization and 2) receding horizon framework is used to both tackle the complexity of the problem and deal with the dynamic nature of the signal and trajectory optimization. The results of this study on an isolated intersection showed that the proposed mathematical model could the total delay by 19.6% - 96.2% compared to a fully-actuated signal control.

Furthermore, we developed a vehicle-level distributed coordination strategy to solve the proposed white phase formulation in real-time. The central optimization model is transformed into vehicle-level distributed mixed-integer non-linear programs that optimizes the trajectory of a single vehicle while proposing a signal timing plan for the entire intersection. In addition, a methodology is developed to form an agreement among all vehicles on their trajectories and intersection signal timing parameters. The agreement on trajectories is formed through an iterative process, where CAVs optimize their trajectories given the trajectories of other vehicles to avoid collisions, then share their trajectories with other vehicles. The signal agreement is reached through a voting process, where the most voted feasible signal timing plan is selected. The case study results on an isolated intersection shows a 3.2% - 94.1% reduction in total delay, compared to a cooperative trajectory and signal optimization.

The proposed distributed coordination strategy could find near optimal solutions in real-time for a single intersection while using up to 80% of the time step length. However, network-level signal and trajectory optimization methods may need to solve the intersection-level signal and trajectory optimization model multiple times to form effective coordination among intersections to push the intersection-level solutions toward network-level optimality. Therefore, we developed an efficient bi-level methodology to solve the intersection-level signal and trajectory optimization fast enough to be useful as a subroutine for network-level optimization algorithms. The upper level of the proposed framework enumerates all the feasible signal timing plans while the lower level uses a shooting heuristic to construct/estimate vehicle trajectories for a given signal timing plan. The numerical results indicate that the proposed methodology could find proper signal timing plans and vehicle trajectories in at most 40 milliseconds, which is twelve times faster than the 500 milliseconds-long updating time step length. In addition, efficient operation of CAVs can decrease the average delay by up to 50.1%, compared to a fleet of CHVs.

The proposed shooting heuristic-based methodology is efficient enough to serve as a subroutine in network-level signal and trajectory optimization algorithms. However, it only uses green signal indications, hence, stops vehicles behind the red light even with 100% CAVs. Therefore, we extend the shooting heuristic-based signal and trajectory optimization framework to accommodate white phases. In this framework, CAV trajectories are constructed in a way to meet rear-end accident prevention, red light running prevention, and vehicle-group safety constraints. To further improve the efficiency of the framework, a platooning algorithm is also incorporated into the framework to operate platoons of vehicles containing one or more vehicle groups. The proposed methodology can find solutions in less than 37 milliseconds for the most complex tested scenario using the available computational power of CAVs. The addition of the white phase decreases the average delay by up to 65%, compared to the same methodology without using the white phase.

7.2. Limitations

In this study we assumed that we could access the location and speed of all vehicles. However, a fully connected fleet may not be achievable in the near future. In addition, we assumed that CAVs are able to precisely implement the acceleration rates that are dictated by the intersection controller, while there is a significant chance that CAVs deviate from the dictated trajectories. Moreover, possibilities like communication delay and cyber attacks are disregarded in this study. Furthermore, we assumed that all CAVs held the same engine and driving characteristics throughout the study period. However, these assumptions may not get satisfied in real world due to different engine and driving behavior of vehicles manufactured by different companies.

We developed concepts and methodologies to operate vehicles though isolated intersections. Although an efficient operation of an intersection in a network can provide local improvements, it may cause gridlocks and queue spillbacks if there is no effective coordination among the intersections of a network, especially within a saturated regime.

7.3. Future research suggestions

Following are the suggestions to continue this research:

1. This research focused on isolated intersections; however, a higher improvement can be achieved if the intersections of a network cooperate with each other. Therefore, extending the concepts proposed in this study is recommended.

2. As shown in this study, CAVs can be used as mobile controllers to enhance the efficiency of intersection control methods. However, the same logic can be used for different parts of the transportation networks like roundabouts and freeways. It is suggested to extend the mobile controller paradigm to different parts of the network.

3. We assumed a single lane for each movement of the intersection. However, most of the intersections in the real world have more than one lane for each movement. It is recommended to incorporate a lane changing logic into the proposed frameworks in this study to accommodate multi-lane intersections.

4. We assumed that CAVs precisely implement the provided trajectories, which is not realistic. It is suggested to consider stochasticity in the location of the CAVs due to their inability to implement the provided trajectories.

5. We did not consider communication delays and cyber-attacks. It is suggested to study the effects of communication delay and cyber attacks in terms of data integrality.
6. It is also suggested to consider different objective functions, engine characteristics, and driving behaviors for CAVs.

REFERENCES

Al Islam, S.M.A. Bin, Hajbabaie, A., 2017. Distributed coordinated signal timing optimization in connected transportation networks. Transp. Res. Part C Emerg. Technol. 80, 272–285.

Amirgholy, M., Gao, H.O., 2023. Optimal traffic operation for maximum energy efficiency in signal-free urban networks: A macroscopic analytical approach. Appl. Energy 329, 120128.

Asadi, B., Vahidi, A., 2010. Predictive cruise control: Utilizing upcoming traffic signal information for improving fuel economy and reducing trip time. IEEE Trans. Control Syst. Technol. 19, 707–714.

Askari, A., Farias, D.A., Kurzhanskiy, A.A., Varaiya, P., 2016. Measuring impact of adaptive and cooperative adaptive cruise control on throughput of signalized intersections. arXiv Prepr. arXiv1611.08973.

Brackstone, M., McDonald, M., 1999. Car-following: a historical review. Transp. Res. Part F Traffic Psychol. Behav. 2, 181–196.

CPLEX, I.B.M.I., 2014. 12.6. CPLEX User's Man.

Dai, P., Liu, K., Zhuge, Q., Sha, E.H.-M., Lee, V.C.S., Son, S.H., 2016. A convex optimization based autonomous intersection control strategy in vehicular cyber-physical systems. In: 2016 Intl IEEE Conferences on Ubiquitous Intelligence & Computing, Advanced and Trusted Computing, Scalable Computing and Communications, Cloud and Big Data Computing, Internet of People, and Smart World Congress (UIC/ATC/ScalCom/CBDCom/IoP/SmartWorld). pp. 203–210.

Deng, Z., Yang, K., Shen, W., Shi, Y., 2023. Cooperative Platoon Formation of Connected and Autonomous Vehicles: Toward Efficient Merging Coordination at Unsignalized Intersections. IEEE Trans. Intell. Transp. Syst.

Dresner, K., Stone, P., 2004. Multiagent traffic management: A reservation-based intersection control mechanism. In: Proceedings of the Third International Joint Conference on Autonomous Agents and Multiagent Systems-Volume 2. pp. 530–537.

Dresner, K., Stone, P., 2008. A multiagent approach to autonomous intersection management. J. Artif. Intell. Res. 31, 591–656.

Du, Y., ShangGuan, W., Chai, L., 2021. A coupled vehicle-signal control method at signalized intersections in mixed traffic environment. IEEE Trans. Veh. Technol. 70, 2089–2100.

Feng, Y., Yu, C., Liu, H.X., 2018. Spatiotemporal intersection control in a connected and automated vehicle environment. Transp. Res. Part C Emerg. Technol. 89, 364–383.

Gettman, D., Head, L., 2003. Surrogate safety measures from traffic simulation models. Transp. Res. Rec. 1840, 104–115.

Ghosh, A., Parisini, T., 2022. Traffic control in a mixed autonomy scenario at urban intersections: An optimal control approach. IEEE Trans. Intell. Transp. Syst. 23, 17325–17341.

Goodall, N.J., Smith, B.L., Park, B., 2013. Traffic signal control with connected vehicles. Transp. Res. Rec. 2381, 65–72.

Guo, Y., Ma, J., Xiong, C., Li, X., Zhou, F., Hao, W., 2019. Joint optimization of vehicle trajectories and intersection controllers with connected automated vehicles: Combined dynamic programming and shooting heuristic approach. Transp. Res. part C Emerg. Technol. 98, 54–72.

Hajbabaie, A., Benekohal, R.F., 2013. Traffic signal timing optimization: Choosing the objective function. Transp. Res. Rec. 2355, 10–19.

Hajbabaie, A., Benekohal, R.F., 2015. A program for simultaneous network signal timing optimization and traffic assignment. IEEE Trans. Intell. Transp. Syst. 16, 2573–2586.

He, Q., Head, K.L., Ding, J., 2012. PAMSCOD: Platoon-based arterial multi-modal signal control with online data. Transp. Res. Part C Emerg. Technol. 20, 164–184.

Helly, W., 1959. Simulation of bottlenecks in single-lane traffic flow.

Jiang, X., Shang, Q., 2022. A Dynamic CAV-Dedicated Lane Allocation Method With the Joint Optimization of Signal Timing Parameters and Smooth Trajectory in a Mixed Traffic Environment. IEEE Trans. Intell. Transp. Syst.

Jung, H., Choi, S., Park, B.B., Lee, H., Son, S.H., 2016. Bi-level optimization for eco-traffic signal system. In: 2016 International Conference on Connected Vehicles and Expo (ICCVE). pp. 29–35.

Lee, J., Park, B., 2012. Development and evaluation of a cooperative vehicle intersection control algorithm under the connected vehicles environment. IEEE Trans. Intell. Transp. Syst. 13, 81–90.

Lee, J., Park, B., Yun, I., 2013. Cumulative travel-time responsive real-time intersection control algorithm in the connected vehicle environment. J. Transp. Eng. 139, 1020–1029.

Li, M., Wu, X., He, X., Yu, G., Wang, Y., 2018. An eco-driving system for electric vehicles with signal control under V2X environment. Transp. Res. Part C Emerg. Technol. 93, 335–350.

Li, P.T., Zhou, X., 2017. Recasting and optimizing intersection automation as a connected-and-automated-vehicle (CAV) scheduling problem: A sequential branch-and-bound search approach in phase-time-traffic hypernetwork. Transp. Res. Part B Methodol. 105, 479–506.

Li, W., Ban, X., 2018. Connected vehicles based traffic signal timing optimization. IEEE Trans. Intell. Transp. Syst.

Li, Z., Elefteriadou, L., Ranka, S., 2014. Signal control optimization for automated vehicles at isolated signalized intersections. Transp. Res. Part C Emerg. Technol. 49, 1–18.

Liang, X., Guler, S.I., Gayah, V. V, 2019. Joint optimization of signal phasing and timing and vehicle speed guidance in a connected and autonomous vehicle environment. Transp. Res. Rec. 2673, 70–83.

Ma, W., Li, J., Yu, C., 2022. Shared-phase-dedicated-lane based intersection control with mixed traffic of human-driven vehicles and connected and automated vehicles. Transp. Res. part C Emerg. Technol. 135, 103509.

Mehrabipour, M., Hajbabaie, A., 2017. A cell-based distributed-coordinated approach for network-level signal timing optimization. Comput. Civ. Infrastruct. Eng. 32, 599–616.

Mirheli, A., Hajibabai, L., 2019. Utilization Management and Pricing of Parking Facilities Under Uncertain Demand and User Decisions. IEEE Trans. Intell. Transp. Syst.

Mirheli, A., Hajibabai, L., Hajbabaie, A., 2018. Development of a signal-head-free intersection control logic in a fully connected and autonomous vehicle environment. Transp. Res. Part C Emerg. Technol. 92, 412–425.

Mirheli, A., Tajalli, M., Hajibabai, L., Hajbabaie, A., 2019. A consensus-based distributed trajectory control in a signal-free intersection. Transp. Res. part C Emerg. Technol. 100, 161–176.

Mohebifard, R., Al Islam, S.M.A. Bin, Hajbabaie, A., 2019. Cooperative traffic signal and perimeter control in semi-connected urban-street networks. Transp. Res. Part C Emerg. Technol. 104, 408–427.

Mohebifard, R., Hajbabaie, A., 2018. Distributed optimization and coordination algorithms for dynamic traffic metering in urban street networks. IEEE Trans. Intell. Transp. Syst. 20, 1930–1941.

Moradi, H., Sasaninejad, S., Wittevrongel, S., Walraevens, J., 2021. Proposal of an integrated platoon-based Round-Robin algorithm with priorities for intersections with mixed traffic flows. IET Intell. Transp. Syst. 15, 1106–1118.

Nguyen, C.H.P., Hoang, N.H., Vu, H.L., 2023. A Joint Trajectory Planning and Signal Control Framework for a Network of Connected and Autonomous Vehicles. IEEE Trans. Intell. Transp. Syst.

Niroumand, R., Hajibabai, L., Hajbabaie, A., 2021. The Effects of Connectivity on Intersection Operations with "White Phase." In: 2021 IEEE International Intelligent Transportation Systems Conference (ITSC). pp. 3839–3844.

Niroumand, R., Hajibabai, L., Hajbabaie, A., Tajalli, M., 2022. Effects of Autonomous Driving Behavior on Intersection Performance and Safety in the Presence of White Phase for Mixed-Autonomy Traffic Stream. Transp. Res. Rec. 03611981221082580.

Niroumand, R., Tajalli, M., Hajibabai, L., Hajbabaie, A., 2020a. Joint Optimization of Vehicle-group Trajectory and Signal Timing: Introducing the White Phase for Mixed-autonomy Traffic Stream. Transp. Res. Part C Emerg. Technol.

Niroumand, R., Tajalli, M., Hajibabai, L., Hajbabaie, A., 2020b. The Effects of the "White Phase" on Intersection Performance with Mixed-Autonomy Traffic Stream. In: 2020 IEEE 23rd International Conference on Intelligent Transportation Systems (ITSC). pp. 1–6.

Pourmehrab, M., Elefteriadou, L., Ranka, S., Martin-Gasulla, M., 2019. Optimizing signalized intersections performance under conventional and automated vehicles traffic. IEEE Trans. Intell. Transp. Syst.

Powell, W.B., 2007. Approximate Dynamic Programming: Solving the curses of dimensionality. John Wiley & Sons.

PTV Group, 2015. PTV Vissim 7 User Manual. PTV AG.

Qian, X., Gregoire, J., Moutarde, F., De La Fortelle, A., 2014. Priority-based coordination of autonomous and legacy vehicles at intersection. In: 17th International IEEE Conference on Intelligent Transportation Systems (ITSC). pp. 1166–1171.

Rey, D., Levin, M.W., 2019. Blue phase: Optimal network traffic control for legacy and autonomous vehicles. Transp. Res. part B Methodol. 130, 105–129.

Shahidi, N., 2010. A delayed response policy for autonomous intersection management.

Tajalli, M., Hajbabaie, A., 2018. Distributed optimization and coordination algorithms for dynamic speed optimization of connected and autonomous vehicles in urban street networks. Transp. Res. Part C Emerg. Technol. 95.

Tajalli, M., Hajbabaie, A., 2021. Traffic Signal Timing and Trajectory Optimization in a Mixed Autonomy Traffic Stream. IEEE Trans. Intell. Transp. Syst.

Tajalli, M., Mehrabipour, M., Hajbabaie, A., 2020. Network-level coordinated speed optimization and traffic light control for connected and automated vehicles. IEEE Trans. Intell. Transp. Syst. 22, 6748–6759.

Vitale, C., Kolios, P., Ellinas, G., 2022. Autonomous intersection crossing with vehicle location uncertainty. IEEE Trans. Intell. Transp. Syst. 23, 17546–17561.

Wu, G., Jiang, R., 2023. Joint optimization for autonomous intersection management and trajectory smoothing design with connected automated vehicles. Transp. B Transp. Dyn. 11, 1234–1255.

Wu, J., Abbas-Turki, A., El Moudni, A., 2012. Cooperative driving: an ant colony system for autonomous intersection management. Appl. Intell. 37, 207–222.

Wu, Y., Chen, H., Zhu, F., 2019. DCL-AIM: Decentralized coordination learning of autonomous intersection management for connected and automated vehicles. Transp. Res. Part C Emerg. Technol. 103, 246–260.

Yao, Z., Jiang, H., Jiang, Y., Ran, B., 2023. A Two-Stage Optimization Method for Schedule and Trajectory of CAVs at an Isolated Autonomous Intersection. IEEE Trans. Intell. Transp. Syst.

Yu, C., Feng, Y., Liu, H.X., Ma, W., Yang, X., 2018. Integrated optimization of traffic signals and vehicle trajectories at isolated urban intersections. Transp. Res. Part B Methodol. 112, 89–112.

Zhang, H., Du, L., 2023. Platoon-centered control for eco-driving at signalized intersection built upon hybrid MPC system, online learning and distributed optimization part I: Modeling and solution algorithm design. Transp. Res. Part B Methodol.